

UNIVERSITY OF CALIFORNIA

IRVINE

Analysis of the Chemical and Photochemical Aging of Organic Aerosols

DISSERTATION

submitted in partial satisfaction of the requirements
for the degree of

DOCTOR OF PHILOSOPHY

in Chemistry

by

Anthony Gomez

Dissertation Committee:
Professor Sergey A. Nizkorodov, Chair
Professor Barbara J. Finlayson-Pitts
Professor Patrick Farmer

2007

Chapter 2 © 2006 American Chemical Society
Chapter 3 © 2006 Royal Society of Chemistry
All other materials © 2007 Anthony Gomez

The dissertation of Anthony Gomez
is approved and accepted in quality
and form for publication on microfilm:

Committee Chair

University of California, Irvine
2007

TABLE OF CONTENTS

	Page
LIST OF FIGURES	vi
LIST OF TABLES	viii
ACKNOWLEDGEMENTS	ix
CURRICULUM VITAE	x
ABSTRACT OF THE DISSERTATION	xi
CHAPTER 1: Introduction / Background	
1.1 Importance of Aerosol Particles	1
1.2 Oxidation by Ozone	2
1.3 Photochemistry	3
1.4 Thesis Objective	3
CHAPTER 2: Ozonolysis and UV Photodissociation Spectroscopy of Oxidized Undecylenic Acid Films Oxidized Undecylenic Acid Films	
2.1 Abstract	5
2.2 Introduction	6
2.3 Experimental	7
2.4 Results	10
2.5 Discussion	18
2.6 Atmospheric Implications	24

2.7	Conclusions	26
2.8	Tables and Figures	28

CHAPTER 3: Ozonolysis and UV Photodissociation Spectroscopy of
Alkene-Terminated Self-Assembled Monolayers on
Amorphous SiO₂ Nanoparticles

3.1	Abstract	43
3.2	Introduction	45
3.3	Experimental	45
3.4	Results	47
3.5	Discussion	50
3.6	Conclusions	57
3.7	Figures	58

CHAPTER 4: Stoichiometry of Ozone-Alkene Reactions in Participating
and Non-Participating Solvents

4.1	Introduction	65
4.2	Experimental	66
4.3	Results	67
4.4	Discussion	69
4.5	Figures	73

REFERENCES:	81
-------------	----

APPENDIX A: CRDS System in Detail

A.1	Lasers and Optics	99
A.2	Optoacoustic Cell	101
A.3	IR CRDS Cavity	101
A.4	Alignment	104
A.5	Photolysis	105
A.6	Ozone Generation	105
A.7	Detector	106
A.8	Triggering	106
A.9	GUI	108
A.10	Figures	110

LIST OF FIGURES

		Page
Figure 2.1	CRDS Diagram	32
Figure 2.2	CRDS Characterization	33
Figure 2.3	UV Absorption Spectra of Oxidized Undecylenic Acid (UA)	34
Figure 2.4	CRDS Survey Scan of UA + O ₃	35
Figure 2.5	CRDS Product Identification of UA + O ₃ / hv	36
Figure 2.6	Photodissociation Spectrum of Oxidized UA	37
Figure 2.7	ESI-MS of UA + O ₃ / hv	38
Figure 2.8	Peroxide Yields of UA + O ₃ vs. Time	39
Figure 2.9	Mechanism of UA + O ₃	40
Figure 2.10	Additional Peroxide / OH Mechanism of UA + O ₃	41
Figure 2.11	Mechanism of UA SOZ Photolysis	42
Figure 3.1	SEM Image of OX-50	58
Figure 3.2	CRDS Product Identification of C6= SAM + O ₃ / hv	59
Figure 3.3	Formic Acid Formation vs Photolysis Wavelength	60
Figure 3.4	Photodissociation Spectrum of Oxidized C6= SAM	61
Figure 3.5	Mechanism of C6= SAM + O ₃	62
Figure 3.6	Additional Peroxide / OH Mechanism of C6= SAM + O ₃	63
Figure 3.7	Mechanism of C6= SAM SOZ Photolysis	64
Figure 4.1	Diagram of the Uptake Apparatus	73

Figure 4.2	Ozone Depletion for Alkene Injections	74
Figure 4.3	Alkene:O ₃ Stoichiometry for Several Fatty Acids and Terpenes	75
Figure 4.4	Temperature and Concentration Effects on Stoichiometry	76
Figure 4.5	Reaction Mechanisms for Different Alkene:O ₃ Ratios	77
Figure 4.6	Effect of Participating Solvents	78
Figure 4.7	Cyclohexane + O ₃ Relative Product Yields	79
Figure 4.8	Alkane:O ₃ Stoichiometry for Cyclohexane	80
Figure A.1	Diagram of the IR CRDS System	110
Figure A.2	CRDS v.1 and V.2 Diagrams	111
Figure A.3	CRDS InSb Detector Sensitivity	112
Figure A.4	Diagram of the CRDS Data Acquisition System	113
Figure A.5	LabView GUI for Data Acquisition and Calculations	114

LIST OF TABLES

Table 2.1	ESI(-)-MS Mass Assignments for UA + O ₃	28
Table 2.2	ESI(-)-MS Mass-Intensity for UA + O ₃ →hv	29

ACKNOWLEDGMENTS

I would like to acknowledge all the people who helped me during my doctoral work:

I would especially like to thank my advisor, Sergey Nizkorodov, for his generous time and commitment. Throughout my doctoral work he encouraged me to develop independent thinking and research skills. It has been a real pleasure working with him on a project that started with an empty room and is now a fully operating laboratory.

I extend many thanks to the Nizkorodov group as a whole for their assistance and support in the lab, their humor in the office, and the never ending supply of coffee.

I'd like to thank members of Finlayson-Pitts group who got my feet wet with our collaboration on self assembled monolayers.

I am grateful for the assistance, and advice I received from John Greaves at the Mass Spec facility. His assistance made it possible for me to analyze complex polymerization mixtures.

Finally, I'd like to thank my family for their constant support. I'm grateful for their encouragement and enthusiasm. I'm especially grateful to Autumn, my dear wife and best friend, who offered me unconditional love and support throughout the course of this degree.

These studies were supported by the National Science Foundation through the Environmental Molecular Science Institute program, grant CHE-0431312 (formerly CHE-0209719), and Atmospheric Chemistry Program, grant ATM-0509248.

CURRICULUM VITAE

B.S. Chemistry, University of California, Irvine, June 2000

Ph.D. Analytical Chemistry, University of California, Irvine, June 2007

Walser, Maggie L.; Park, Jiho; Gomez, Anthony L.; Russell, Ashley R.; Nizkorodov, Sergey A., "*Photochemical Aging of Secondary Organic Aerosol Particles Generated from the Oxidation of d-Limonene*", *Journal of Physical Chemistry A* 2007, 111, 1907-1913

Gomez, Anthony L.; Park, Jiho; Walser, Maggie L.; Lin, Ao; Nizkorodov, Sergey A., "*UV Photodissociation Spectroscopy of Oxidized Undecylenic Acid Films*", *Journal of Physical Chemistry A* 2006, 110, 3584-3592.

Park, Jiho; Gomez, Anthony L.; Walser, Maggie L.; Lin, Ao; Nizkorodov, Sergey A.; "*Ozonolysis and Photolysis of Alkene-Terminated Self-Assembled Monolayers on Quartz Nanoparticles: Implications for Photochemical Aging of Organic Aerosol Particles*", *Physical Chemistry Chemical Physics* 2006, 8, 2506-2512.

Y. Dubowski, J. Vieceli, D.J. Tobias, A. Gomez, A. Lin, S.A. Nizkorodov, T. McIntire, B.J. Finlayson-Pitts, "*The Interaction of Gas-Phase Ozone at 296 K with Unsaturated SAMs: A New Look at an Old System*", *Journal of Physical Chemistry B* 2004, 108 (2004) 10473-10485

ABSTRACT

Analysis of the Chemical and Photochemical Aging of Organic Aerosols

By

Anthony Gomez

Doctor of Philosophy in Chemistry

University of California, Irvine, 2007

Professor Sergey Nizkorodov, Chair

The 2007 Intergovernmental Panel on Climate Change released a report which thoroughly reviewed the various components of radiative forcing on the global climate. Some anthropogenic contributions to radiative forcing such as greenhouse gases are reasonably well understood, whereas the indirect effect of aerosol particles is poorly understood. Knowledge of the climate effects of aged organic aerosol particles is especially lacking. Understanding how organic aerosol particles age is complicated by their varied composition and morphology.

Ozone is one of the key atmospheric oxidants responsible for aging of organic aerosol particles. Application of the well-known Criegee mechanism of ozonolysis to a typical atmospheric alkene predicts a relatively small number of oxidation products; however our work reveals a large number of unanticipated products, including extensive oligomerization. In order to understand how organic aerosols age chemically and photochemically, a more complete mechanism of ozonolysis of atmospherically relevant olefins is needed.

In this thesis, several techniques are used to improve our understanding of organic aerosol aging by ozone and solar radiation. These techniques include cavity ringdown spectroscopy (CRDS), which is used to identify small gas phase molecules generated from chemical and photochemical processing of olefins. GC-MS, CI-MS and ESI-MS are used to analyze larger products after processing. Idometric tests are carried out to quantify peroxide formation in ozonolysis of relevant alkenes. FTIR and UV-Vis spectroscopies are used to measure changes in the spectra of model aerosol particles as a function of oxidation. Stoichiometry of oxidation of alkenes by ozone is also investigated with an uptake apparatus.

This work finds that oxidation of atmospherically relevant alkenes by ozone shifts their photoabsorption into atmospherically relevant region of the solar spectrum, reinforcing the importance of solar radiation on the aging of organic particles. Observation of small molecules released into the gas phase upon solar photolysis, coupled with results from other experiments described herein, indicate that secondary ozonides (SOZ) are likely to be common components of aged organic aerosols. The total peroxide analysis of oxidized alkenes indicates upwards of 60% alkene-to-peroxide conversion efficiency. Ozone:alkene reaction stoichiometry displays surprising temperature and concentration dependence resulting from free radical contributions to the ozonolysis.

Chapter I

Introduction / Background

1.1 Importance of Aerosol Particles

Aerosol particles have a tremendous impact on the chemistry and energy balance of the atmosphere, and affect both human health and local air quality.¹⁻³ Although there have been numerous studies on the impact of aerosol particles on climate, unresolved issues and discrepancies persist.⁴

In recent years, chemical processes occurring at aerosol particle-air interfaces have received strong interest from the atmospheric chemistry community.⁵⁻¹⁶ Indeed, the chemical properties of air-particle interfaces affect the ability of particles to act as efficient cloud condensation nuclei (CCN).¹⁷ The high surface-to-volume ratio of solid aerosol particles both increases the adsorptivity of the surface and significantly amplifies interface-specific chemical processes. Even in aqueous particles with highly dynamic air-water interfaces, certain anions (e.g., Cl^- and NO_3^-) have been shown to favor the interfacial layer, potentially enhancing the efficiency of chemical reactions involving such ions.^{9, 18}

Field observations of aerosol composition show that a large fraction of atmospheric aerosol particles contains significant amounts of organic material^{1, 19-29}. Such organic aerosol particles can undergo significant oxidation during their lifetime in the atmosphere as they are continuously oxidized by reactions with atmospheric oxidants

including ozone (O₃) and hydroxyl radicals (OH).^{30,31} This oxidative processing modifies important physicochemical properties of aerosol particles including their composition, size, toxicity, and ability to act as nuclei for cloud droplet growth.

1.2 Oxidation by Ozone

Ozone is a key oxidant for atmospheric organic molecules containing unsaturated carbon-carbon bonds,³²⁻³⁹ e.g., unsaturated fatty acids frequently found in urban⁴⁰ and marine^{28,41} aerosol particles. Thus, ozonation of atmospherically relevant organic films^{35,42,43} and aerosol particles^{14,15,44,45} has received a lot of scientific attention in recent years.

The accepted mechanism of ozonolysis of olefins^{15,46,47} involves a rate-limiting formation of a primary ozonide (POZ) followed by a unimolecular decomposition of the POZ into a stable carbonyl and an unstable carbonyl oxide (Criegee intermediate). In non-participating solvents, the carbonyl oxide normally reacts with the geminate carbonyl to form a secondary ozonide (SOZ). In the gas-phase, collisional stabilization of carbonyl oxides is less efficient, and their fates are dominated by various decomposition and isomerization processes.⁴⁸⁻⁵³ In the presence of liquid or gaseous water, acids or alcohols, the stabilized carbonyl oxide reacts with them to form hydroxylhydroperoxides and related compounds.⁵⁴⁻⁵⁸ From the aerosol particle photochemistry point of view, the reactions involved in ozonolysis of olefins are very interesting because they generate many products (aldehydes, peroxides, etc.) with significant photodissociation cross sections in the tropospheric actinic window ($\lambda > 295$ nm).

1.3 Photochemistry

Organic aerosols are continuously modified in the atmosphere by chemical reactions with O_3 , O_2 , NO_3 , and OH ^{30, 31, 59} resulting in a rather complex organic surface composition. Such oxidation of the organic surface is expected to shift its absorption cross section to the red as the aerosol ages. The increase in the absorption cross section is primarily due to aldehydes, ketones and peroxides formed during oxidation. Indeed, the gas phase absorption cross section of formaldehyde (~ 300 nm maxima) and peroxides extend to longer wavelengths compared to those of saturated hydrocarbons and carboxylic acids (~ 220 nm).

The key question is whether this red shift is significant enough to measurably accelerate aerosol aging via photolysis processes within the particles, or even turn organic aerosol particles into diffuse sources of small organic molecules and free radicals. There are strong reasons to believe that oxidatively aged organic aerosols should also be highly photochemically active. Surface photolysis is already known to play a significant role in atmospheric photochemistry, e.g., photolysis of HNO_3 into HONO on surfaces^{60, 61} or photochemical production of aldehydes⁶²⁻⁶⁴ and HONO⁶⁵ in snowpack.

1.5 Thesis Objectives

The main objective of this work is to study of the mechanism of oxidative aging of organic aerosol particles containing unsaturated carbon-carbon bonds by ozone. The second objective is to investigate the mechanism of photochemical processing of aged organic aerosol particles. Thin films (Chapter 2), self assembled monolayers (Chapter 3),

and aqueous solutions (Chapter 4) are investigated as idealized models of organic aerosol particles. The final objective of this work is to develop novel and unique tools for studying aerosol particle photochemistry (Appendix A).

Chapter II

Ozonolysis and UV Photodissociation Spectroscopy of Oxidized Undecylenic Acid Films

Reproduced with permission from *Gomez, A.L.; Park, J.; Walser, M. L.; Lin, A.; Nizkorodov, S. A., J. Phys. Chem. A 2006, 110, 3584-3592*. Copyright 2006 American
Chemical Society

2.1 Abstract

Oxidation of thin multilayered films of undecylenic (10-undecenoic) acid by gaseous ozone was investigated using a combination of spectroscopic and mass spectrometric techniques. The UV absorption spectrum of the oxidized undecylenic acid film was significantly red-shifted compared to that of the initial film. Photolysis of the oxidized film in the tropospheric actinic region ($\lambda > 295$ nm) readily produced formaldehyde and formic acid as gas-phase products. Photodissociation action spectra of the oxidized film suggest that organic peroxides are responsible for the observed photochemical activity. The presence of peroxides was confirmed by mass-spectrometric analysis of the oxidized sample and an iodometric test. Significant polymerization resulting from secondary reactions of Criegee radicals during ozonolysis of the film was observed. The data strongly imply the importance of photochemistry in aging of atmospheric organic aerosol particles.

2.2 Introduction

This work focuses on mechanisms of chemical and photochemical processes occurring at the air-particle interface in organic aerosols. Numerous field observations of aerosol composition have shown that a substantial fraction of tropospheric aerosols can be classified as organic.^{22-29, 66, 67} Even aerosol particles that have traditionally been regarded as inorganic (sea-salt, dust, soot) have been shown to carry an organic coating.^{28, 41, 68-72}

To help better understand the importance of photochemical processes occurring at particle-air interfaces in organic aerosols, we studied the photochemistry of thin multilayered films of pure undecylenic acid (10-undecenoic acid) oxidized by gaseous ozone. Although ω -oxocarboxylic (alkene-terminated) acids, such as undecylenic acid, are rarely found in ambient aerosol particles,⁷³ larger unsaturated fatty acids and their oxidation products are quite common in organic particulate matter.^{28, 40, 73, 74} Oxidation of unsaturated fatty acids by ozone has been studied by many researchers.^{15, 33, 35, 37, 44, 45, 75-77} Related reactions of ozone with ordered Langmuir films of phospholipids on water^{38, 39, 78} or with unsaturated SAM (Self-Assembled Monolayers)^{32, 34, 79-82} have also been examined. As a result, both the gas-phase and surface products of ozonolysis of unsaturated fatty acids are relatively well understood. This provides a convenient foundation for interpretation of our new results on the photolysis of the oxidized acids.

2.3 Experimental

The approach relies on Infrared Cavity Ring-Down Spectroscopy (IR CRDS) for real-time, sensitive detection of gas-phase molecules in the immediate vicinity of a sample exposed to gas-phase chemicals and/or tunable UV radiation (Fig. 2.1 and Appendix A). To prepare the sample, a film of undecylenic acid was spread on the inner wall of a 14-mm ID quartz tube. The tube was pre-coated with an organic self-assembled monolayer by treating it with alkylchlorosilanes to improve the uniformity of the undecylenic acid film.^{80, 83-85} After applying undecylenic acid, the inside of the tube was thoroughly wiped with a Kimwipe until it appeared fully transparent (the number of molecular layers in the film was not quantified but the film was optically thin in the examined UV spectral range). The coated tube was placed in a vacuum-tight CRDS cavity. The sample was first oxidized by passing a flow from a commercial ozonizer containing 10^{14} - 10^{15} molec cm^{-3} of ozone in oxygen through the tube. The ozone density was measured with two homemade absorption cells operating on the 253.65 nm mercury line (napierian absorption cross section of O_3 at 253.65 nm is 1.136×10^{-17} cm^2).⁸⁶ After the oxidation was complete, the flow of ozone was replaced by a flow of UHP-grade helium, and the oxidized film was photolyzed. All gas flows into the cavity were measured by calibrated mass-flow controllers. The pressure was measured by a capacitance manometer; most experiments described here were conducted at 1-20 torr (1 torr = 133.32 Pa).

A pair of CRDS cavity mirrors with a stated reflectivity of 99.98% at 3.3 μm was spaced by about 60 cm and protected by a constant purging flow of dry helium. The

cavity was pumped by an infrared optical parametric oscillator laser characterized by 0.1 cm⁻¹ spectral resolution, 8 ns pulse duration, 15 mJ/pulse energy, and 20 Hz repetition rate. CRDS experiments described here used a small spectral window at 3.3 μm that contains easily distinguishable lines of formic acid and formaldehyde (expected gas-phase products of ozonolysis of undecylenic acid). The cavity ring-down signal was detected with an InSb detector (>5 MHz bandwidth), averaged for 20 laser pulses, and digitized with an oscilloscope. A Labview-based program was used to process and store the resulting traces. An optoacoustic spectrum (of H₂O, CH₂O, or HCOOH) was recorded in parallel with the CRDS spectrum for wavelength calibration and line identification purposes.

Intrinsic ring-down time is around $\tau_0 = 4\text{-}7 \mu\text{s}$, which is close to the theoretical limit of 10 μs for this cavity configuration. The effective absorption coefficient, α , is calculated using a well-known relationship⁸⁷

$$\alpha(\text{cm}^{-1}) = \frac{1}{c} \left(\frac{1}{\tau} - \frac{1}{\tau_0} \right)$$

where c is the speed of light, τ is the ring-down time for a cavity containing an absorber, and τ_0 is the intrinsic ring-down time. As the laser line width (0.1 cm⁻¹) is larger than the pressure and Doppler broadened line widths of individual H₂CO and HCOOH lines (~0.01 cm⁻¹), the method does not actually provide absolute absorbance via $A = \alpha \times L$.⁸⁷ Furthermore, the cavity ring-down traces are not singly exponential under such conditions, and the presence of mirror-purging flows makes the actual absorption

pathlength (L) somewhat uncertain. Nevertheless, absolute concentrations can still be obtained from the data using an explicit calibration and/or fitting algorithms accounting for the poly-exponential decay. Figure 2.2 shows a representative calibration plot for CH₄. The minimal (RMS-equivalent) absorption coefficient sensitivity achieved with 1 s integration time (20 laser shots) was $3 \times 10^{-8} \text{ cm}^{-1}$. This is similar to the detection sensitivity achieved by other pulsed CRDS instruments.⁸⁷ For CH₂O lines near 3.3 μm with integrated line strengths of about $5 \times 10^{-20} \text{ cm}^2 \text{ molec}^{-1} \text{ cm}^{-1}$, this translates into the minimal detectable concentration of $6 \times 10^{10} \text{ molec cm}^{-3}$.

A UV lamp/monochromator illumination system was used for photolysis experiments. The illuminator covers the usual Xe-lamp range (200–800 nm) with a variable 1–20 nm resolution. The output of the monochromator illuminated a small section ($\sim 1 \text{ cm}^2$) of the quartz cell. The UV-radiation power was on the order of 10 mW at 300 nm. The power was considerably lower at lower irradiation wavelengths. Depending on the experiment, photobleaching was accounted for in one of two ways: i) a different section of the tube was irradiated every two experiments; ii) photolysis product yields of a specific molecule were monitored throughout the experiment at a reference UV exposure wavelength. In broadband photolysis experiments, the monochromator was replaced by a suitable long-pass or band-pass optical filter. All photolysis experiments were done under UHP He flow conditions.

The experiments were performed in several modes. In CRDS scanning mode, the UV frequency was fixed while the IR laser was scanned to probe chemical identities of the gas-phase photolysis products. In the action spectrum mode, the UV radiation source

was tuned while IR frequency was fixed to examine the UV wavelength dependence for a particular photolysis product. The apparatus can also be used in a “reaction mode”, wherein the photolysis radiation source was replaced by chemical exposure. In kinetics mode, the CRDS signal was tracked as a function of time with all other conditions fixed.

Because the IR CRDS method does not provide information on the composition of the organic film, the film was examined off-line (before and after each experiment) using electrospray ionization mass spectrometry in either positive or negative ion mode. Additionally, the reacted film was characterized by UV/Vis spectroscopy.

2.4 Results

2.4a *Effect of ozonolysis on UV/Vis absorption spectrum of undecylenic acid*

The primary goal of this work is to understand the effect of simulated atmospheric oxidation of undecylenic acid on its photochemistry. The initial organic film had no photochemical activity in the tropospheric actinic window ($\lambda > 295$ nm) because unsaturated fatty acids do not strongly absorb above 250 nm. Figure 2.3 compares the UV absorption spectrum of an undecylenic acid film before and after ozone treatment. The ozonolysis clearly produced a strong red-shift in the absorption spectrum presumably caused by the presence of aldehyde and peroxy groups in the oxidized sample. Ozonolysis of undecylenic acid in a non-participating solvent (CH_2Cl_2) had a similar effect on its absorption spectrum (Fig. 2.3). Note that the characteristic 290 nm band of

the –CHO group was not visible suggesting that the absorption of the oxidized undecylenic acid was dominated by peroxy groups (see section 2.4e).

2.4b Gas-phase products of ozonolysis of undecylenic acid

In agreement with previous studies of ozonolysis of liquid terminal alkenes,^{32, 34, 35, 80} the IR CRDS spectra taken during ozonolysis of pure undecylenic acid films detect formaldehyde as the major volatile product. Figure 2.4 shows a typical CRDS spectrum obtained during ozonolysis of the film in the 2800-3100 cm⁻¹ window. The lines appeared on a slowly changing background determined by the CRDS mirror reflectivity (the largest reflectivity and the longest ring-down time are achieved at 3000 cm⁻¹). The majority of the lines can be assigned to ro-vibrational transitions of formaldehyde by an explicit comparison with its reference spectrum. Formic acid was also detected but in smaller amounts; the measured [HCOOH]/[H₂CO] branching ratio was 0.25±0.15. These observations were in good agreement with those of Ref. ^{32, 35}, who detected little HCOOH in the ozonolysis of long-chain terminal alkenes.

A search for spectral signatures of the simplest Criegee intermediate, H₂C·OO·, and the simplest dioxirane, H₂CO₂, was also attempted. Band-contour simulations predicted that CH-stretching bands of H₂C·OO· and H₂CO₂ should be easily distinguishable from those of H₂CO at the 0.1 cm⁻¹ spectral resolution. Furthermore, fairly accurate CH-stretching frequencies were available for both species from theoretical calculations.⁸⁸⁻⁹¹ In spite of an extensive search, no CH-stretching bands corresponding to H₂C·OO· and H₂CO₂ were found. This suggests that H₂C·OO· rapidly isomerizes into

HCOOH, reacts to form secondary ozonides and hydroxyhydroperoxides, or decomposes before it can escape from the film. This conclusion was supported by the analysis of the reaction products remaining in the condensed-phase (see below). Even if $\text{H}_2\text{C}\cdot\text{OO}\cdot$ does escape to the gas-phase, it may be too short-lived to be detected by IR CRDS under the present conditions.^{52, 53}

2.4c *Gas-phase products of photolysis of oxidized undecylenic acid*

Unlike unoxidized undecylenic acid, which showed no measurable photodissociation activity, the oxidized film released formic acid as the primary, and H_2CO as the secondary volatile product upon UV photolysis. Both products were sensitively and unambiguously detected by IR CRDS via their highly structured IR absorptions. Figure 2.5 shows small sections of the CRDS spectra in the vicinity of 2920 cm^{-1} . Explicit comparison of the CRDS spectra with reference spectra clearly shows that formic acid was the dominant product of photolysis of the oxidized film. More rigorous determination of the branching ratio using absolute absorption cross sections from the Northwest Infrared library⁹² leads to the following result for $\lambda > 290\text{ nm}$ photolysis: $[\text{HCOOH}]/[\text{H}_2\text{CO}] = 2.5 \pm 1.0$. Although this ratio depends on the extent of oxidation of the film and the extent of photolysis, HCOOH remained the dominant observed product under all conditions.

Note that the CRDS instrument was limited by its mirrors to the IR range of 2850 to 3150 cm^{-1} , and was blind to molecules with no CH-stretching vibrations. Possible gas-phase photolysis products are not necessarily limited to H_2CO and HCOOH. We have

attempted to detect other expected gas-phase products of ozonolysis (e.g., H₂O, CO and CO₂) with an electron impact mass-spectrometer but ran into difficulties with the high background signal for these molecules. However, the mass-spectroscopic analysis of the film before and after photolysis indicates very clear signatures of loss of CO (-28 amu), H₂O (-18 amu), HCOOH (-46 amu), and formaldehyde (-30 amu) induced by UV photolysis.

Additional information about the photochemistry of freshly oxidized undecylenic acid can be obtained from an action photodissociation spectrum measured by monitoring the appearance of a specific photolysis product as a function of the UV photolysis wavelength. Figure 2.6 shows an action spectrum for the HCOOH formation channel obtained in pure helium flow. The data in Fig. 2.6 are obtained by fixing the IR CRDS laser on a chosen absorption line of HCOOH, and stepping the monochromator in the UV illuminator in the range of 260 nm – 350 nm in 10 nm increments. The CRDS signal was converted into an absorption coefficient and normalized with respect to the UV radiation power transmitted through the sample cell. The photolysis-induced signal was easily detectable even at 350 nm, i.e., quite far into the tropospheric actinic window. The shape of the photodissociation spectrum was almost identical to the UV direct absorption spectrum of the oxidized undecylenic acid (Fig. 2.3) suggesting that HCOOH must be a product of photolysis of one of the primary absorbers in the film.

2.4d Condensed-phase products of ozonolysis/photolysis of undecylenic acid

The oxidized undecylenic acid was analyzed by electrospray ionization mass spectrometry in both positive and negative ion modes. In both cases, methanol was used as the solvent. The negative ion mode was particularly useful because nearly every product of ozonolysis of undecylenic acid contains at least one -COOH group. Therefore, the major peaks correspond to -COO- anions appearing in the (M-1) channels with minimal fragmentation and polymerization. Figure 2.7 shows a sample negative ion mass spectrum of pure undecylenic acid (MW = 184 amu). The spectrum was clearly dominated by a single peak at 183 amu. The second largest peak, which appears only if an over-concentrated solution of undecylenic acid was injected, corresponds to a complex between an undecylenic acid monomer and its anion (MW = 367 amu). Larger complexes do not appear in the mass spectrum under the present experimental conditions. The positive ion mode spectra were somewhat more complicated but still assignable. The primary peaks correspond to complexes of a parent molecule with Na^+ ion (M+23) and, in the case of carboxylic acids, complexes of a Na-salt of a parent acid with another Na^+ ion (M+45).

The oxidized films were dissolved in the same volume of methanol as the volume used for the undecylenic acid reference spectrum (Fig. 2.7). The resulting spectrum contained many peaks corresponding to previously identified products. For example, sebacic acid, $\text{HOOC-(CH}_2)_8\text{-COOH}$, and sebaldehydic acid, $\text{HOOC-(CH}_2)_8\text{-COH}$, are reproducibly observed in comparable amounts in the mass-spectrum. Both acids are expected products of decomposition of the primary ozonide of undecylenic acid (Fig. 2.9). However, nonanoic acid was not an observed product as found in a previous study of

ozonolysis of undecylenic acid.³⁵ No significant signal corresponding to the SOZ of undecylenic acid was observed; it is likely to be destroyed by the high temperature of the ionization source. Table 1 summarizes the observed peak positions and proposed assignments for the mass-spectra of products of ozonolysis of undecylenic acid films. Ozone + multilayered film of undecylenic acid, and ozone + undecylenic acid dissolved in a non-participating solvent resulted in a similar set of observed products. Table 2.2 lists the full set of observed peaks.

In addition to the known low molecular weight products of ozonolysis of undecylenic acid, many previously unidentified oligomeric products were also observed. For example, the mass spectrum shown in Fig. 2.7 had several well-defined "clusters" of peaks between 300 and 1000 amu. This mass spectrum corresponded to a strongly oxidized sample with almost no remaining undecylenic acid, but we observed similar clusters of peaks in mass-spectra with a lower degree of oxidation. The most prominent peaks within each cluster were separated by the mass of an oxygen atom (16 amu). The clusters themselves were separated from each other by the mass of the larger carbonyl oxide formed in the decomposition of the primary ozonide of undecylenic acid (202 amu). This pattern of peaks can be interpreted as a result of various polymerization reactions taking place during the ozonolysis. The upper limit for the mass spectrum is 1000 amu, and the largest observed cluster of peaks corresponds to a "pentamer". However, based on the peak intensity distribution in the mass spectrum, even larger oligomers are likely to be present in the oxidized film. The chemical identity of some of these oligomers will be discussed below.

The presence of oligomers in an analyte can sometimes be confused with an complex formation in the electrospray ion source. The latter possibility can be ruled out based on: i) the lack of oligomers (other than the dimer) in the reference spectrum of undecylenic acid obtained under the same conditions; ii) reproducible presence of oligomer peaks in the mass spectrum irrespective of the concentration of the oxidized sample in the solvent; iii) appearance of the same oligomers in both negative ion (M-1) and positive ion (M+23, M+45) mass-spectra.

The products of the UV photolysis of the oxidized film were also examined. The photolysis was carried out with a 295 nm longpass filter in dry air at atmospheric pressure. Figure 2.7 displays a sample mass spectrum. The UV exposure clearly had several reproducible effects on the spectrum. The peaks corresponding to molecules containing aldehyde and peroxy groups were reduced in intensity. For example, the intensity of the sebaldehydic acid peak was considerably reduced relative to that of sebacic acid. The oligomeric clusters of peaks survive the UV exposure but they were clearly shifted to somewhat lower masses. The observed UV-induced fragmentation corresponds to the loss of CO (-28 amu), H₂O (-18 amu), HCOOH (-46 amu), and formaldehyde (-30 amu). Only a small fraction of peaks can be assigned to specific molecules.

2.4e Iodometric test for the formation of peroxides

Iodometric tests⁹³ were carried out in an attempt to quantify the total number of peroxy bonds formed in the oxidized undecylenic acid. Undecylenic acid was dissolved in a non-participating solvent (hexadecane) to make a 1.0 mM solution, and ozone (1×10^{16} #/cm³) was bubbled through the solution at room temperature for various lengths of time covering 0 to 100% alkene oxidation. The resulting solution was thoroughly degassed with dry helium to remove any dissolved oxygen and acidified with 20 μ l of glacial acetic acid. The product mixture was then reacted with KI in the dark for 30 minutes and was analyzed with UV/Vis spectrometry. As every peroxy bond produces one I₃⁻ by oxidation of 2I⁻ to I₂ followed by complexation of I₂ with I⁻ in the presence of acids, measured absorbance of I₃⁻ (using $\epsilon_{470 \text{ nm}} = 817 \text{ L mol}^{-1} \text{ cm}^{-1}$)⁹³ were directly related to the concentration of peroxy bonds. A calibration experiment using H₂O₂ reproduced the H₂O₂ concentration with better than 10% accuracy, with one molar equivalent of peroxy bonds producing one molar equivalent of I₃⁻.

Initially, the amount of peroxides formed were proportional to the amount of ozone reacted., and eventually plateau at approximately 60% alkene to peroxide conversion (Fig. 2.8). This was consistent with other observations also yielding high conversion of olefins to peroxides by ozone.^{15, 93} Peroxide analysis of ozonized alkane solvent indicated no peroxide formation. This was qualitatively consistent with the mass-spectrometric results, which showed that the majority of the oxidation products have hydroperoxy functionalities. Additional experiments would be needed to determine how R-COOH, R-OH and H₂O affect peroxide yields.⁹⁴

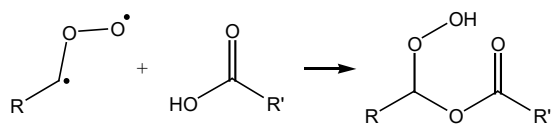
2.5 Discussion

2.5a Mechanism of ozonolysis of undecylenic acid

The major gas-phase and liquid-phase products of ozonolysis of undecylenic acid were generally consistent with the Criegee mechanism of ozonolysis of alkenes.⁴⁶ Figure 2.9 shows the most important initial reactions taking place in this system. The initial ozone attack on the double bond of undecylenic acid (I) results in a highly-unstable POZ (not shown). POZ rapidly decomposes into two sets of products: sebaldehydic acid (II) and a small carbonyl oxide (III); formaldehyde (IV) and a large carbonyl oxide (V). Formic (VI) and sebacic (VIII) acids are produced by isomerization of the corresponding carbonyl oxides. SOZ (VII) is produced by recombination of fragments of POZ decomposition; production of SOZ is known to be efficient in liquids and is also likely to occur in thin films as well. Apart from SOZ, all of the stable products shown in Fig. 2.9 were directly observed by mass-spectrometry and/or cavity ring-down spectroscopy in this work. In a similar experiment done with oleic acid, $2M_{\text{SOZ}+1}$ was observed.

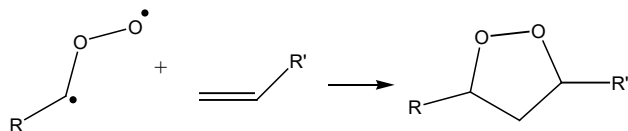
The excess of gas-phase formaldehyde over formic acid was consistent with previous work on ozonolysis of multilayered films and SAM of terminal alkenes.^{32, 34, 35,}
⁸⁰ It is likely that the initial splitting of POZ occurs with nearly equal probability for the formaldehyde and sebaldehydic acid channels. Indeed, (II) and (VIII) were generated in comparable amounts in the oxidized film. However, not all of the carbonyl oxide (III) will isomerize into formic acid; the ratio measured here, $\text{HCOOH}/\text{H}_2\text{CO} = 0.25 \pm 0.15$, was considerably below unity.

Oligomeric compounds were recently observed in chamber studies of the oxidation of organic aerosol particles.⁹⁵⁻⁹⁹ The chemistry responsible for polymerization was attributed to acid-catalyzed aldol and gem-diol condensation. In the present case, the polymerization mechanism was entirely different. Indeed, many oligomeric compounds observed in the mass spectrum could be assigned as products of reactions of carbonyl oxides with the carboxylic groups in undecylenic acid and in the ozonolysis products.



The mass spectrum in Fig. 2.7 contained sizable peaks corresponding to "dimeric" structures (X, XI, XII) which resulted from condensation of carbonyl oxide (V) with undecylenic, sebaldehydic, and sebacic acids, respectively (Fig. 2.9). In addition, there were peaks with larger masses corresponding to further additions of carbonyl oxide (V) to (X, XI, XII) and to larger oligomers. The largest detected oligomers correspond to "pentamers". Even larger oligomers probably exist in the oxidized mixture but they fall outside the mass range of the mass-spectrometer. Surprisingly, there was no evidence of the smaller carbonyl oxide (III) addition to undecylenic acid and/or other molecules. Therefore, we presume that the dominant reaction pathways for (III) are decomposition to CO, CO₂, etc. and isomerization to formic acid.

It was suggested⁴⁴ that carbonyl oxides can also add to double bonds in unsaturated fatty acids to form peroxidic 5-member rings:



The mass-spectrometer would not be able to differentiate between the products of addition of a carbonyl oxide to the carboxylic or alkene groups of undecylenic acid because such products would have identical molecular weights. However, if the chemistry was dominated by the double bond addition, the extensive polymerization would not take place as the reaction would terminate at the "dimer" level. On the contrary, addition to the carboxylic end of undecylenic acid can be propagated further as it leaves a double bond in the product ready for the next cycle of ozonolysis + polymerization. The observed distribution of oligomers in the mass spectrum shown in Fig. 2.9 suggests that reaction of carbonyl oxide with the carboxylic groups was the dominant polymerization route.

The small HCOOH/HCHO ratio and absence of condensation reaction products for carbonyl oxide (III) imply that its decomposition into HCO and OH radicals may be quite efficient (HCO then quickly reacts with oxygen to produce HO₂ and CO). A fraction of carbonyl oxide (V) can also decompose to produce OH and peroxy radical (IX). Such decomposition reactions are known to play an important role in gas-phase alkene ozonolysis;^{48-50, 100, 101} results of this work suggest that such decomposition may also take place in the liquid phase or possibly on the surface of the film. Once OH is generated, it can either add to the double bond in undecylenic acid or abstract a hydrogen atom from one of the neighboring CH₂ groups. Figure 2.10 shows an example of a reaction sequence initiated by OH addition to undecylenic acid. This sequence ultimately

generates peroxy groups via $\text{RO}_2 + \text{HO}_2$ reactions, but it is also capable of installing multiple oxygen atoms in the molecules via $\text{RO}_2 + \text{R}'\text{O}_2$ reactions, followed by facile isomerization of the resulting alkyloxy radicals, followed by addition of O_2 . Note that an abstraction of a hydrogen atom by OH would initiate a similar chain of events.

The insertion of multiple oxygen atoms into the various reaction products were clearly evident from the mass spectrum (Fig. 2.7). Indeed, there were several families of peaks in the mass spectrum separated from each other by either 16 (or 32) atomic mass units. Table 1 was constructed in an attempt to tie the major peaks to common precursor molecules through a sequence of $+n\text{O}_2$ additions. Such a representation accounts for nearly half of the products formed during ozonolysis. The peaks that could not be assigned to specific structures also appear in families separated by 16 and/or 32 mass units. One could generate a similar table assuming single O (16 amu) additions (Fig. 2.10). However, the aldehyde-terminated and carboxylic acid-terminated products differ by one O-atom leading to overlapping series. Mass-spectrometry would not be able to distinguish the series resulting from single-O and double-O additions in this particular case.

As the oligomer size grows from monomer to pentamer, the propensity for O_2 insertions increases. In fact, the intensity of $\text{M}+\text{O}_2$ peaks relative to that of M peaks grows approximately proportionally to the size of M (M stands for any molecule). For example, the $[\text{M}+\text{O}_2]/[\text{M}]$ ratio is 0.3, 1.2, 2.4, 3.4 and 4.0 for $\text{M} = \text{sebaldehydic acid} + 0, 1, 2, 3, \text{ and } 4$ units of carbonyl oxide (V), respectively. This observation is fully consistent with the increase in available reactive sites for the OH attacks.

2.5b Mechanism of photolysis

HCOOH and HCHO were easily observed in the photolysis of oxidized undecylenic acid (Fig. 2.5). This was a curious observation as neither sebacic acid (VIII) nor sebaldehydic acid (II) can directly photolyze into HCOOH and HCHO under the mild UV excitation conditions of the present work. Norrish type II splitting of sebaldehydic acid would produce the enol corresponding to acetaldehyde, $\text{CH}_2=\text{CH-OH}$, and α -cleavage of sebaldehydic acid would yield HCO or CO. These processes do occur but neither of them can account for formic acid being the primary observed photolysis product.

Due to the complexity of the oxidized film, it was not trivial to assign a specific precursor responsible for the photoinduced release of these two molecules. However, close similarity between the action spectrum and absorption spectrum of oxidized undecylenic acid (Fig. 2.6), the characteristic shape of the action spectrum, and the large amount of peroxy bonds measured by the iodometric test suggest that photochemistry must be initiated by splitting one of the $-\text{O}-\text{O}-$ bonds. One possibility would be photolysis of hydroxylhydroperoxides such as (X, XI, XII) releasing OH, with secondary reactions of OH with oligomeric ozonolysis reaction products producing HCOOH and HCHO.

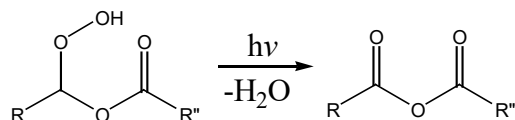
Another possible precursor of both HCHO and HCOOH is terminal SOZ such as (VII). Previous research on ozonides suggest that UV photolysis must break the weakest $-\text{O}-\text{O}-$ bond, with subsequent isomerization processes resulting in release of an aldehyde

or carboxylic acid in the gas phase.^{46, 102, 103} Such a mechanism could explain the preferred formation of formic acid relative to formaldehyde in the photolysis: the pathway leading to HCOOH is less sterically hindered (Fig. 2.11). One potential problem with this mechanism was that it requires formation of SOZ in high yields, and also relatively high stability of the resulting SOZ. The high stability of SOZs is not unprecedented; SOZ obtained by ozonolysis of 2,3-dimethyl-butene remains stable for days in solutions¹⁰⁴ and for hours in the gas-phase¹⁰⁵ at room temperature. We do not observe large peaks corresponding to (VII) and larger secondary ozonides in the mass spectrum. However, it is possible that SOZ of undecylenic acid was not as stable as heavily substituted SOZ of 2,3-dimethyl-butene, and it decomposes into an aldehyde-acid pair under high-temperature conditions of the electrospray ion source. We do observe SOZs corresponding to ozonolysis of oleic acid, as do other researchers.¹⁵ This reflects higher stability of the substituted SOZ relative to the terminal ones.

2.5c *Photolysis products remaining in the film*

The mass spectrum of oxidized undecylenic acid film changed considerably after photolysis (Fig. 2.7). The most prominent change was the increase in relative intensity of the sebacic acid peak because this was more or less the only product molecule that was resilient to photolysis under these conditions ($\lambda > 290$ nm). On the contrary, all the peaks assigned to photochemically unstable aldehydes (e.g., II) and peroxides (X, XI, XII, etc.) are reduced in intensity.

The second most apparent change was the appearance of many new mass peaks in the mass spectrum (Fig. 2.7). The mass spectrum still maintained the general periodic appearance of clusters of peaks, although the clusters were shifted toward smaller masses compared to the mass spectrum obtained before photolysis. In addition to peaks corresponding to loss of HCOOH and HCHO, there were peaks corresponding to loss of CO resulting from photolysis of aldehydes, and loss of H₂O resulting from photolysis of hydroxylhydroperoxides:



There is evidence for multiple losses of H₂O from the same precursor molecules corresponding to the photolysis of products containing multiple hydroperoxy moieties.

2.6 Atmospheric Implications

Results of this work strongly suggest that UV photolysis in aerosol particle phase may play a significant role in atmospheric processing of primary (POA) and secondary (SOA) organic aerosol particles. Indeed, a large fraction of POA in urban areas comes from cooking emissions,^{40, 106} which contain unsaturated fatty acids, cholesterol, and other unsaturated organics. Reactions of these molecules with ozone and OH will make them photochemically active and open new pathways for aerosol particle photochemistry. Aerosol particle processing by solar radiation is also likely to be important for SOA generated by oxidation of terpenes. For example, a strong effect of UV-radiation on the

yield of SOA in terpene ozonolysis was reported in Ref. ^{107, 108} The SOA yield is presumably reduced by the UV-radiation because of the photolytic splitting of primary oxidation products into smaller, more volatile species. Based on the results of this work, photolysis of organic peroxides is the most likely reason for the observed effects of UV-radiation on the SOA yields.

A rough estimate of the relative importance of photolysis in aging of organic aerosol particles can be made assuming typical urban concentrations, $[\text{OH}] = 10^6 \text{ cm}^{-3}$, $[\text{O}_3] = 10^{12} \text{ cm}^{-3}$, and using measured surface reaction probabilities for OH ($\gamma > 0.1$ on solid organic surfaces)⁵⁹ and O₃ ($\gamma > 10^{-5}$ on frozen surfaces of fatty acids).³³ Taking oleic acid as a representative component of an organic aerosol particle, one can estimate the lifetime of double bonds with respect to the attack by O₃ as $<10^3$ s, and the lifetime of –CH₂– groups with respect to OH-oxidation as $<10^5$ s. The observed lifetime of oleic acid in multiphase aerosol particles is actually longer because the molecules are buried inside the particle.⁴³ The carbonyl groups and peroxy groups appearing in the oxidation will have a photolysis lifetime around 3×10^4 s and 10^5 s, respectively (calculated for zero solar zenith angle, "best estimate" surface albedo,¹ and absorption cross sections for acetaldehyde and hydrogen peroxide).¹⁰⁹ Furthermore, the relative rate of photolysis will increase in the upper troposphere. For example, the lifetime of acetone, the most common atmospheric ketone, is dominated by photolysis, not by reaction with OH, in the upper troposphere.¹ Therefore, photolysis and OH-oxidation may have comparable contributions to the rates of chemical transformations occurring in organic aerosol particles.

Although the results of this work are highly suggestive, they cannot be immediately applied to the actual atmosphere without resolving several limitations of the present approach. Dry oxidation conditions, unrealistically large ozone concentration, photolysis under low pressure in an oxygen and NO_x free environment, and use of a pure multilayered film instead of a multi-component organic aerosol may distort the potential importance of photochemical processes discussed here in actual atmospheric aerosol particles.

2.7 Conclusions

This work represents the first experimental inquiry into the role of solar radiation in atmospheric processing of organic aerosols. Although the molecule selected for this study (undecylenic acid) is not a common constituent of airborne particulate matter,⁷³ the general conclusions of this work are likely to hold for all organic aerosol particles containing significant amounts of unsaturated organics:

1. Oxidation of unsaturated organic molecules in aerosol particles is expected to make them absorb radiation in the tropospheric actinic window ($\lambda > 295$ nm). This prediction is explicitly verified in this work for the case of ozonolysis of terminal alkenes.
2. Photochemistry occurring in the oxidized aerosol particles is expected to contribute significantly to the atmospheric processing of organic aerosols.

Furthermore, such photochemical processes may generate products that evaporate from the particle into the gas-phase. For the present case of ozonolysis of terminal alkenes, the observed gas-phase photolysis products are formaldehyde and formic acid.

3. Prolonged solar photolysis is likely to significantly affect the chemical composition of organic aerosol particles. For example, we observe a clear effect of UV post-treatment on the degree of polymerization and product distribution in the oxidized undecylenic acid. The photolysis acts to reduce the oxidative state of the aerosol components, thus opposing the oxidative aging of aerosols by free radicals.

In addition to the general conclusions, this work provides new information on the mechanistic details of ozonolysis of undecylenic acid. The most interesting observations include a large degree of oligomerization in the ozonolysis products caused by sequential additions of carboxyl oxides to -COOH groups, and a very large concentration of peroxy moieties in the oxidized products also mediated by carbonyl oxide reactions. Even for such a simple molecule, only a fraction of the final ozonolysis products could be assigned to specific chemical structures.

2.8 Tables and Figures

Table 2.1: List of assigned peaks in the negative-ion electrospray mass spectrum of oxidized undecylenic acid. Approximately 50% of the primary-isotope peaks with intensities above 10% of the maximum were assignable. All peaks were detected in M-1 channel corresponding to de-protonation of $-\text{COOH}$ groups. Roman numbers for organic molecules are defined in Fig.

	M-1	M-1 +O ₂	M-1 +2O ₂	M-1 +3O ₂	M-1 +4O ₂
Undecylenic Acid (I)	183.2	215.2	247.2	279.2	311.4
(I + V \equiv X)	385.3	417.3	449.3	481.3	-
(I + 2V)	587.4	619.4	651.4	683.4	-
(I + 3V)	789.5	821.5	853.5	885.5	-
(I + 4V)	991.6	-	-	-	-
Sebaldehydic Acid (II)	185.1	217.1	-	-	-
(II + V \equiv XI)	387.3	419.3	-	-	-
(II + 2V)	589.4	621.4	-	-	-
(II + 3V)	791.5	823.5	-	-	-
(II + 4V)	993.6	-	-	-	-
Sebacic acid (VIII)	201.2	233.2	265.2	297.2	-

(VIII + V \equiv XII)	403.3	435.3	467.3	499.3	531.3
(VIII + 2V)	605.5	637.5	669.5	701.5	733.5
(VIII + 3V)	809.6	841.6	873.6	905.6	937.6

Table 2.2: List of mass-intensities in negative ion ESI mass spectrum of sample obtained by ozonolysis (left) of undecylenic acid film followed by photolysis (>295nm) (right). Only peaks > 10% and 5% of the maximum are listed for ozonolysis and photolysis respectively.

O₃		hν	
Mass	Intensity	Mass	Intensity
185.1	405.5	157.1	39.1
186.1	44.9	185.1	110
201.1	199.8	185.1	85.2
387.2	312.3	201.1	723.5
403.2	324.3	202.1	83.2
404.2	68.1	217.1	43.1
417.3	80	385.2	135.7
419.3	277	387.2	87.8
420.3	61.6	403.2	375.3
433.2	220.8	404.2	98.9
434.3	52.3	417.3	39.7
435.3	52.1	419.3	76.4
455.2	107.3	433.2	115.7

457.3	45.8	449.3	48.6
463.3	80.9	543.4	84.2
465.3	41.4	545.4	60.6
469.2	154.7	559.4	37.4
470.2	43.5	561.4	44.6
471.2	101.4	573.4	55.6
482.3	53.9	587.4	83.8
485.2	64.5	589.4	253.5
496.2	83.8	590.4	88.7
515.2	50.2	591.4	43.8
589.4	102.5	603.4	61.4
605.4	104.7	605.4	154.5
619.4	79.5	606.4	48.3
621.4	259.9	617.4	43.2
622.4	76.9	619.4	72.6
635.4	373.4	621.4	55
636.4	140.2	635.4	99.7
637.4	65.7	651.4	38.1
651.4	211	745.5	39.5
652.4	77.9	773.5	47.4
657.4	44.2	775.5	50.2
665.4	152.6	789.5	48.2
666.4	53	791.5	102.4
667.4	106.9	792.5	45.9
681.4	111.7	805.5	37.6
697.4	71.9	807.5	68.2
711.4	57.1	821.5	73.8

791.5	49.2	837.5	54.5
807.5	92.2	977.6	51.4
808.5	44.7	993.6	48.3
821.5	100.5		
823.5	174.4		
824.5	74.7		
837.5	275		
838.5	118.3		
839.5	106.4		
840.5	40.7		
853.5	232.9		
854.5	107.5		
855.5	59.2		
867.5	211.3		
868.5	105.1		
869.5	126.1		
883.5	132		
899.5	79.4		
913.5	71.9		
1009.6	62		
1023.6	84.9		
1025.6	106.7		
1039.6	158.7		

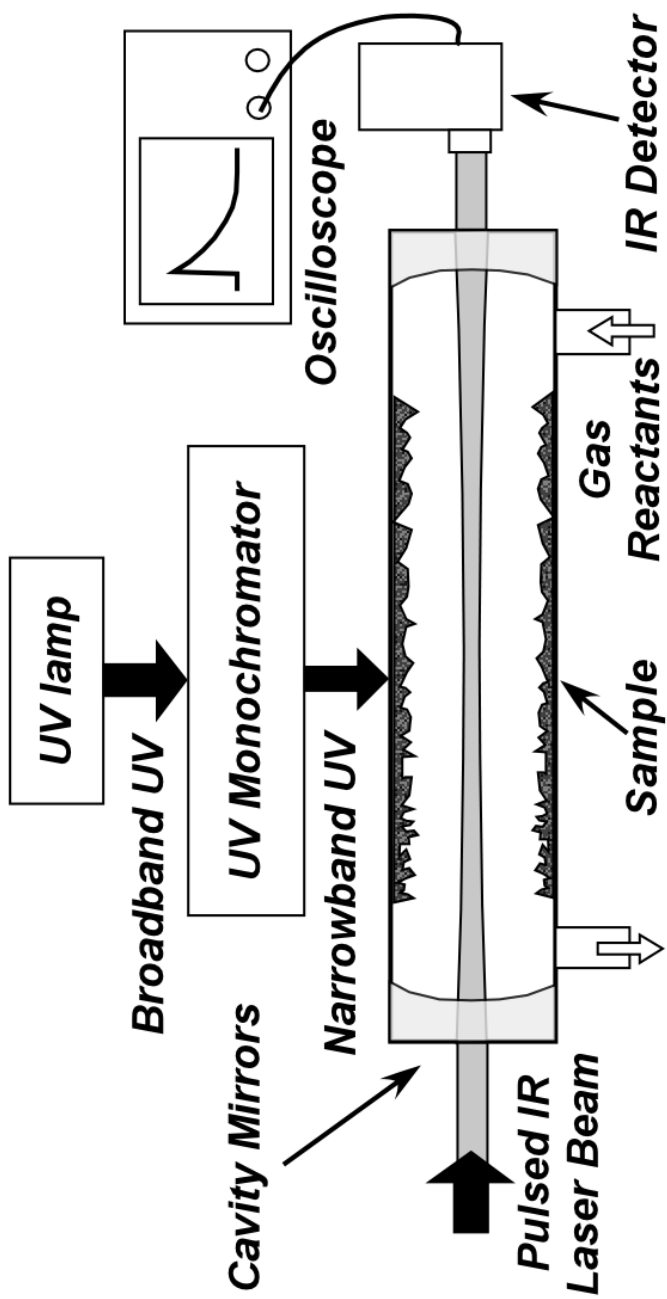


Figure 2.1: Experimental setup. Quartz flow tube coated with a sample of interest was exposed to gas reactants and/or tunable UV radiation. Gas phase products are detected using IR CRDS along the flow tube axis

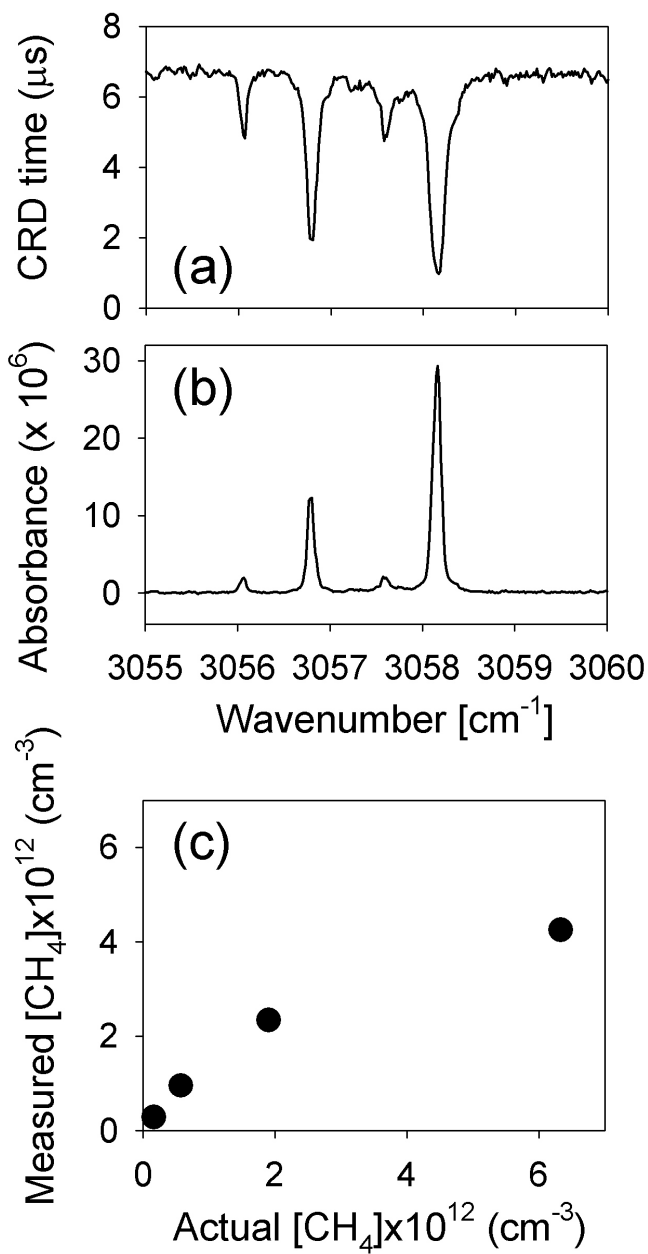


Figure 2.2: Characterization of the CRDS setup. (a) Cavity ring-down time measured with 1.4×10^{13} molec/cm³ of CH₄ in the cell. (b) Absorbance calculated from the ring-down time. (c) Measured and actual density of CH₄. The observed non-linearity was due to the low spectral resolution of the pump laser.

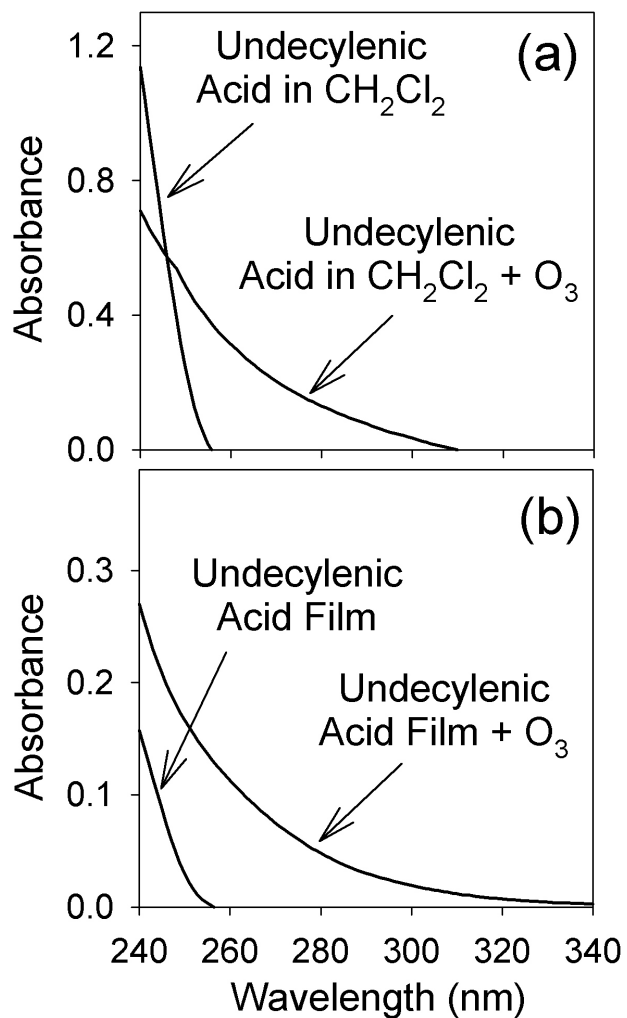


Figure 2.3: UV absorption spectra of undecylenic acid and its oxidation products. The ozonolysis reaction was carried out: (a) in the liquid phase; (b) on the surface of a thin multilayered film.

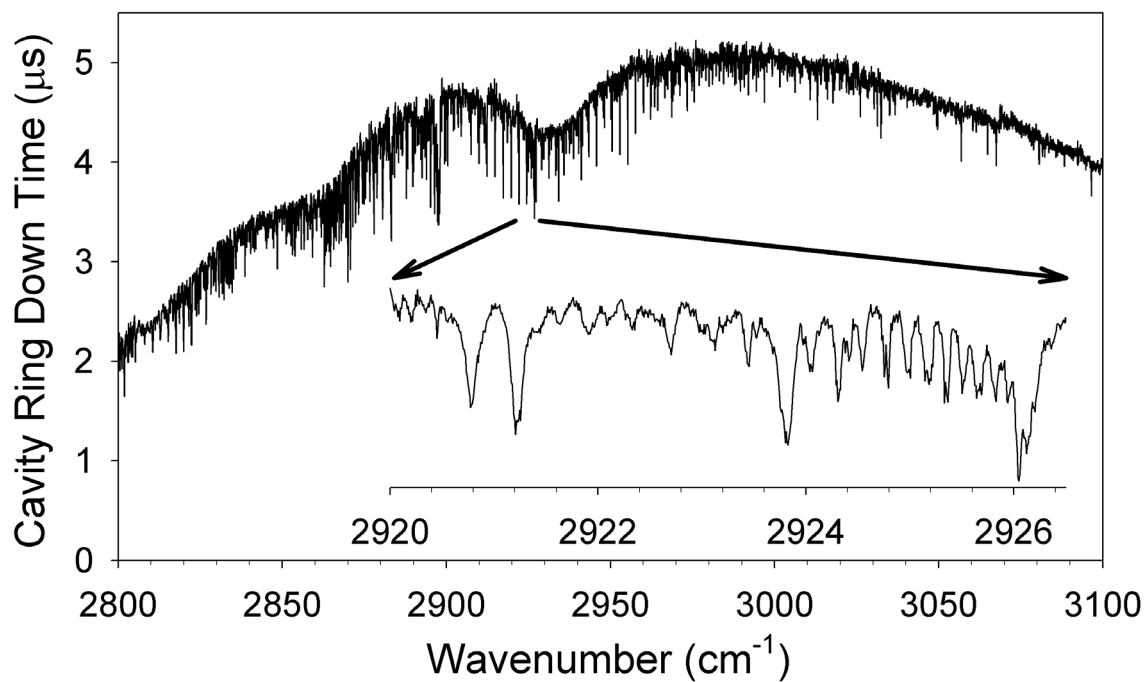


Figure 2.4: CRDS spectrum of the gas-phase oxidation products of undecylenic acid.

The fine structure is mostly due to formaldehyde, and the overall shape of the spectrum is due to the reflectivity profile of the cavity mirrors. Present experiments use the narrow window between 2920 and 2927 cm^{-1} showed in the zoomed portion.

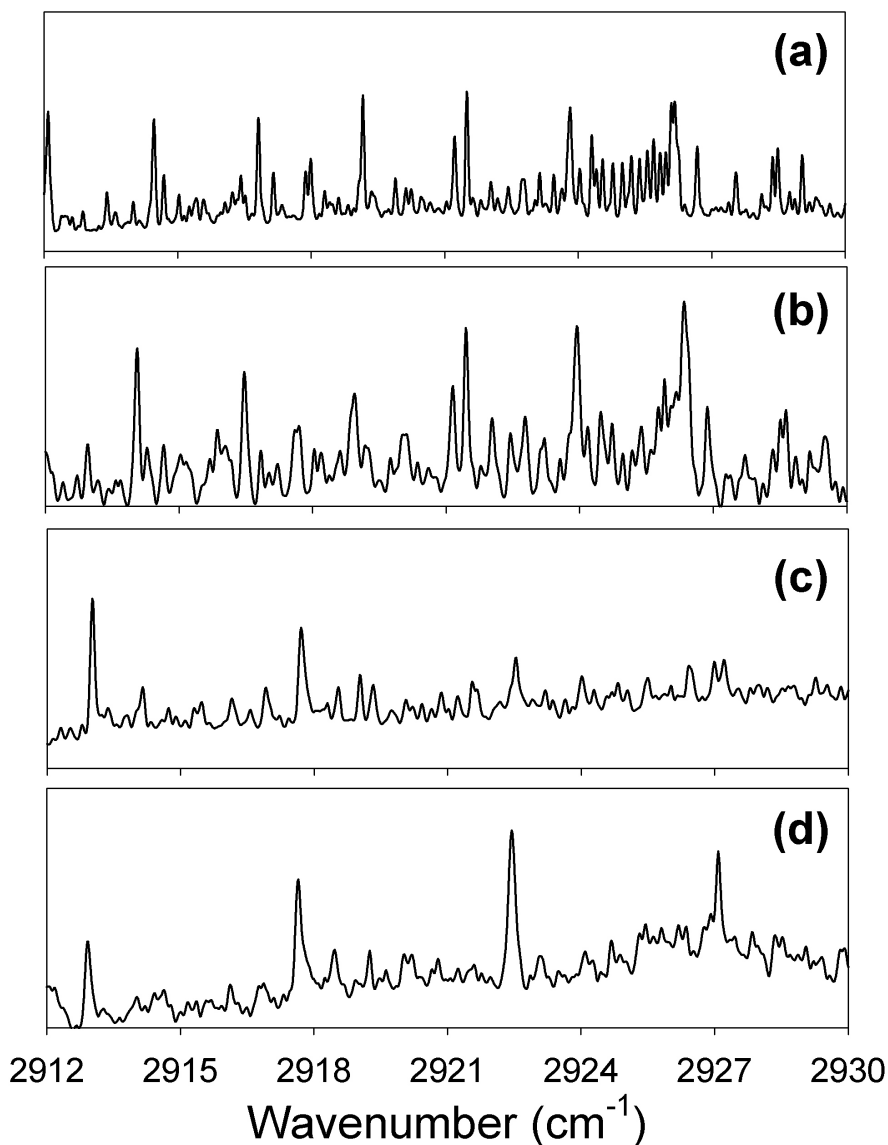


Figure 2.5: CRDS spectra taken during ozonolysis and subsequent photolysis of undecylenic acid: (a) reference spectrum of formaldehyde convoluted to the CRDS laser linewidth; (b) CRDS spectrum taken during the ozonolysis; (c) CRDS spectrum taken during UV photolysis of oxidized undecylenic acid; (d) reference optoacoustic spectrum of formic acid taken in parallel with CRDS.

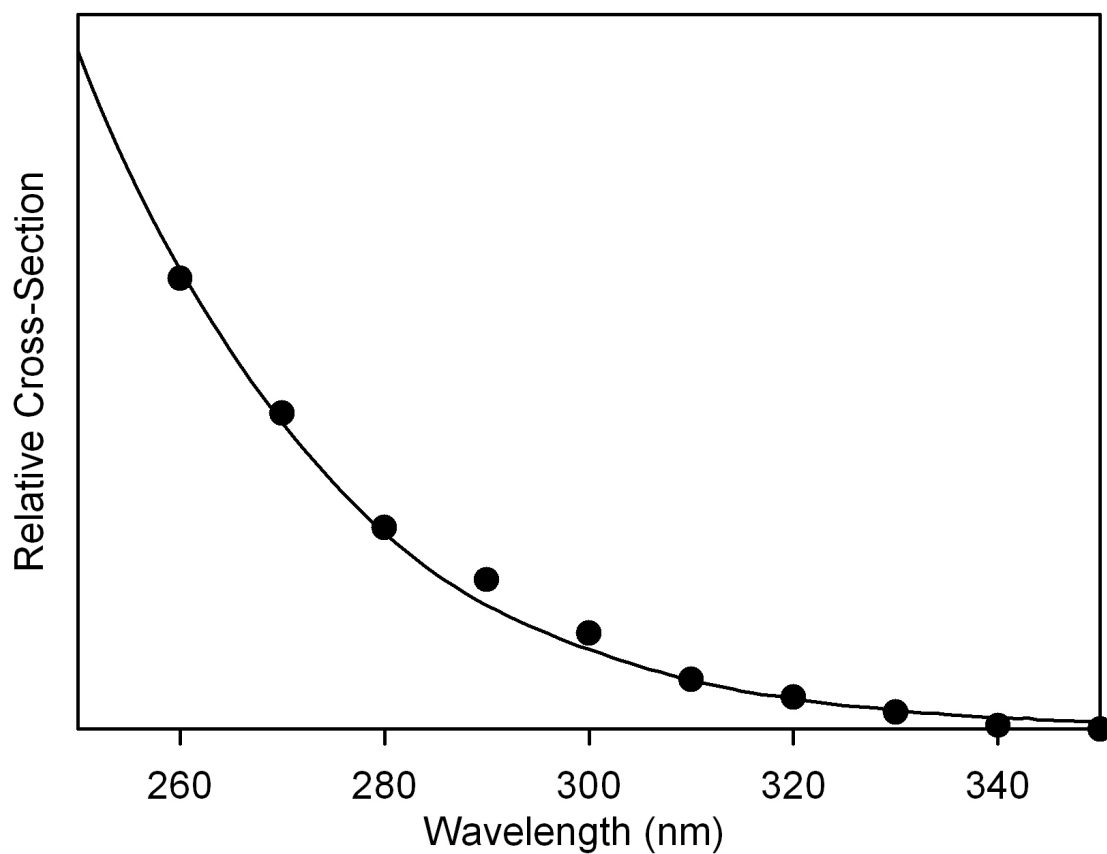


Figure 2.6: Comparison of action photodissociation (filled circles) and absorption (solid line) spectra of oxidized undecylenic acid. The action spectrum was arbitrarily scaled to fit the absorption data.

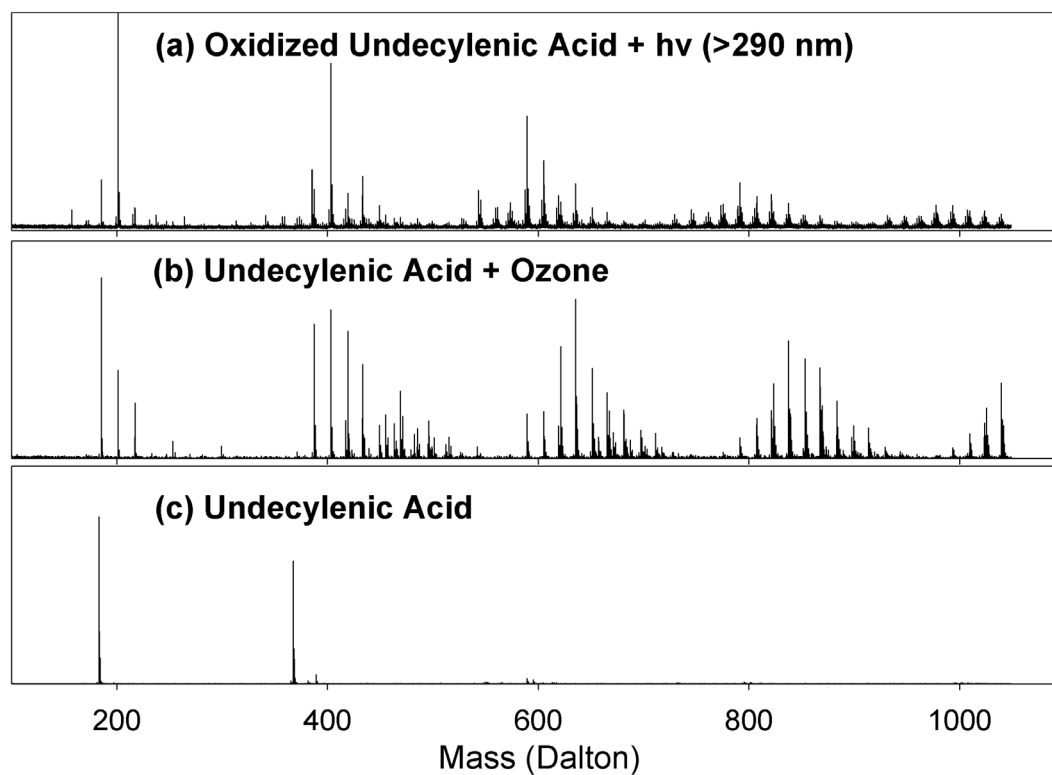


Figure 2.7: Negative ion electrospray mass-spectra of: (a) undecylenic acid film subjected to ozonolysis and then to photolysis ($\lambda > 295$ nm) in dry air; (b) oxidized undecylenic acid; (c) pure undecylenic acid

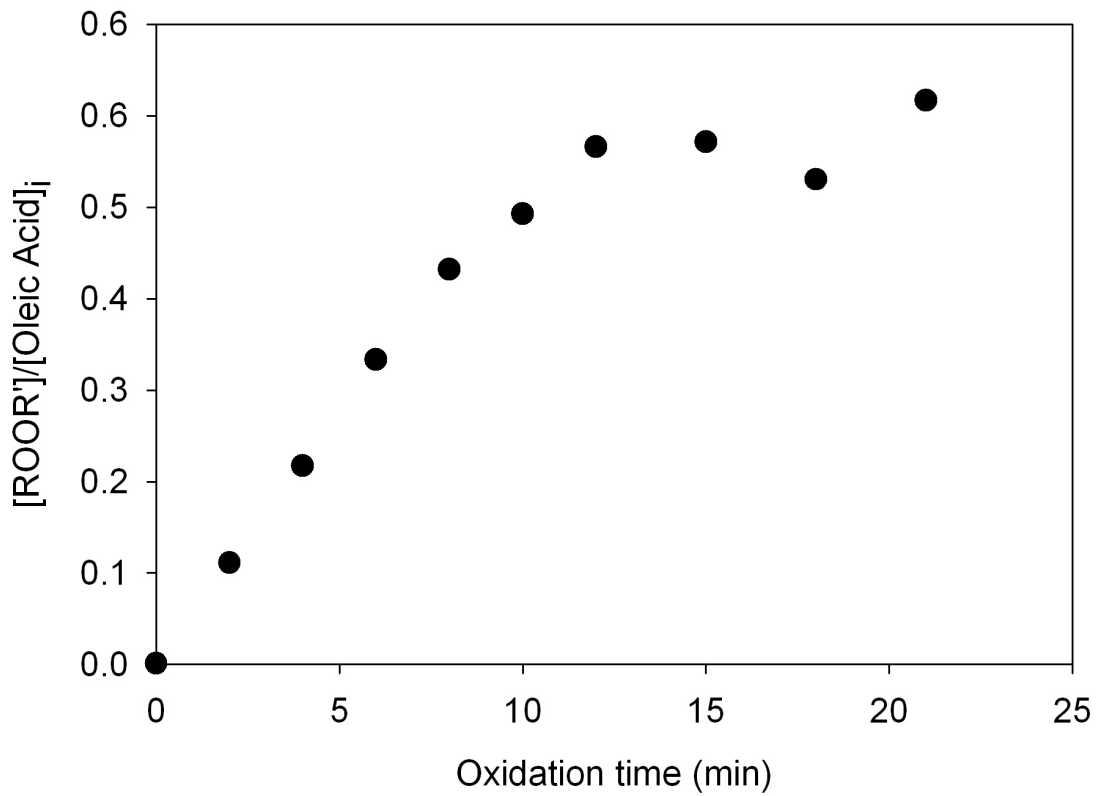


Figure 2.8: Iodimetric tests on oxidized Oleic acid/methanol solutions show significant peroxide formation with upwards of 60% conversion of double bonds into various peroxy groups.

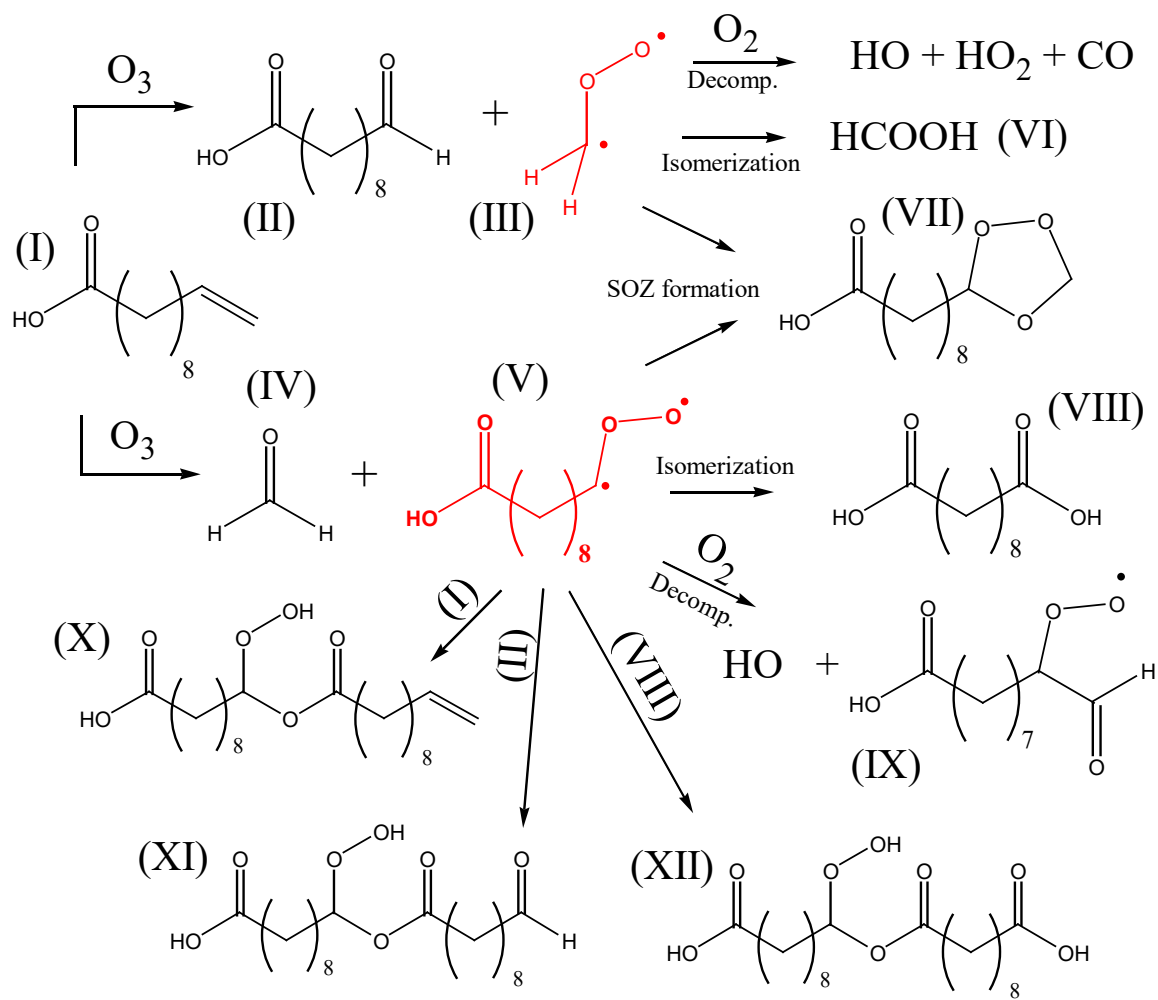


Figure 2.9: Primary reactions taking place during ozonolysis of undecylenic acid film.

Products (II, IV, VI, VIII) could be observed directly. SOZ (VII) and carbonyl oxides (III, V) participate in secondary reactions such as decomposition and oligomerization (not shown).

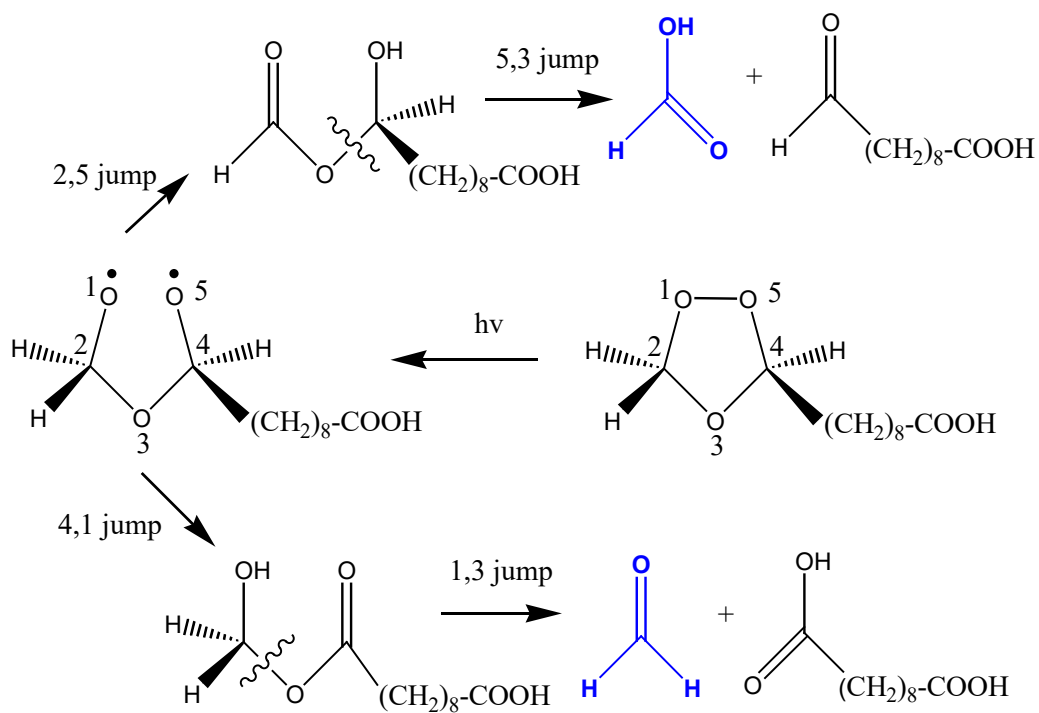


Figure 2.11: One of the possible mechanisms of photolytic production of HCHO and HCOOH from the oxidized undecylenic acid. Preferential formation of HCOOH can be explained by steric hindrance in the H-transfer step.

Chapter III

Ozonolysis and UV Photodissociation Spectroscopy of Alkene-Terminated Self-Assembled Monolayers on Amorphous SiO₂ Nanoparticles

Reproduced in part from *Park, J.; Gomez, A. L.; Walser, M. L.; Lin, A.; Nizkorodov, S. A., PCCP 2006, 8, 2506-2512*, with permission of the PCCP Owner Societies.

3.1 Abstract

Photolysis of alkene-terminated self assembled monolayers (SAM) deposited on Degussa SiO₂ nanoparticles is studied following oxidation of SAM with a gaseous ozone/oxygen mixture. Infrared cavity ring-down spectroscopy is used to observe gas-phase products generated during ozonolysis and subsequent photolysis of SAM in real time. Reactions taking place during ozonolysis transform alkene-terminated SAM into a photochemically active state capable of photolysis in the tropospheric actinic window ($\lambda > 295$ nm). Formaldehyde and formic acid are the observed photolysis products. Photodissociation action spectra of oxidized SAM and the observed pattern of gas-phase products are consistent with the well-established Criegee mechanism of ozonolysis of terminal alkenes. There is strong evidence for the presence of secondary ozonides (1,3,4-trioxalones) and other peroxides on the oxidized SAM surface. The data imply that

photolysis plays a role in atmospheric aging of primary and secondary organic aerosol particles.

3.2 Introduction

In this work, alkene-terminated molecules adsorbed on the surface of silicon oxide are used as a surrogate for aerosol particles coated by an organic surfactant. The main objective of this work is to investigate the effect of oxidation by ozone on the photochemical properties of the organic surface in contrast to results presented in chapter 2 which describe ozonolysis and photolysis of thin organic films. By studying SAM, the surface effects are emphasized relative to the bulk. To this end, the UV photodissociation spectrum of the oxidized surface is measured using action spectroscopy, wherein gas-phase formaldehyde and formic acid photolysis product concentrations are carefully measured at different excitation wavelengths.

3.3 Experimental

Powdery silicon oxide was functionalized to prepare SAM of alkene-terminated organic silanes using the method reported by Usher et al.⁷⁹ Briefly, SiO₂ powder (Degussa OX50) was dried at ~ 400 K overnight prior to use and dispersed in dry toluene (1.5g/100 ml). Ten drops (~ 210 mg) of 5-hexenyldimethylchlorosilane (Gelest) and five drops (~ 120 mg) of pyridine were added to the SiO₂/toluene suspension. The temperature of the resulting solution was kept at 360 K for about 3 hours of vigorous stirring. Treated SiO₂ particles coated with 5-hexenyldimethylchlorosilane were collected using vacuum filtration and stored in dry toluene after washing them with clean toluene at least three times (Fig. 3.1).

A fraction of the toluene slurry containing freshly prepared organic-coated SiO₂ powder (C6= SAM on SiO₂ nanoparticles) was transferred onto the inner wall of a quartz tube and dried by flowing helium gas over it. Only one side of the tube was coated to allow UV radiation to enter the tube through the uncoated side. After installing the quartz tube between two highly reflective mirrors of a cavity ring-down spectrometer, residual toluene was pumped out overnight before proceeding with the ozonolysis experiment.

All experiments were performed at room temperature (295 K). The SAM adsorbed on the inner wall of quartz tube (ID = 1.27 cm) was exposed to ozone in the dark at a concentration of $\sim 10^{14}$ - 10^{15} molecules cm⁻³ until nearly complete oxidation of surface alkenes was achieved. The ozone concentration was considerably higher than a typical atmospheric value. However, this study mainly focused on the photolysis of ozonized terminal alkenes adsorbed on the silicone oxide surface, and not on the ozonolysis reaction. The carrier gas contained O₂ and He at a total pressure of 5-30 torr. The gas-phase products of the ozonolysis of SAM were probed in real-time IR-CRDS. In the majority of experiments, the film was oxidized on a time scale of 30-60 minutes making it possible to complete several IR-CRDS scans (5-10 min. each) in the process. More details about the IR-CRDS system are provided Appendix A.

Before the photolysis experiments, the cell containing ozonized SAM was evacuated in the dark for several hours to remove volatile products formed during ozonolysis. Radiation from a 150W Xe-arc lamp was directed through a 295 nm long-pass filter or a monochromator to select the wavelength (resulting wavelength resolution ~ 10 nm), and the sample cell was illuminated at a right angle to the IR-CRDS cavity axis.

The maximal UV-radiation power (at 310 nm) was 17.5 mW distributed over an irradiation area of 1 cm². The power was considerably lower for shorter irradiation wavelengths. The rest of the cell was protected from scattered radiation by foil. There was no correlation between the observed rate of photolysis and the location of the photolysis spot suggesting that the oxidized SAM was relatively homogeneous. All photolysis experiments were also carried out at room temperature (295 K) under slow flow conditions (~1-5 min cavity flushing time) using ultra high purity helium as a bath gas at 5-30 torr. An optoacoustic reference spectrum of HCOOH vapor (1 torr of HCOOH in 10-100 torr N₂ buffer) was recorded in parallel with the IR-CRDS spectrum for wavelength calibration purposes.

3.4 Results

3.4a Ozonolysis

Sample IR-CRDS absorption scans of gas phase products from ozonolysis (a) and subsequent photolysis (b) of SAM are shown in Figure 3.2. The reference absorption spectrum of formaldehyde (c) and optoacoustic spectrum of formic acid (d) are also plotted for comparison. We explicitly verified⁸⁰ that no HCHO or HCOOH gas-phase products are emitted during the ozonolysis of fully saturated organic SAM deposited on flat Si(111) wafers (ozone reacts very slowly with saturated hydrocarbons and it does not destroy the O-Si-C bridges in SAM). On the contrary, ozonolysis of alkene-terminated SAM on Si wafers generated HCHO as the major gas-phase product.⁸⁰ The results

obtained here are qualitatively similar but the signal-to-noise ratio is considerably improved because of the considerably larger combined surface area of SiO₂ nanoparticles compared to the Si wafer.

Similar to the results for Si wafers,⁸⁰ large signals from HCHO and smaller signals from HCOOH were detected during ozonolysis of alkene-terminated SAM on SiO₂ particles (Figure 3.2(a)). The absolute ratio between HCHO and HCOOH formation was obtained by simulating the IR CRDS spectra using the known absorption cross-sections for these two molecules. (make ref: Northwest-Infrared Vapor Phase Infrared Spectral Library. Northwest National Laboratory, <http://nwir.pnl.gov>) The laser bandwidth (0.1 cm⁻¹) is larger than the bandwidth of individual ro-vibrational transitions in HCHO and HCOOH (0.01 cm⁻¹), which makes the apparent IR-CRDS absorption coefficient depend on concentration in a non-linear way.¹¹⁰ However, the branching ratio obtained from well-isolated HCHO and HCOOH lines with comparable line strengths and intrinsic line widths is expected to be fairly quantitative.

Analysis of the IR-CRDS spectra provides an approximate ratio of HCOOH/HCHO = 0.65±0.20. This ratio represents a time-averaged value over the initial stages of ozonolysis (~10 min). This time was comparable to the half-time for complete film oxidation and gas-SAM equilibration (~10 min). Our data suggest that the HCOOH/HCHO ratio remains approximately the same at later stages of ozonolysis implying that there is no drastic change in the mechanism of POZ decomposition as the organic film ages.

3.4b Photolysis

A sample CRDS spectrum obtained during the broadband photolysis of the oxidized surface with a 295 nm long-pass filter is shown in Figure 3.2(b). The spectrum unambiguously shows that both formaldehyde and formic acid are produced during photolysis. These molecules were not detected during UV irradiation of the SAM surface before it was processed with ozone. We also explicitly verified that the observed emission of HCHO and HCOOH was not a result of simple thermal desorption caused by radiative heating of the sample. A K-type thermocouple was attached to the sample cell during photolysis, and no significant temperature elevation at the irradiated surface was observed.

The primary focus of this work is the effect of oxidation of SAM on its photochemical activity in the tropospheric actinic window ($\lambda > 295$ nm). We studied the wavelength-dependent photolysis of the oxidized sample by taking its action photodissociation spectrum in the HCOOH product channel. Specifically, a small section (~ 1 cm²) of oxidized SAM was photolyzed with a tunable UV source, while keeping the IR-CRDS laser frequency fixed on a strong absorption line of formic acid at ~ 2917.9 cm⁻¹. Figure 3.3 shows the observed change in formic acid concentration as a function of photolysis time at several different photolysis wavelengths. The steady-state is achieved after 10-20 minutes of photolysis, with the formic acid concentration at steady-state increasing at shorter photolysis wavelengths. We attribute the long time required to reach the steady-state to slow desorption of formic acid from high surface area SiO₂ particles.

The wavelength-dependent relative yield of formic acid corrected for the UV lamp power and quartz cell transmission is plotted in Figure 3.4. The action spectrum is characteristic of absorption by peroxy groups, with the photodissociation yield of HCOOH smoothly increasing towards the blue end of the spectrum. It should be noted that significant formation of formic acid is detected at wavelengths where the initial alkene-terminated SAM is stable to photolysis. This observation is in line with the results from our study of photolysis of ozonized undecylenic acid with the same approach.¹¹⁰

We have attempted to characterize the surface products of SAM oxidation and photolysis by electrospray ionization mass spectrometry (ESI-MS). The ESI-MS approach was very helpful in unraveling the mechanism of ozonolysis and photolysis of undecylenic acid reported in Ref.¹¹⁰. Unfortunately, ESI-MS of products of SAM hydrolysis gave incomprehensively complex mass spectra in both positive and negative ion mode. The authors of Ref.¹¹¹ had similar difficulties in analyzing the composition of surface products of ozonolysis of SAM on Si wafers.

3.5 Discussion

3.5a Ozonolysis

The general mechanism of ozonolysis of unsaturated hydrocarbons has been extensively studied by many research groups.^{32, 80; Usher, 2003 #615]} The effect of light radiation during/after ozonolysis has not been significantly considered and it will be

discussed in the later parts of this paper. Only a brief discussion necessary to support the photolysis results will be given in this section.

A schematic diagram of the primary reactions between alkene-terminated SAM and ozone is shown in Figure 3.5. The POZ produced in the initial ozone-double bond addition decomposes in one of two ways to produce either formaldehyde and a surface-bound Criegee intermediate (I) or a surface-bound aldehyde (II) and a gas-phase Criegee intermediate (III). Product molecules that are not bound to the surface may then escape from the SAM environment into the gas-phase or undergo secondary reactions within the SAM.

Gas-phase ozonolysis of terminal alkenes is known to produce HCHO, HCOOH, and other volatile products. For example, a study by Neeb et al.⁹⁴ showed that the branching ratio for the HCHO formation channel in ozonolysis of terminal alkenes at 730 torr is 0.5, whereas the branching ratio for the HCOOH formation channel through the isomerization of the Criegee intermediate is as low as 0.05. Ozonolysis of alkene-terminated SAM also favor the HCHO product.⁷⁹; [Dubowski, 2004 #955]

Whereas the gas-phase products of ozonolysis of C6= SAM on SiO₂ nanoparticles are the same as previously observed, the HCOOH yield measured by the CRDS technique (0.4±0.1) is substantially higher than that measured by mass-spectrometry study (<0.05).

³² We stress that both methods of detection are prone to experimental artifacts: selective wall adsorption in mass-spectrometry and insufficient spectral resolution leading to non-linearity in absorbance in IR-CRDS. In addition, line strengths and pressure broadening

coefficients for HCOOH transitions are not known with good precision. However, it is possible that reduced stabilization of the escaping Criegee intermediate (III) under the low pressure conditions of this work does produce an increased yield of formic acid.

In view of the lack of strong spatial constraints in the decomposition of singly-substituted POZ, the branching ratio between channels a and b in Figure 5 should be close to 1:1. The observed <50% yield of HCOOH implies that only a fraction of Criegee intermediate (III) can isomerize to HCOOH. One possibility is that III is rapidly decomposing into HCO, OH, CO₂, CO, H₂, and H₂O. The latter occurs, for example, in the gas phase ozone-propene reaction where yields of (CO + CO₂) were measured to be 67% compared to 11% for formic acid.¹¹² Our CRDS instrument in its present configuration is blind to CO and CO₂.

A more likely fate for III is stabilization followed by secondary reactions with neighboring SAM molecules. Indeed, there are several possible secondary reactions that take place in SAM after POZ decomposition. Criegee intermediates, I and III, can recombine with formaldehyde and surface aldehyde, respectively, to form surface secondary ozonides (sSOZ). This reaction is believed to be very efficient in liquids due to the solvent cage effect,¹¹³ and it is conceivable that it also occurs in the semi-liquid SAM environment. The production of gas phase secondary ozonide (gSOZ) from the reaction between formaldehyde and Criegee intermediate (III) is also possible, and there have been several reports of gas phase SOZ formation from ozonation of alkenes in various pressure ranges.¹¹⁴⁻¹¹⁶

As the SAM oxidation proceeds and surface products accumulate, new reaction channels open up due to the close proximity of surface bound molecules in SAM. For example, association reaction of surface aldehyde (II) with surface Criegee intermediate (I) can form surface SOZ dimer (V) shown in Figure 6. Criegee radical (I) can also attack double bonds and carboxylic groups in neighboring molecules to form other surface peroxides. Similar selective condensation reactions among I, I', III, and unreacted terminal alkene (OS-SiO₂) are also possible, again yielding various peroxides (structures IV, VI, VII, and VIII in Figure 6). Even more complicated surface polymerization reactions initiated by the Criegee intermediates are possible as suggested in recent reports by Dreyfus et al.¹¹⁷ and Hung et al.¹¹⁸ For example, McIntire and co-workers¹¹¹ studied ozonolysis of unsaturated SAM on silica wafers using atomic force microscopy, and found unusually large organic aggregates formed with unknown chemical composition on the oxidized surface.

3.5b Photolysis

Photolysis experiments lend strong support to the assumption that sSOZ and/or other peroxides products are present on the surface after ozonolysis. As described in the previous section, we found significant amounts of formic acid and formaldehyde produced during photolysis of oxidized SAM. Photolytic elimination of HCHO and HCOOH is not very common, and it strongly restricts the molecular nature of their possible photochemical precursors. For example, direct photochemical formation of HCHO and HCOOH from the photolysis of surface acid (I') and surface aldehyde (II) cannot occur at these excitation frequencies. Excitation of surface peroxides (IV-VIII)

would sever the -O-O- bond but the resulting rearrangement products would remain attached to the surface and/or produce hydroxyl radicals. Although photolysis of gSOZ could give rise to both HCHO and HCOOH, gSOZ should be removed by pumping on the flow cell for several hours before starting the photolysis experiments. In addition, SOZ of ethene may not be stable enough to remain in the system for so long.⁹⁴

The most likely source of these photoproducts is photolysis of sSOZ. The suggested mechanism is shown in Figure 7. Because the O-O bonds in SOZ molecules are relatively weak, they are easily broken by UV photons¹⁰²; Andrews, 1982 #434; Khachatryan, 1997 #1008] to produce an intermediate (IX). Rearrangement of IX can proceed via two possible pathways: 1,4- Ha shift and 3,5-Hb shift forming intermediate species, X and XI, respectively. Depending on the H-transfer pathway, formic acid (from X through Ha migration) or formaldehyde (from XI through Hb migration) are produced together with surface aldehyde (II) and surface acid (I').

The large delay between oxidation of the sample and photolysis experiments (several hours) implies that sSOZ in SAM do not decompose on timescales of hours at room temperature. Such high stability of substituted SOZ compounds is not unusual. For example, SOZ obtained by ozonolysis of 2,3-dimethyl-butene remains stable for days in solutions¹⁰⁴ and for hours in the gas-phase at room temperature.¹⁰⁵ SOZ of many other singly-substituted molecules have been successfully prepared and characterized by analytical techniques, some of which require heating the sample (GC/MS and ESI-MS).

104, 105, 114, 115, 119

A previous study of the photolysis of 3,5-dimethyl-1,2,4-trioxolane (secondary ozonide of 2-butene)¹⁰⁵ showed that the SOZ photolytic decomposition mechanism is wavelength-dependent. The authors reported that photolysis by hard UV radiation (ArF laser, 193 nm) produced many different products, including formic acid, whereas photolysis by mild UV radiation (N₂ laser, 337 nm) was a much slower process, which could not compete with SOZ oligomerization occurring on the reactor walls under their experimental conditions. Although sSOZ oligomerization cannot be ruled out, we do not observe a change in the HCHO/HCOOH ratio over the action spectrum (Figure 4) wavelength range of 270-310 nm.

The surface bound hydroperoxides (VI and VIII) are also expected to photolyze by cleavage of the -O-OH bond releasing OH and/or H₂O and leaving surface products on the surface. The highly reactive OH radical is likely to either add to double bonds remaining on the SAM surface or abstract an H-atom from a neighboring chain. Subsequent reactions with trace O₂ molecules in the buffer gas-flow will produce surface-bound RO₂ radicals. We cannot rule out a possibility that one of the secondary reactions involving RO₂ radicals can generate HCHO and HCOOH as secondary products of photolysis; more information on photochemistry of hydroperoxides in the condensed organic phase is necessary to address this question.

3.5c Atmospheric Implications

In spite of the incomplete characterization of the surface products in this work, it is clear that oxidation of unsaturated organic films by ozone has a strong effect on the

photochemical properties of the resulting surface. The photodissociation cross-section of the oxidized film is characteristic of absorption by peroxidic groups. This observation has important implications for photochemical aging of both primary organic aerosol (POA), which is emitted directly in particulate form, and secondary organic aerosol (SOA), formed by condensation of low volatility products of atmospheric oxidation of hydrocarbons. Indeed, a substantial fraction of POA in urban areas comes from cooking emissions^{25, 120} containing an array of unsaturated organics such as oleic acid, linoleic acid, cholesterol derivatives, etc. Oxidation of these unsaturated molecules will convert them into more photoactive forms permitting further processing induced by solar radiation.

SOA formation from monoterpene oxidation by ozone has been extensively investigated,¹²¹⁻¹²⁴ and its aging by UV-radiation is likely to be equally important to the POA case, especially for SOA generated by ozonolysis in the dark. Several research groups are currently working on this important area.¹⁰⁷ Presto et al. reported a significant effect of UV-radiation on the yield reduction of SOA in terpene ozonolysis and concluded that SOA yield is likely to depend on actinic flux. Our preliminary measurements of the photochemical properties of SOA generated by ozonolysis of α -pinene and d-limonene reveal even stronger photoactivity than reported here for alkene-terminated SAM. The results on SOA photolysis will be reported elsewhere.

Photochemical processing of organic particles can not only change their chemical properties but also serve as a potential source of free organic aldehydes and carboxylic acids. Verification of this hypothesis is an ongoing research effort in our group, and it

requires a careful quantification of photodissociation cross-sections of model POA and SOA particles generated under realistic atmospheric conditions.

3.6 Conclusions

Ozonolysis of assembled organic monolayers deposited on SiO₂ nanoparticles and photolysis of the resulting oxidized surface have been studied. Such SiO₂ nanoparticles are characterized by a high surface-to-volume ratio that is ideal for investigation of surface-specific reactions occurring at the organic aerosol-air interface. The observed pattern of products implies rich chemistry resulting in formation of complex oxygenated products on the SAM surface. Some of these products are photoactive in the tropospheric actinic window ($\lambda > 295$ nm), and release formaldehyde, formic acid, and possibly other small molecules in the gas-phase during UV irradiation. The wavelength dependence of formic acid yield strongly suggests the presence of peroxides such as secondary ozonides on the oxidized SAM surface. The main implication of this work is the potential role of solar radiation in photoaging of primary and secondary organic aerosols.

3.7 Figures

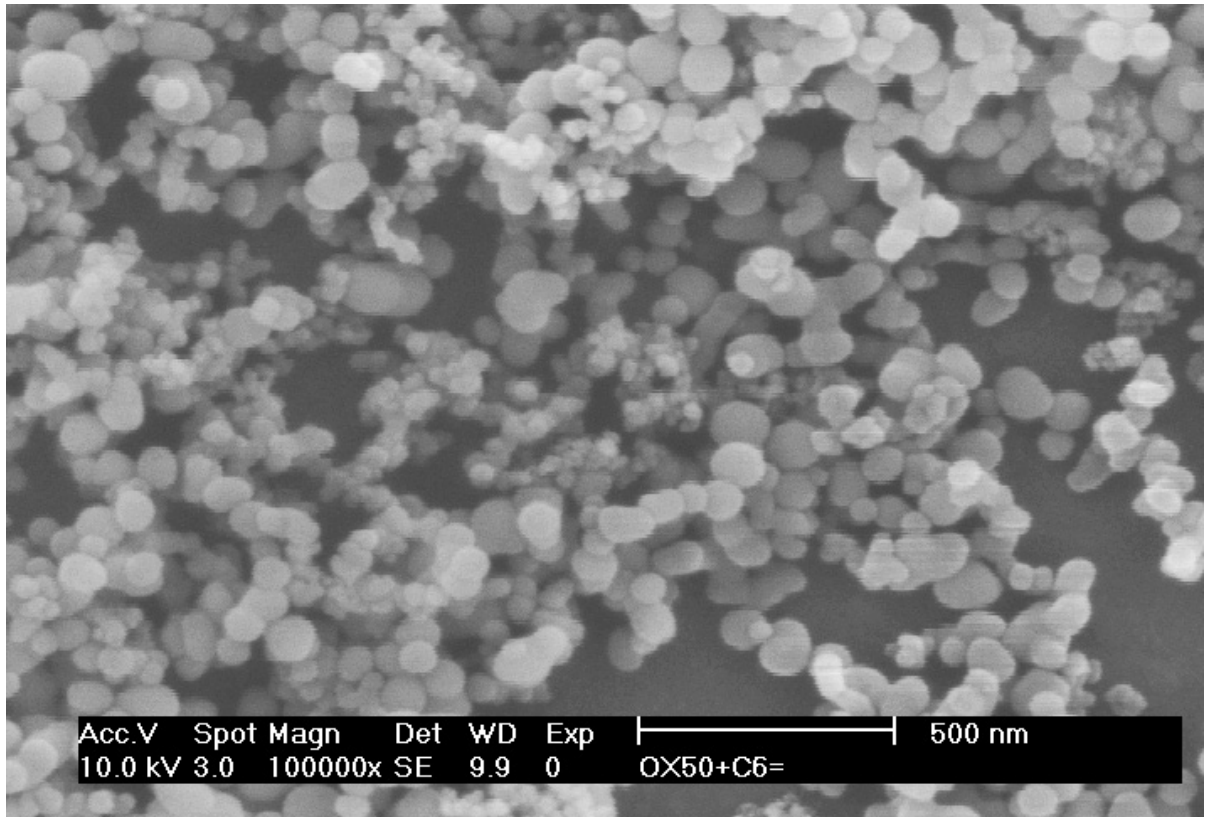


Figure 3.1: SEM image of Degussa OX-50 SiO₂ particles after treatment with 5-hexenyldimethylchlorosilane

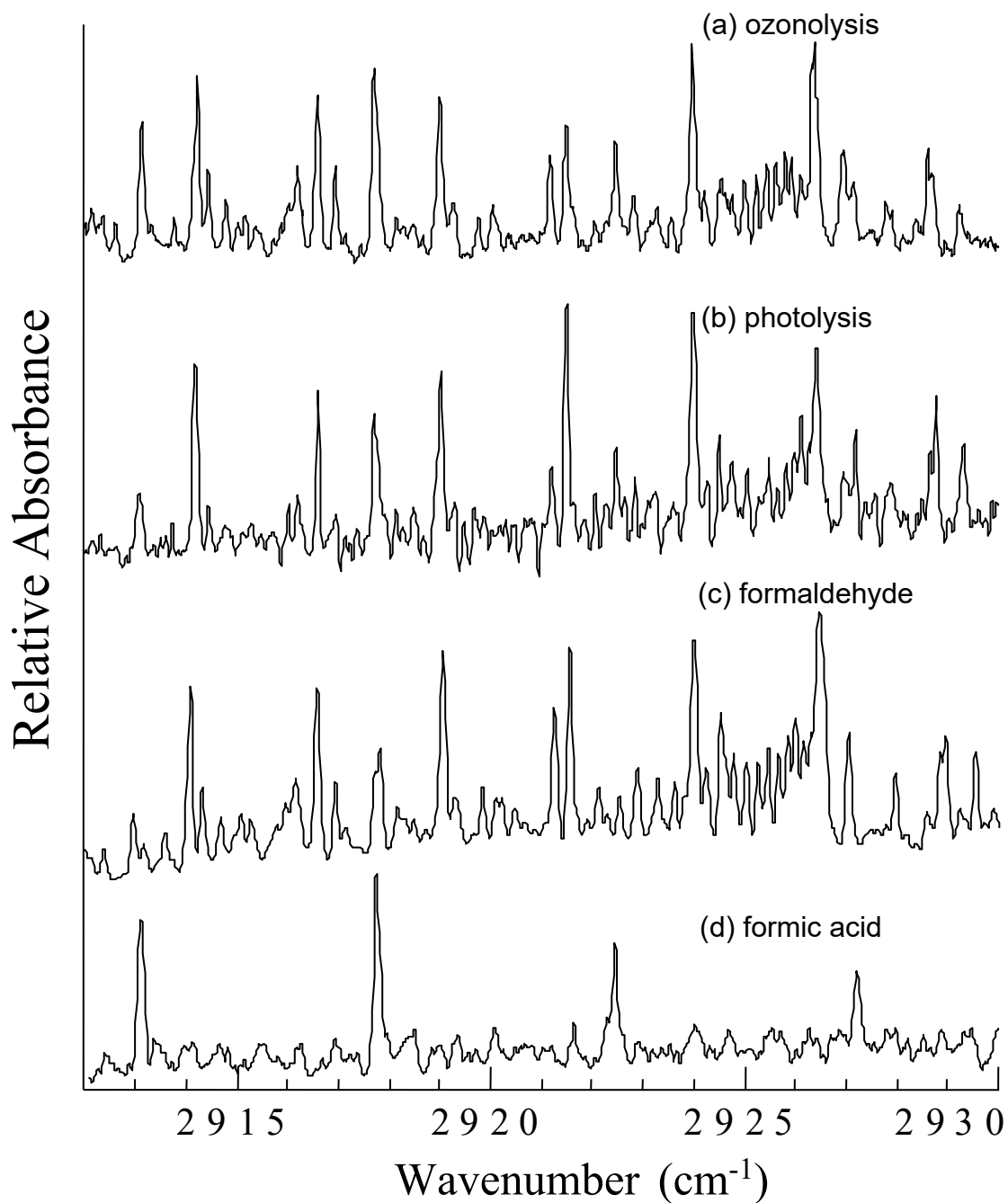


Figure 3.2: IR CRDS spectra of gas products from (a) ozonolysis and (b) photolysis ($\lambda > 295$ nm) of SAM on SiO₂ nanoparticles. Spectrum (b) was obtained after SAM was oxidized by ozone. Reference spectrum of formaldehyde (c) and optoacoustic spectrum of formic acid (d) are plotted for comparison.

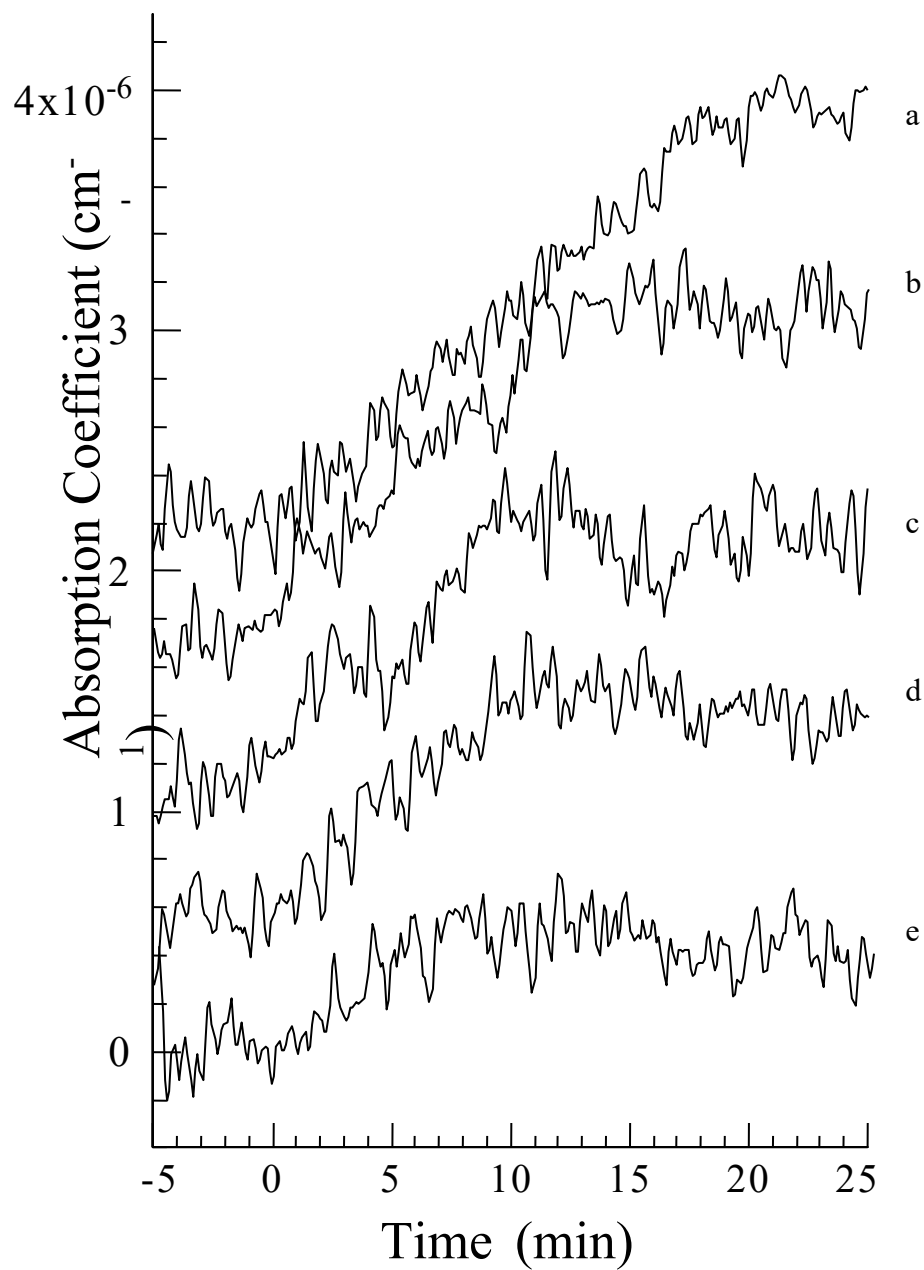


Figure 3.3: Formic acid formation during photolysis of ozonized SAM as a function of photolysis time. Photolysis wavelengths are (a) 270 nm, (b) 280 nm, (c) 290 nm, (d) 300 nm, and (e) 310 nm. The baselines are offset for clarity.

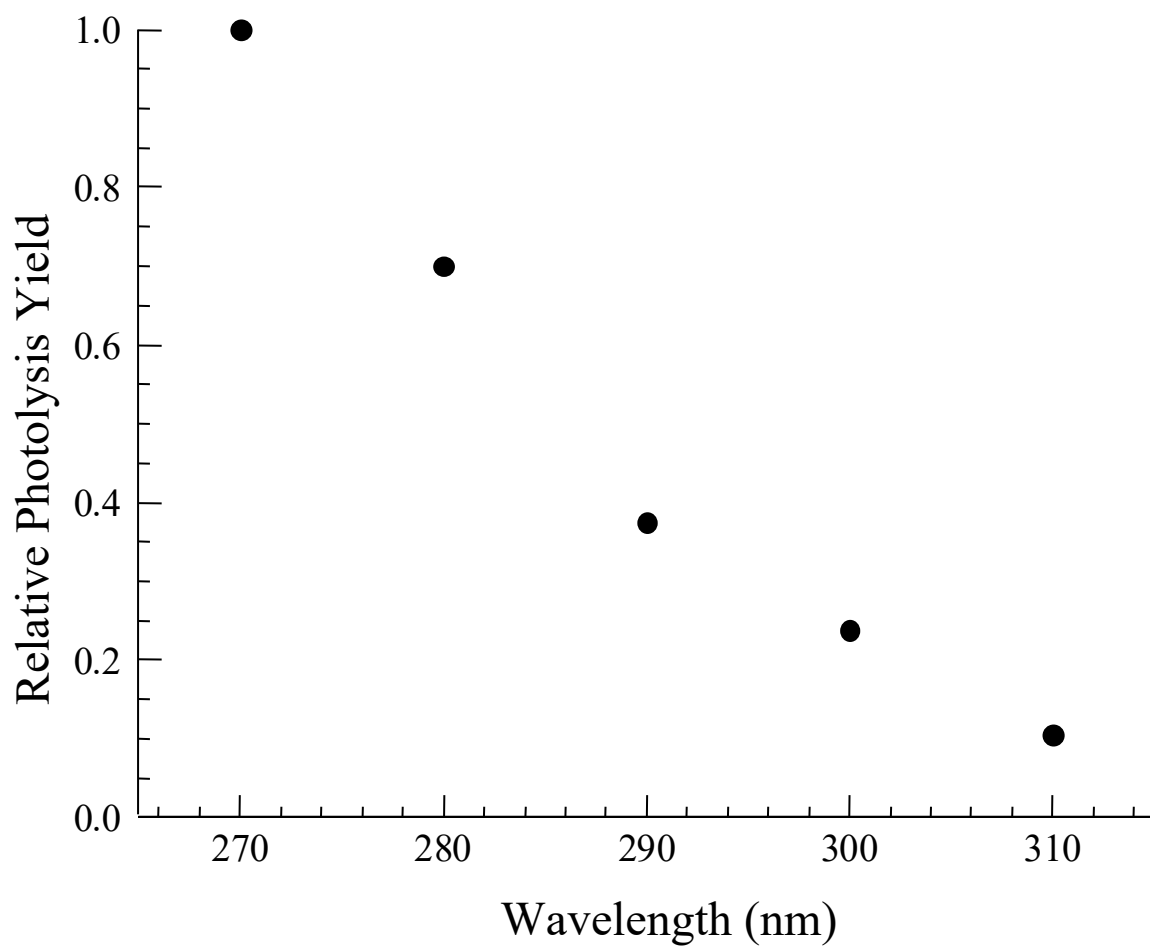


Figure 3.4: Relative yield of formic acid from the photolysis of ozonized SAM as a function of the photolysis wavelength (normalized to the UV power).

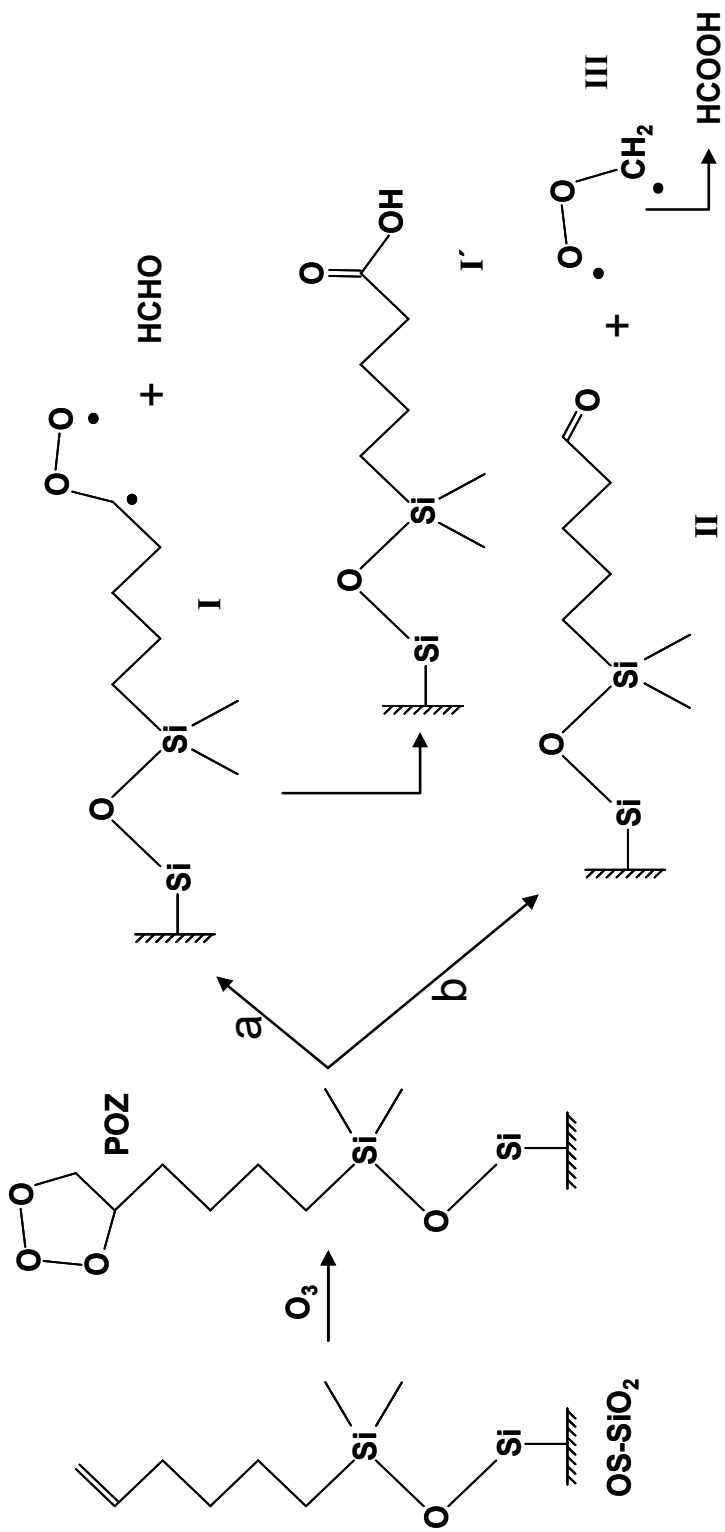


Figure 3.5: Primary reactions taking place during ozonolysis of alkene-terminated SAM. OS-SiO₂ stands for the organic silane initially deposited on the SiO₂ surface.

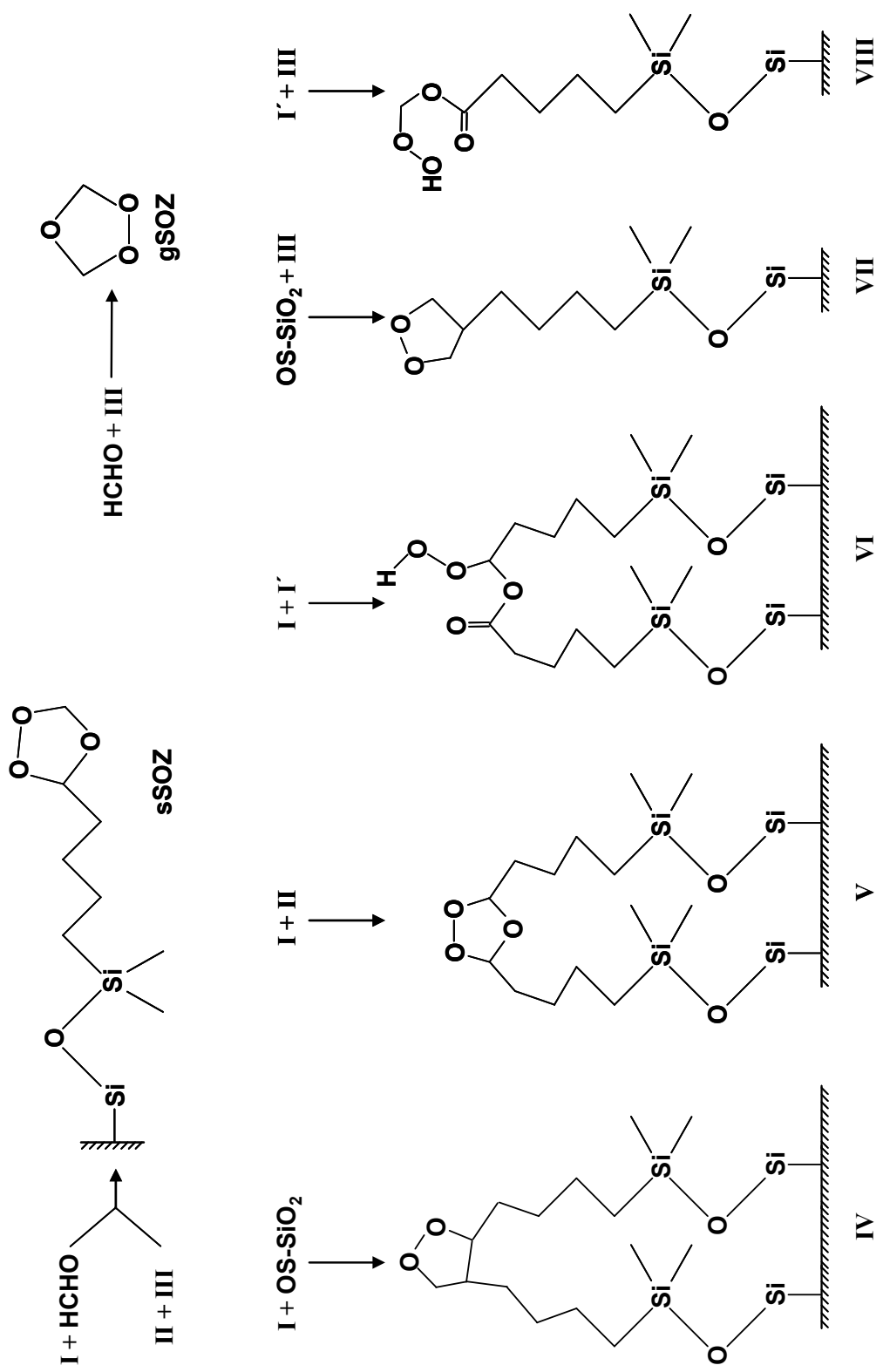


Figure 3.6: Possible secondary reactions taking place during ozonolysis of alkene-terminated SAM

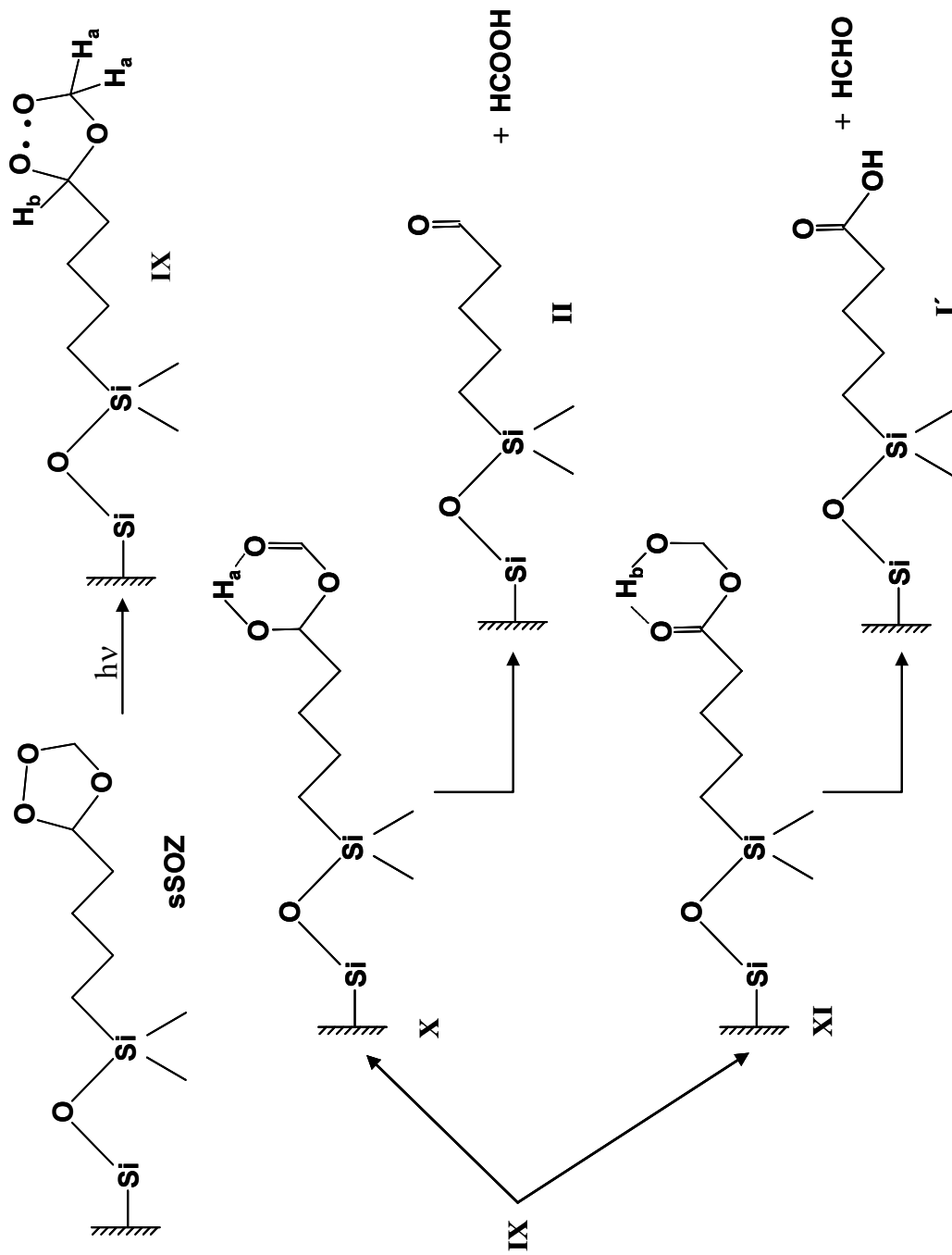


Figure 3.7: Mechanism of sSOZ photolysis leading to photochemical release of HCHO and HCOOH

Chapter IV

Stoichiometry of Ozone-Alkene Reactions in Participating and Non-Participating Solvents

4.1 Introduction

This work is an in-progress effort to understand how reaction conditions affect ozone-alkene reaction stoichiometry. It is generally assumed that ozone reacts with unsaturated organics in a well-defined stoichiometric ratio, with one carbon-carbon double bond consumed per ozone molecule reacted.^{1, 46, 125} However, our preliminary data suggests that a single ozone molecule in the presence of excess molecular oxygen can destroy several double bonds in dilute solutions of monoterpenes and unsaturated fatty acids, likely via a branched radical reaction mechanism. This surprising effect appears to be especially important near room temperature, and it may have implications for the atmospheric chemistry of organic aerosol particles.

Furthermore, ozonation is frequently used for the synthesis of aldehydes and carboxylic acids from olefins. The reaction conditions are optimized for the maximal yield of the desired product; any deviations from the expected reaction stoichiometry are usually regarded as a nuisance. However, a recent study of ozonation of triptene reported 1.05-1.56:1 olefin-to-ozone stoichiometry for the complete triptene consumption and classified this result as “surprising”¹²⁶. Our work suggests that such a deviation from the 1:1 stoichiometry in ozonation of unsaturated organics is a general effect, and quantifies it for several atmospherically-relevant molecules.

4.2 Experimental

Figure 4.1 shows a schematic of the experimental setup used in this study. The reaction stoichiometry was measured by bubbling a calibrated flow of O₃/O₂ gas mixture through a solution, which was periodically spiked with a known quantity of an unsaturated organic reactant. Specifically, an oxygen flow of $F = 20$ sccm (standard cubic centimeters per second) containing ozone at a concentration of $[O_3] = 5 \times 10^{15} - 7 \times 10^{16}$ molec/cm³ was bubbled into 5 mL of a stirred solvent contained in a 10 mL septum-sealed reaction vial immersed in a temperature-controlled bath. Organic reactants pre-diluted to millimolar concentrations with the same solvent were injected into the vial in small volumes (1 to 150 μ L) with a graduated GC syringe. The reactants included unsaturated fatty acids (undecylenic, oleic, linoleic, and linolenic acids) and monoterpenes (α -pinene, β -pinene, and d-limonene). Non-participating solvent reactions were performed in n-hexadecane and nonane for room and low temperature experiments, respectively. To measure the effect of participating solvents, the experiment was repeated at room temperature with oleic acid as a reactant in methanol, 1% acetic acid in methanol, and 10% acetic acid in methanol used as solvents.

The concentration of ozone in the gas effluent was measured with a calibrated home-made Hg-lamp photometer using base- e absorption cross-section of $\sigma_{253.65\text{nm}} = 1.136 \times 10^{-17}$ cm².⁸⁶ Figure 4.2 shows that the measured concentration of ozone exiting the reaction volume dropped after each organic reactant injection, and returned to its initial steady state value, $[O_3]_{ss}$, after all double bonds in the reactants were consumed.

Successive injections were performed either with monotonically increasing reactant concentration or in a random order, with no difference in the results. To keep the ozone solubility and self-decomposition rate in the solution at constant levels, each experimental run was limited to a maximum of 10 injections. The solution remained clear after the injections with no evidence of precipitation.

The reaction products were characterized by electrospray ionization mass-spectrometry (ESI-MS) in negative ion mode, which is ideally suited for the detection of carboxylic acids via their ($m/z-1$) anions. The mass-spectra confirmed that every injection of unsaturated fatty acid reactants resulted in a complete removal of all double bonds from the mixture by O_3 . In the case of monoterpene reactants, the removal of double bonds was not explicitly tested, but it was assumed that it was complete based on similarity of the reaction conditions.

4.3 Results

4.3a *Non-participating Solvents*

The absolute number of ozone molecules needed for the oxidation of double bonds in the organic reactant was obtained by integration of the time dependent ozone concentration (Figure 4.2) for each injection (F is the gas flow rate):

$$\text{molec } O_3 = F \times \int ([O_3]_{ss} - [O_3](t)) dt$$

The absolute number of organic reactant molecules was calculated from the known injection volumes and concentrations.

Figure 4.3 shows a molecule-per-molecule plot for all organic reactants measured at room temperature in non-participating solvents. The dashed line corresponds to the expected stoichiometric 1:1 ozonation of reactants with a single double bond. Clearly, under these experimental conditions, consumption of one ozone molecule results in an elimination of more than one double bond. Furthermore, careful examination of the plot reveals that the olefin-to-ozone stoichiometry depends on the initial amount of the olefin. These effects are reproducible and extend over a fairly wide range of conditions. For example, ozonation of undecylenic acid was studied at ozone steady-state levels of 6×10^{15} and 6×10^{16} molec/cm³, and the data from these two experiments agreed with each other over 3 orders of magnitude of reactant concentrations.

The average number of double bonds depleted by each ozone molecule is plotted against the reactant concentration in Figure 4.4 for several temperatures. Clearly, this ratio converges at the conventional double bond-to-ozone stoichiometry of 1:1 only at the highest concentrations and lowest temperatures used in this work. At room temperature, this ratio converges to 2-3 at the higher reactant concentrations, and it increases to 4-5 at the lower concentrations. At lower temperatures, this effect is less dramatic, with the number of consumed double bonds approaching 1.5 at the lowest concentrations probed in this work.

4.3b Participating Solvents

To investigate the reaction mechanism, these uptake experiments were repeated in participating solvents (methanol, 1% acetic acid in methanol, and 10% acetic acid in methanol). Figure 4.6 shows a comparison of the uptake of oleic acid in various

participating solvent mixtures, at room temperature. The uptake ratio increases as the solvent becomes “more participating” with ratios reaching 10:1 for higher concentrations and 20:1 for low concentrations in methanol/acetic acid solvent mixtures.

4.3 Discussion

The accepted mechanism of ozonation of olefins involves cycloaddition of ozone across the double bond followed by a fast decomposition of the resulting primary ozonide into an aldehyde & carbonyl oxide pair.^{15, 46} The solvents employed in this work are classified as either participating or non-participating depending on whether they react with ozone and/or the carbonyl oxide intermediates. The usual fate of the carbonyl oxides in non-participating solvents is recombination with the geminate aldehydes to give a secondary ozonide (SOZ). This reaction pathway results in 1:1 olefin-to-ozone stoichiometry (Figure 4.5), but it is consistent with present observations only for the lower temperature conditions. Indeed, our ESI-MS spectra confirmed that SOZ (observed at $m/z = 2M_{\text{SOZ}} - 1$) is the primary product of ozonation of unsaturated fatty acids at lower temperatures, but SOZ yield is reduced considerably at higher temperatures.

Isomerization of carbonyl oxides into the corresponding carboxylic acids would similarly result in a double bond-to-ozone ratio of 1:1 (Figure 4.5). This isomerization process is known to be fairly efficient as carboxylic acids are very common products of ozonation of olefins in solutions, gas-phase, and aerosol phase.^{15, 33, 35, 44, 75, 77, 110, 118} In this work we also find very clear signatures of the isomerization products in the ESI-MS spectra.

Carbonyl oxides do not normally attack double bonds directly.⁴⁶ However, some researchers have proposed that carbonyl oxide's cycloaddition across a double bond is possible (e.g., Ref. ⁴⁴). Such a cycloaddition, if efficient, would result in 2:1 double bond-to-ozone stoichiometry. Although this possibility cannot be ruled out by the data, it still does not account for the observed stoichiometric ratios in excess of 2:1. Furthermore, stabilized carbonyl oxides are much more likely to add to carboxylic groups in solutions containing organic acids.^{15, 110}

To account for the observed stoichiometric ratios in excess of 2:1, we initially speculated that reaction intermediates undergo decomposition into OH and an organic radical. The decomposition of the carbonyl oxide intermediate into OH and an organic radical, is a well known reaction pathway in the gas-phase ozonation of olefins⁵⁰. In the presence of water, alcohols and carboxylic acids, this pathway is quenched and leads to the formation of hydroxyhydroperoxides (Fig 5) thus decreasing the depletion ratio. To test this hypothesis, uptake experiments were performed in participating solvents (Fig 6). However, much to our surprise, reactions in participating solvents resulted in even *higher* alkene:ozone stoichiometric ratios. While this would first indicate that the decomposition of carbonyls into OH is not responsible for higher uptake ratios, it does not rule out other sources of radicals. This also indicates that the solvent may play a significant role in the oxidation pathway.

Our second hypothesis was that free radicals needed for >1:1 stoichiometry are generated even before the alkene is added to the mixture as a result of slow reactions between ozone and organic solvents. Although gas-phase reactions of ozone with saturated hydrocarbons are exceedingly slow, with rate constants well below $10^{-20} \text{ cm}^3 \text{ s}^{-1}$

molecule⁻¹, ozone does produce measurable amounts of oxidation products when bubbled through organic solvents at room temperature. The reaction likely proceeds via hydrogen atom abstraction, and generates OH, alkyl radical, and oxygen molecule. Therefore, a small steady-state concentration of free radicals can exist in a solution through which ozone is bubbled.

In order to gauge the total OH production by ozone-solvent reactions, the reaction was performed in pure cyclohexane. Oxidation of cyclohexane by hydroxyl radical or ozone in the presence of molecular oxygen should predominately result in cyclohexanone and cyclohexanol. Bubbling 0.1% O₃/O₂ mixture through cyclohexane for 0-60 minutes did result in cyclohexanol, cyclohexanone and an additional unidentified compound detected by GC-MS (Fig. 4.7). Furthermore, the cyclohexanone yield was quantified by GC-MS as a function of oxidation time. On average, one cyclohexanone molecule is produced for every ~8 ozone molecules passed through the solution (Fig. 4.8).

Cyclohexane, n-hexadecane and nonane are considered non-participating solvents with respect to the Criegee intermediates. Our preliminary conclusion is that these solvents may be indirectly participating in the oxidation of alkenes. Our results suggest that ozone-solvent reactions may generate free radicals in quantities significant for oxidizing with small amounts of added alkenes.

Additional experiments are currently underway to determine the effect of temperature on this ozone-solvent chemistry. Since the apparent reaction stoichiometry depends on temperature and approaches the normal 1:1 alkene:ozone value at lower temperatures, we expect that the solvent-ozone reactions generating free radicals should be quenched at reduced temperatures. The low temperature reactions are being carried

out in cyclopentane (melting point: -97°C as compared to 7°C for cyclohexane). The result from these temperature-dependent experiments will hopefully be the final piece in the puzzle of unusual alkene:ozone reaction stoichiometry.

4.7 Figures.

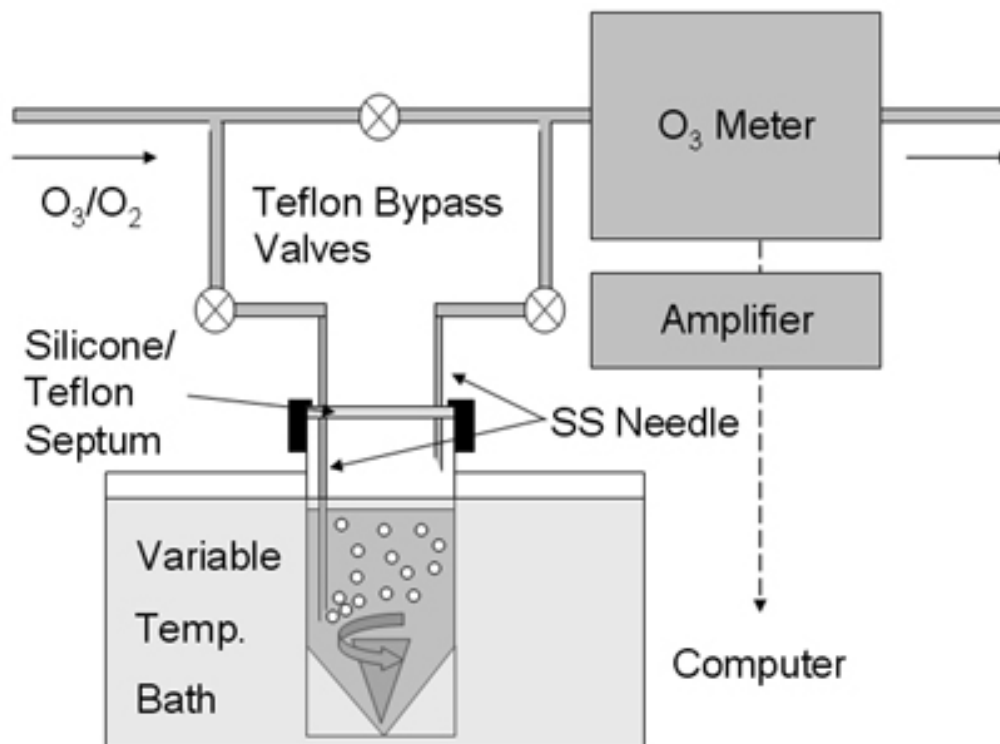


Figure 4.1: Schematics of the experimental setup used to measure the olefin-to-ozone reaction stoichiometry. The O_3/O_2 flow through the reaction vial is maintained at a steady level (20 sccm). A small amount of olefin dissolved in an inert solvent is periodically injected in the vial with a GC syringe.

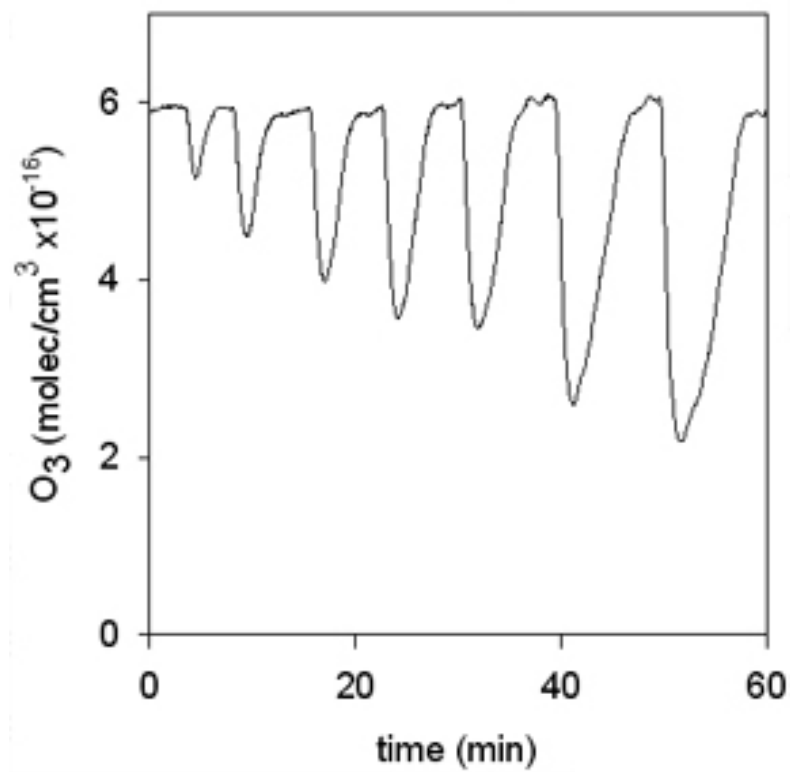


Figure 4.2: Sample experimental data showing the concentration of ozone exiting the reaction vial. Injection of a small volume of olefin into the vial leads to a reduction in ozone concentration followed by a slower recovery to the steady state level. In this case, the amount of injected olefin is monotonically increased for every new injection.

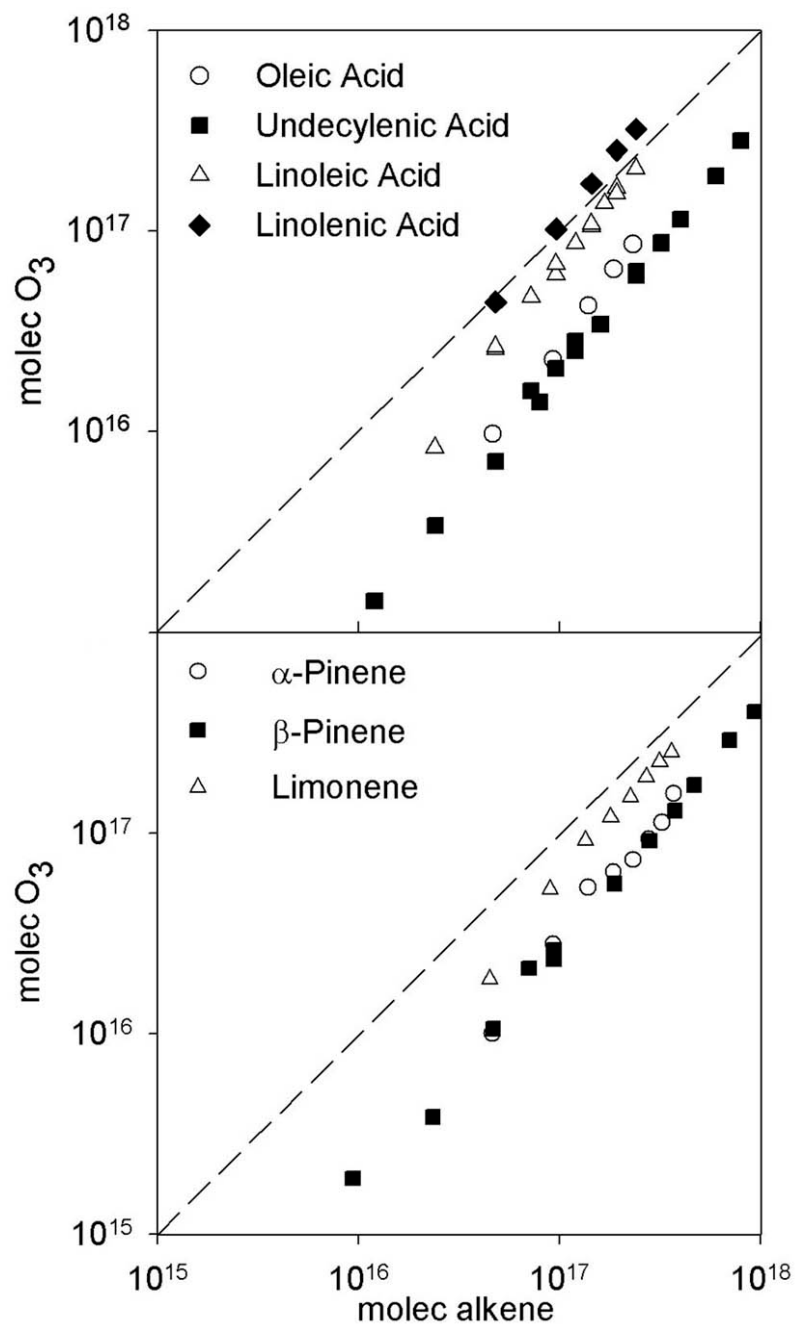


Figure 4.3: Number of ozone molecules required to completely remove double bonds in solutions of unsaturated fatty acids (top) and terpenes (bottom). The dashed line represents a 1:1 reaction. All molecules have one double bond except linoleic acid (2), limonene (2), and linolenic acid (3 double bonds).

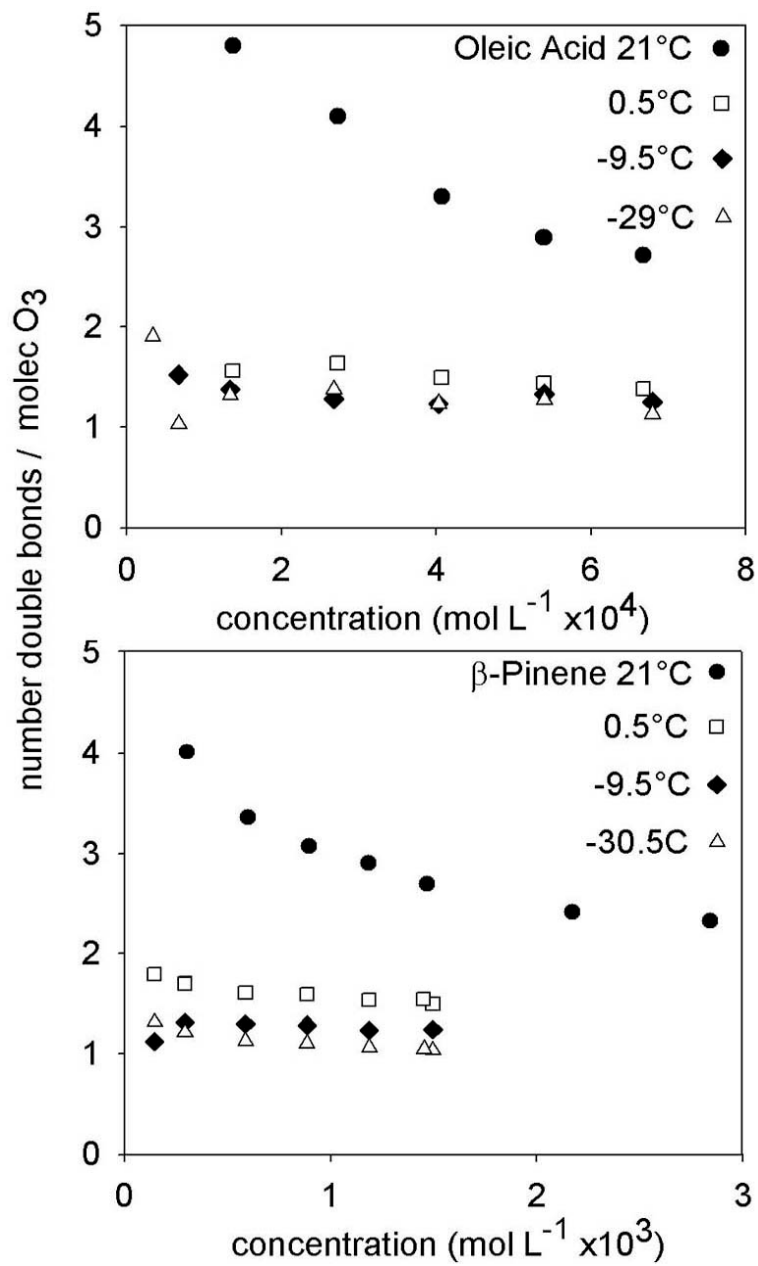


Figure 4.4.: Temperature and concentration dependence of the olefin-to-ozone stoichiometry for ozonation of oleic acid (top) and β -pinene (bottom).

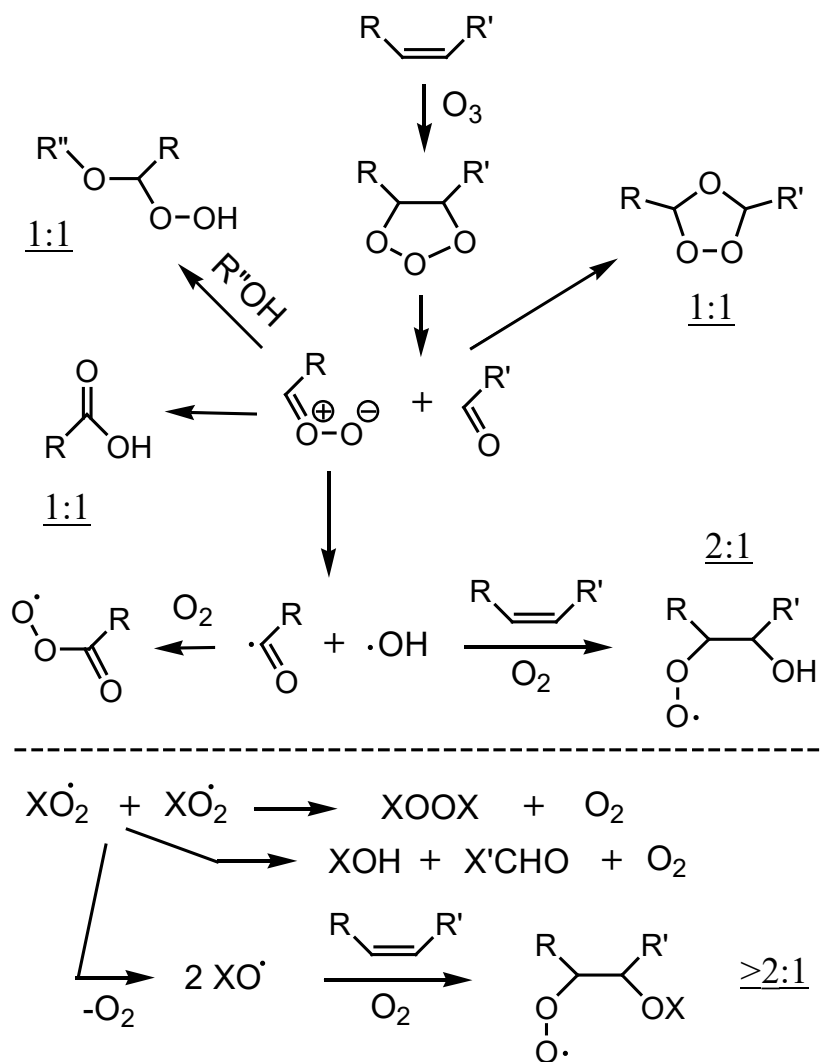


Figure 4.5: Expected double bond:ozone stoichiometry for different reaction channels is shown next to the products. For high alkene concentration, the key process is likely unimolecular decomposition of carbonyl oxide leading to generation of two free radicals. The oxidation is then propagated by self-reactions of alkylperoxyradicals. For low concentrations, radicals generated from ozone-alkane reactions dominate.

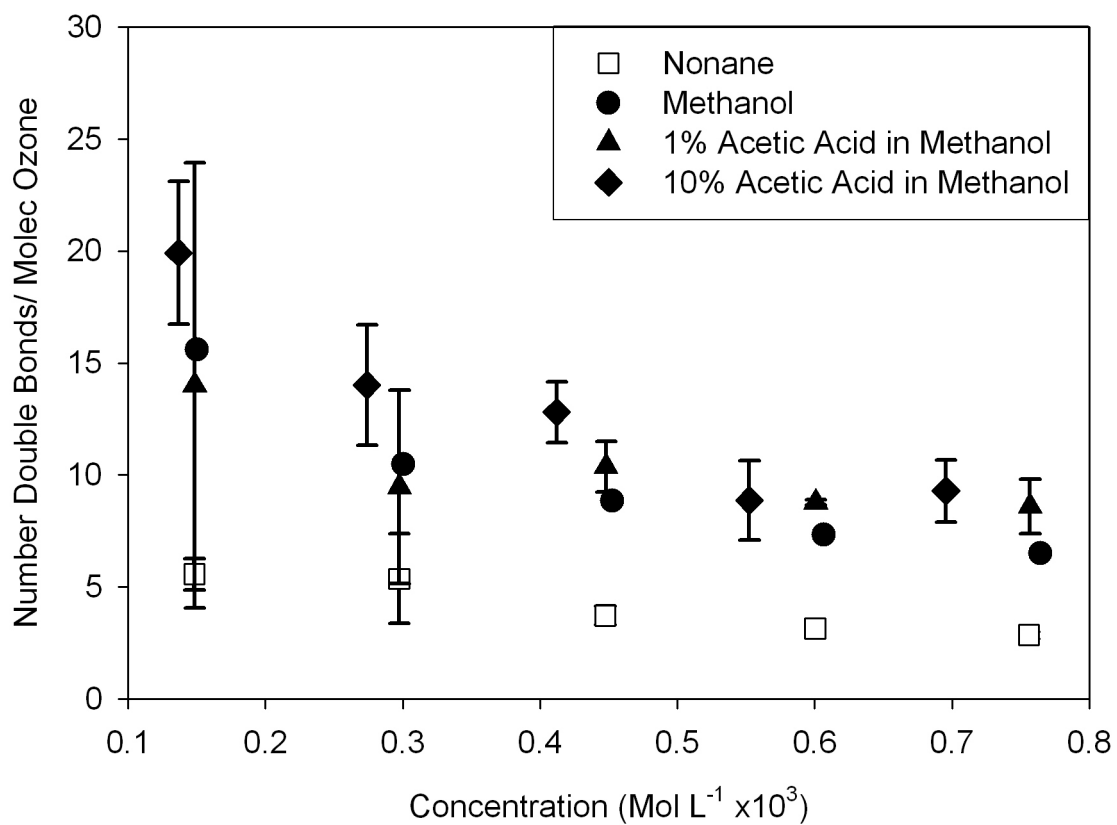


Figure 4.6: Concentration dependence of the olefin-to-ozone stoichiometry for ozonation of oleic acid in various participating solvent mixtures.

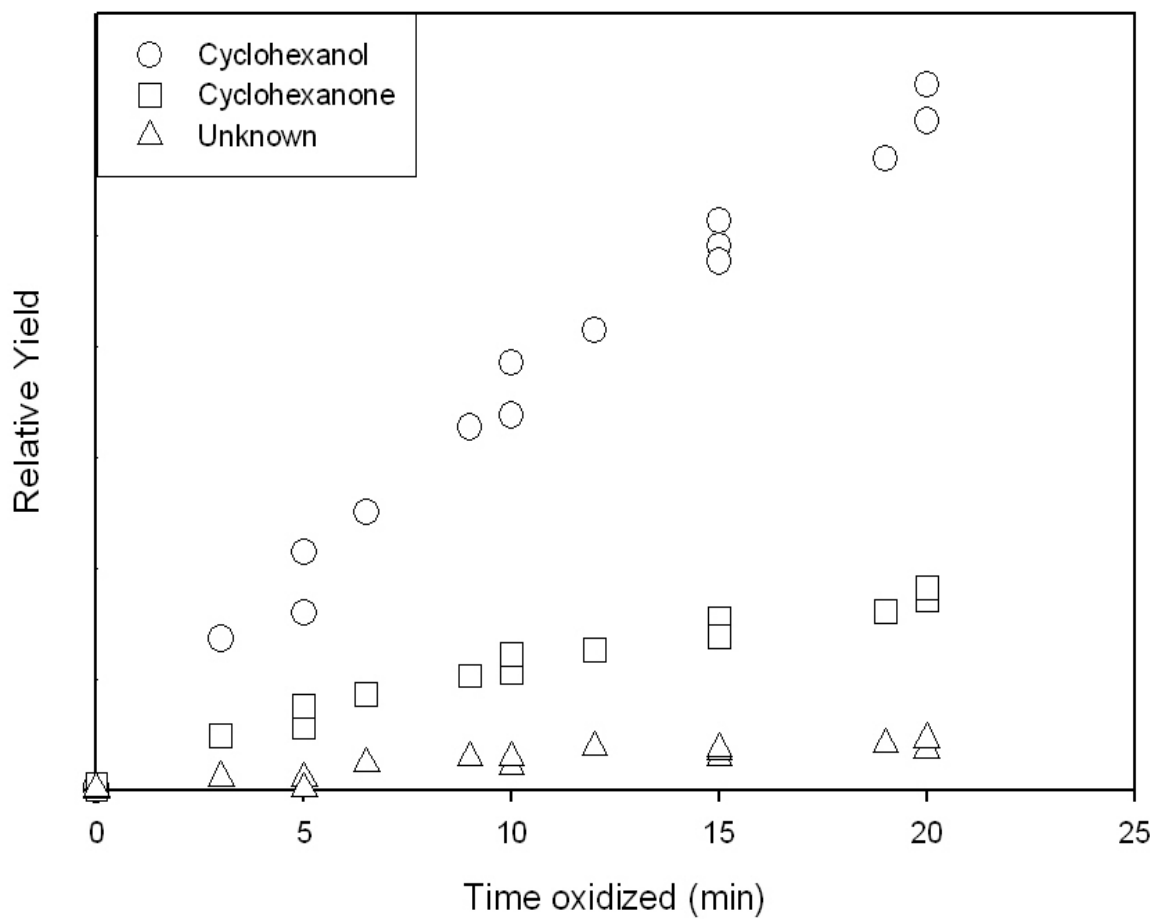


Figure 4.7: Yields of cyclohexanol, cyclohexanone and an unknown product from the ozonolysis of cyclohexane, relative to an internal standard.

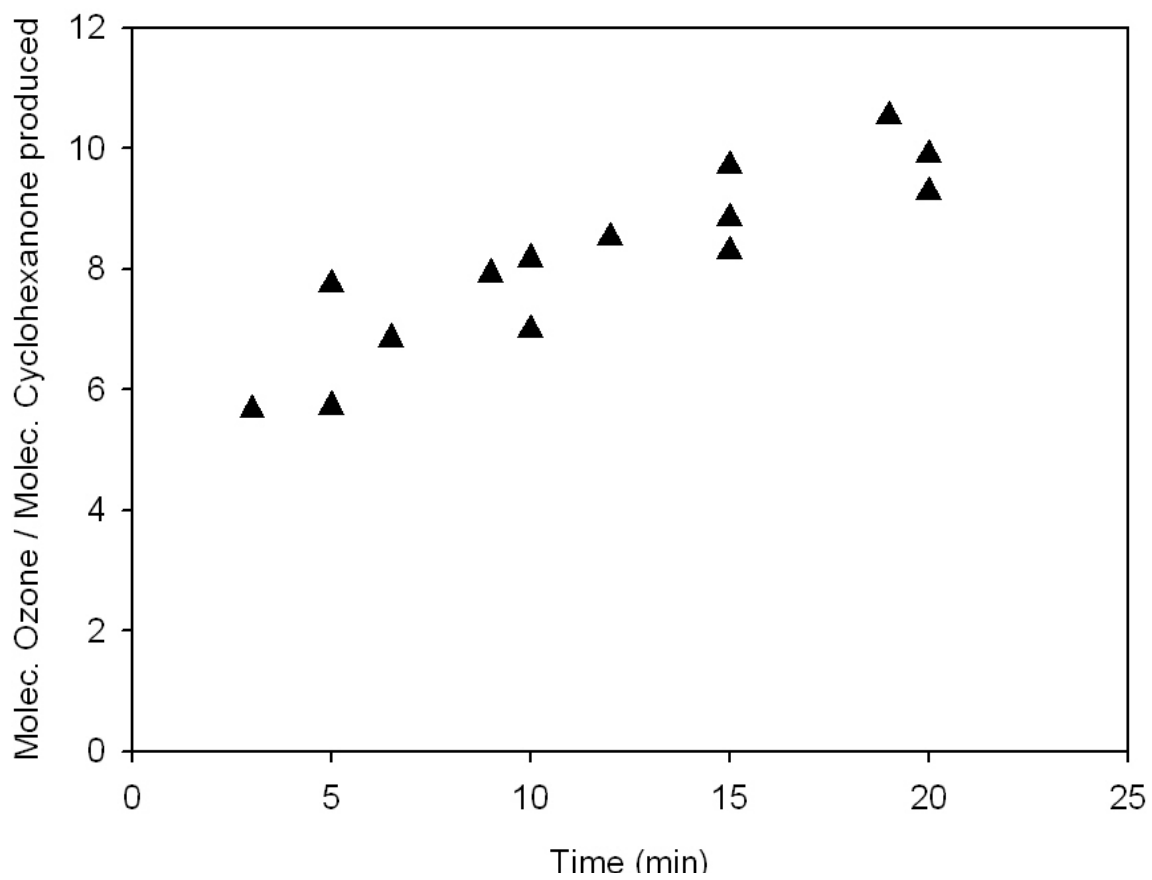


Figure 4.8: Number of ozone molecules required to produce one molecule of cyclohexanone.

REFERENCES

1. Finlayson-Pitts, B. J.; Pitts, J. N., *Chemistry of the Upper and Lower Atmosphere: Theory, Experiments, and Applications*. Academic Press: 2000; p 1040 pp.
2. Seinfeld, J. H.; Pandis, S. N., *Atmospheric Chemistry and Physics: From Air Pollution to Climate Change*. 1998; p 1326 pp.
3. Pope, C. A., III; Burnett, R. T.; Thun, M. J.; Calle, E. E.; Krewski, D.; Ito, K.; Thurston, G. D., Lung cancer, cardiopulmonary mortality, and long-term exposure to fine particulate air pollution. *J. Amer. Med. Assoc.* 2002, 287, (9), 1132-1141.
4. Penner, J. E.; Andreae, M. O.; Annegarn, H.; Barrie, L.; Feichter, J.; Hegg, D. A.; Jayaraman, A.; Leaitch, R.; Murphy, D. M.; Nganga, J.; Pitari, G., Aerosols, their Direct and Indirect Effects. In *Climate Change 2001: The Scientific Basis. Contribution of Working Group I to the Third Assessment Report of the Intergovernmental Panel on Climate Change.*, Houghton, J. T.; Ding, Y.; Griggs, D. J.; Noguer, M.; van der Linden, P. J.; Dai, X.; Maskell, K.; Johnson, C. A., Eds. Cambridge University Press: New York, USA, 2001; p 881.
5. Nathanson, G. M.; Davidovits, P.; Worsnop, D. R.; Kolb, C. E., Dynamics and Kinetics at the Gas-Liquid Interface. *J. Phys. Chem.* 1996, 100, (31), 13007-13020.
6. Garrett, B. C., Ions at the Air/Water Interface. *Science* 2004, 303, 1146-47.
7. Reid, J. P.; Sayer, R. M., Heterogeneous atmospheric aerosol chemistry: laboratory studies of chemistry on water droplets. *Chemical Society Reviews* 2003, 32, (2), 70-79.

8. Mmereki, B. T.; Donaldson, D. J., Direct observation of the kinetics of an atmospherically important reaction at the air-aqueous interface. *Journal of Physical Chemistry A* 2003, 107, (50), 11038-11042.
9. Jungwirth, P.; Tobias, D. J., Ions at the Air/Water Interface. *Journal of Physical Chemistry B* 2002, 106, (25), 6361-6373.
10. Knipping, E. M.; Lakin, M. J.; Foster, K. L.; Jungwirth, P.; Tobias, D. J.; Gerber, R. B.; Dabdub, D.; Finlayson-Pitts, B. J., Experiments and simulations of ion-enhanced interfacial chemistry on aqueous NaCl aerosols. *Science* 2000, 288, (5464), 301-306.
11. Abbatt, J. P. D., Interactions of Atmospheric Trace Gases with Ice Surfaces: Adsorption and Reaction. *Chemical Reviews* 2003, 103, (12), 4783-4800.
12. Liu, D.; Ma, G.; Levering, L. M.; Allen, H. C., Vibrational Spectroscopy of Aqueous Sodium Halide Solutions and Air-Liquid Interfaces: Observation of Increased Interfacial Depth. *Journal of Physical Chemistry B* 2004, 108, (7), 2252-2260.
13. Usher, C. R.; Michel, A. E.; Grassian, V. H., Reactions on Mineral Dust. *Chemical Reviews* 2003, 103, (12), 4883-4939.
14. Hearn, J. D.; Smith, G. D., Measuring rates of reaction in supercooled organic particles with implications for atmospheric aerosol. *Physical Chemistry Chemical Physics* 2005, 7, (13), 2549-2551.
15. Ziemann, P. J., Aerosol products, mechanisms, and kinetics of heterogeneous reactions of ozone with oleic acid in pure and mixed particles. *Faraday Discussions* 2005, 130, (Atmospheric Chemistry), 469-490.

16. Symes, R.; Sayer, R. M.; Reid, J. P., Cavity enhanced droplet spectroscopy: Principles, perspectives and prospects. *Physical Chemistry Chemical Physics* 2004, 6, (3), 474-487.
17. Broekhuizen, K.; Kumar, P. P.; Abbatt, J. P. D., Partially soluble organics as cloud condensation nuclei: Role of trace soluble and surface active species. *Geophysical Research Letters* 2004, 31, (1), L01107/1-L01107/5.
18. Petersen, P. B.; Saykally, R. J., Confirmation of enhanced anion concentration at the liquid water surface. *Chemical Physics Letters* 2004, 397, (1-3), 51-55.
19. Kanakidou, M.; Seinfeld, J. H.; Pandis, S. N.; Barnes, I.; Dentener, F. J.; Facchini, M. C.; Van Dingenen, R.; Ervens, B.; Nenes, A.; Nielsen, C. J.; Swietlicki, E.; Putaud, J. P.; Balkanski, Y.; Fuzzi, S.; Horth, J.; Moortgat, G. K.; Winterhalter, R.; Myhre, C. E. L.; Tsigaridis, K.; Vignati, E.; Stephanou, E. G.; Wilson, J., Organic aerosol and global climate modelling: A review. *Atmospheric Chemistry and Physics* 2005, 5, (4), 1053-1123.
20. Rogge, W. F.; Mazurek, M. A.; Hildemann, L. M.; Cass, G. R.; Simoneit, B. R. T., Quantification of urban organic aerosols at a molecular level: identification, abundance and seasonal variation. *Atmos. Environ., Part A* 1993, 27A, (8), 1309-30.
21. Novakov, T.; Penner, J. E., Large contribution of organic aerosols to cloud-condensation-nuclei concentrations. *Nature* 1993, 365, (6449), 823-6.
22. Murphy, D. M.; Thomson, D. S.; Mahoney, M. J., In situ measurements of organics, meteoritic material, mercury, and other elements in aerosols at 5 to 19 kilometers. *Science* 1998, 282, (5394), 1664-1669.

23. Jacobson, M. C.; Hansson, H. C.; Noone, K. J.; Charlson, R. J., Organic atmospheric aerosols: review and state of the science. *Reviews of Geophysics* 2000, 38, (2), 267-294.
24. Duce, R. A.; Mohnen, V. A.; Zimmerman, P. R.; Grosjean, D.; Cautreels, W.; Chatfield, R.; Jaenicke, R.; Ogren, J. A.; Pellizzari, E. D.; Wallace, G. T., Organic material in the global troposphere. *Reviews of Geophysics and Space Physics* 1983, 21, (4), 921-52.
25. Hildemann, L. M.; Markowski, G. R.; Cass, G. R., Chemical composition of emissions from urban sources of fine organic aerosol. *Environ. Sci. Technol.* 1991, 25, (4), 744-59.
26. Middlebrook, A. M.; Murphy, D. M.; Thomson, D. S., Observations of organic material in individual marine particles at Cape Grim during the First Aerosol Characterization Experiment (ACE 1). *Journal of Geophysical Research* 1998, 103, (D13), 16475-16483.
27. Alves, C.; Pio, C.; Duarte, A., Composition of extractable organic matter of air particles from rural and urban Portuguese areas. *Atmospheric Environment* 2001, 35, (32), 5485-5496.
28. Mochida, M.; Kitamori, Y.; Kawamura, K.; Nojiri, Y.; Suzuki, K., Fatty acids in the marine atmosphere: factors governing their concentrations and evaluation of organic films on sea-salt particles. *Journal of Geophysical Research* 2002, 107, (D17), AAC1/1-AAC1/10.

29. Liu, D.-Y.; Wenzel, R. J.; Prather, K. A., Aerosol time-of-flight mass spectrometry during the Atlanta Supersite Experiment: 1. Measurements. *Journal of Geophysical Research* 2003, 108, (D7), SOS 14/1-SOS 14/16.
30. Rudich, Y., Laboratory Perspectives on the Chemical Transformations of Organic Matter in Atmospheric Particles. *Chemical Reviews* 2003, 103, (12), 5097-5124.
31. Ellison, G. B.; Tuck, A. F.; Vaida, V., Atmospheric processing of organic aerosols. *J. Geophys. Res.* 1999, 104, (D9), 11633-11641.
32. Thomas, E. R.; Frost, G. J.; Rudich, Y., Reactive uptake of ozone by proxies for organic aerosols: Surface-bound and gas-phase products. *J. Geophys. Res.* 2001, 106, (D3), 3045-3056.
33. Moise, T.; Rudich, Y., Reactive Uptake of Ozone by Aerosol-Associated Unsaturated Fatty Acids: Kinetics, Mechanism, and Products. *Journal of Physical Chemistry A* 2002, 106, (27), 6469-6476.
34. Moise, T.; Rudich, Y., Reactive uptake of ozone by proxies for organic aerosols: Surface versus bulk processes. *J. Geophys. Res.* 2000, 105, (D11), 14667-14676.
35. Eliason, T. L.; Aloisio, S.; Donaldson, D. J.; Cziczo, D. J.; Vaida, V., Processing of unsaturated organic acid films and aerosols by ozone. *Atmospheric Environment* 2003, 37, (16), 2207-2219.
36. Smith, G.; Hauser, C.; Baer, T.; Miller, R. E.; Woods, E., III, Reactions of ozone with organic aerosols analyzed by single-particle time-of-flight mass spectrometry. *Abstracts of Papers, 222nd ACS National Meeting, Chicago, IL, United States, August 26-30, 2001* 2001, HYS-364.

37. Morris, J. W.; Davidovits, P.; Jayne, J. T.; Jimenez, J. L.; Shi, Q.; Kolb, C. E.; Worsnop, D. R.; Barney, W. S.; Cass, G., Kinetics of submicron oleic acid aerosols with ozone: a novel aerosol mass spectrometric technique. *Geophysical Research Letters* 2002, 29, (9), 71/1-71/4.
38. Wadia, Y.; Tobias, D. J.; Stafford, R.; Finlayson-Pitts, B. J., Real-Time Monitoring of the Kinetics and Gas-Phase Products of the Reaction of Ozone with an Unsaturated Phospholipid at the Air-Water Interface. *Langmuir* 2000, 16, (24), 9321-9330.
39. Lai, C. C.; Yang, S. H.; Finlayson-Pitts, B. J., Interactions of monolayers of unsaturated phosphocholines with ozone at the air-water interface. *Langmuir* 1994, 10, (12), 4637-44.
40. Rogge, W. F.; Hildemann, L. M.; Mazurek, M. A.; Cass, G. R.; Simoneit, B. R. T., Sources of fine organic aerosol. 1. Charbroilers and meat cooking operations. *Environ. Sci. Technol.* 1991, 25, (6), 1112-25.
41. Tervahattu, H.; Juhanaja, J.; Kupiainen, K., Identification of an organic coating on marine aerosol particles by TOF-SIMS. *Journal of Geophysical Research* 2002, 107, (D16), ACH18/1-ACH18/7.
42. Asad, A.; Mmereki, B. T.; Donaldson, D. J., Enhanced uptake of water by oxidatively processed oleic acid. *Atmospheric Chemistry and Physics* 2004, 4, (8), 2083-2089.
43. Knopf, D. A.; Anthony, L. M.; Bertram, A. K., Reactive Uptake of O₃ by Multicomponent and Multiphase Mixtures Containing Oleic Acid. *Journal of Physical Chemistry A* 2005, 109, (25), 5579-5589.

44. Katrib, Y.; Martin, S. T.; Hung, H.-M.; Rudich, Y.; Zhang, H.; Slowik, J. G.; Davidovits, P.; Jayne, J. T.; Worsnop, D. R., Products and Mechanisms of Ozone Reactions with Oleic Acid for Aerosol Particles Having Core-Shell Morphologies. *Journal of Physical Chemistry A* 2004, 108, (32), 6686-6695.
45. Smith, G. D.; Woods, E., III; DeForest, C. L.; Baer, T.; Miller, R. E., Reactive Uptake of Ozone by Oleic Acid Aerosol Particles: Application of Single-Particle Mass Spectrometry to Heterogeneous Reaction Kinetics. *Journal of Physical Chemistry A* 2002, 106, (35), 8085-8095.
46. Bailey, P. S., *Organic Chemistry, Vol. 39, Pt. 1: Ozonation in Organic Chemistry, Vol. 1: Olefinic Compounds*. Academic Press: 1978; p 272 pp.
47. Criegee, R., Mechanism of ozonolysis. *Angew. Chem.* 1975, 87, (21), 765-71.
48. Rickard, A. R.; Johnson, D.; McGill, C. D.; Marston, G., OH Yields in the Gas-Phase Reactions of Ozone with Alkenes. *Journal of Physical Chemistry A* 1999, 103, (38), 7656-7664.
49. Horie, O.; Moortgat, G. K., Decomposition pathways of the excited Criegee intermediates in the ozonolysis of simple alkenes. *Atmospheric Environment, Part A: General Topics* 1991, 25A, (9), 1881-96.
50. Paulson, S. E.; Chung, M. Y.; Hasson, A. S., OH Radical Formation from Gas-Phase Reaction of Ozone with Terminal Alkenes and the Relationship between Structure and Mechanism. *J. Phys. Chem. A* 1999, 103, (41), 8125-8138.
51. Kroll, J. H.; Donahue, N. M.; Cee, V. J.; Demerjian, K. L.; Anderson, J. G., Gas-Phase Ozonolysis of Alkenes: Formation of OH from Anti Carbonyl Oxides. *Journal of the American Chemical Society* 2002, 124, (29), 8518-8519.

52. Kroll, J. H.; Clarke, J. S.; Donahue, N. M.; Anderson, J. G.; Demerjian, K. L., Mechanism of HO_x Formation in the Gas-Phase Ozone-Alkene Reaction. 1. Direct, Pressure-Dependent Measurements of Prompt OH Yields. *Journal of Physical Chemistry A* 2001, 105, (9), 1554-1560.
53. Kroll, J. H.; Sahay, S. R.; Anderson, J. G.; Demerjian, K. L.; Donahue, N. M., Mechanism of HO_x formation in the gas-phase ozone-alkene reaction. 2. prompt versus thermal dissociation of carbonyl oxides to form OH. *Journal of Physical Chemistry A* 2001, 105, (18), 4446-4457.
54. Tobias, H. J.; Ziemann, P. J., Kinetics of the Gas-Phase Reactions of Alcohols, Aldehydes, Carboxylic Acids, and Water with the C₁₃ Stabilized Criegee Intermediate Formed from Ozonolysis of 1-Tetradecene. *Journal of Physical Chemistry A* 2001, 105, (25), 6129-6135.
55. Ziemann, P. J., Formation of Alkoxyhydroperoxy Aldehydes and Cyclic Peroxyhemiacetals from Reactions of Cyclic Alkenes with O₃ in the Presence of Alcohols. *Journal of Physical Chemistry A* 2003, 107, (12), 2048-2060.
56. Hasson, A. S.; Orzechowska, G.; Paulson, S. E., Production of stabilized Criegee intermediates and peroxides in the gas phase ozonolysis of alkenes. 1. Ethene, trans-2-butene, and 2,3-dimethyl-2-butene. *Journal of Geophysical Research* 2001, 106, (D24), 34131-34142.
57. Hasson, A. S.; Ho, A. W.; Kuwata, K. T.; Paulson, S. E., Production of stabilized Criegee intermediates and peroxides in the gas phase ozonolysis of alkenes. 2. Asymmetric and biogenic alkenes. *Journal of Geophysical Research* 2001, 106, (D24), 34143-34153.

58. Baker, J.; Aschmann, S. M.; Arey, J.; Atkinson, R., Reactions of stabilized Criegee intermediates from the gas-phase reactions of O₃ with selected alkenes. *International Journal of Chemical Kinetics* 2002, 34, (2), 73-85.
59. Bertram, A. K.; Ivanov, A. V.; Hunter, M.; Molina, L. T.; Molina, M. J., The reaction probability of OH on organic surfaces of tropospheric interest. *Journal of Physical Chemistry A* 2001, 105, (41), 9415-9421.
60. Zhou, X.; Gao, H.; He, Y.; Huang, G.; Bertman, S. B.; Civerolo, K.; Schwab, J., Nitric acid photolysis on surfaces in low-NO_x environments: significant atmospheric implications. *Geophysical Research Letters* 2003, 30, (23), ASC 12/1-ASC 12/4.
61. Zhou, X.; He, Y.; Huang, G.; Thornberry, T. D.; Carroll, M. A.; Bertman, S. B., Photochemical production of nitrous acid on glass sample manifold surface. *Geophysical Research Letters* 2002, 29, (14), 26/1-26/4.
62. Sumner, A. L.; Shepson, P. B., Snowpack production of formaldehyde and its effect on the Arctic troposphere. *Nature* 1999, 398, (6724), 230-233.
63. Guimbaud, C.; Grannas, A. M.; Shepson, P. B.; Fuentes, J. D.; Boudries, H.; Bottenheim, J. W.; Domine, F.; Houdier, S.; Perrier, S.; Biesenthal, T. B.; Splawn, B. G., Snowpack processing of acetaldehyde and acetone in the Arctic atmospheric boundary layer. *Atmospheric Environment* 2002, 36, (15-16), 2743-2752.
64. Domine, F.; Shepson, P. B., Air-snow interactions and atmospheric chemistry. *Science* 2002, 297, (5586), 1506-1510.
65. Zhou, X.; Beine, H. J.; Honrath, R. E.; Fuentes, J. D.; Simpson, W.; Shepson, P. B.; Bottenheim, J. W., Snowpack photochemical production of HONO: A major source

of OH in the Arctic boundary layer in springtime. *Geophysical Research Letters* 2001, 28, (21), 4087-4090.

66. Alves, C.; Carvalho, A.; Pio, C., Mass balance of organic carbon fractions in atmospheric aerosols. *Journal of Geophysical Research* 2002, 107, (D21), ICC7/1-ICC7/9.

67. Raes, F.; Bates, T.; McGovern, F.; Van Liedekerke, M., The 2nd Aerosol Characterization Experiment (ACE-2): general overview and main results. *Tellus, Series B: Chemical and Physical Meteorology* 2000, 52B, (2), 111-125.

68. Falkovich, A. H.; Schkolnik, G.; Ganor, E.; Rudich, Y., Adsorption of organic compounds pertinent to urban environments onto mineral dust particles. *Journal of Geophysical Research* 2004, 109, (D2), D02208/1-D02208/19.

69. Diamond, M. L.; Gingrich, S. E.; McCarry, B. E.; Stern, G. A.; Tomy, G., Evidence for an organic film on impervious urban and rural surfaces. *Organohalogen Compounds* 1999, 41, 343-346.

70. Tervahattu, H.; Hartonen, K.; Kerminen, V.-M.; Kupiainen, K.; Aarnio, P.; Koskentalo, T.; Tuck, A. F.; Vaida, V., New evidence of an organic layer on marine aerosols. *Journal of Geophysical Research* 2002, 107, (D7 & D8), AAC 1/1-AAC 1/9.

71. Gill, P. S.; Graedel, T. E.; Weschler, C. J., Organic films on atmospheric aerosol particles, fog droplets, cloud droplets, raindrops, and snowflakes. *Reviews of Geophysics and Space Physics* 1983, 21, (4), 903-20.

72. Donaldson, D. J.; Anderson, D., Adsorption of atmospheric gases at the air-water interface. 2. C1-C4 alcohols, acids, and acetone. *Journal of Physical Chemistry A* 1999, 103, (7), 871-876.

73. Kawamura, K., Identification of C2-C10 α -oxocarboxylic acids, pyruvic acid, and C2-C3 α -dicarbonyls in wet precipitation and aerosol samples by capillary GC and GC/MS. *Analytical Chemistry* 1993, 65, (23), 3505-11.
74. Blazso, M.; Janitsek, S.; Gelencser, A.; Artaxo, P.; Graham, B.; Andreae, M. O., Study of tropical organic aerosol by thermally assisted alkylation-gas chromatography mass spectrometry. *Journal of Analytical and Applied Pyrolysis* 2003, 68-69, 351-369.
75. Thornberry, T.; Abbatt, J. P. D., Heterogeneous reaction of ozone with liquid unsaturated fatty acids: detailed kinetics and gas-phase product studies. *Physical Chemistry Chemical Physics* 2004, 6, (1), 84-93.
76. Eliason, T. L.; Gilman, J. B.; Vaida, V., Oxidation of organic films relevant to atmospheric aerosols. *Atmospheric Environment* 2004, 38, (9), 1367-1378.
77. Hearn, J. D.; Lovett, A. J.; Smith, G. D., Ozonolysis of oleic acid particles: evidence for a surface reaction and secondary reactions involving Criegee intermediates. *Physical Chemistry Chemical Physics* 2005, 7, (3), 501-511.
78. Lai, C. C.; Finlayson-Pitts, B. J.; Willis, W. V., Formation of secondary ozonides from the reaction of an unsaturated phosphatidylcholine with ozone. *Chemical Research in Toxicology* 1990, 3, (6), 517-23.
79. Usher, C. R.; Michel, A. E.; Stec, D.; Grassian, V. H., Laboratory studies of ozone uptake on processed mineral dust. *Atmospheric Environment* 2003, 37, (38), 5337-5347.
80. Dubowski, Y.; Vieceli, J.; Tobias, D. J.; Gomez, A.; Lin, A.; Nizkorodov, S. A.; McIntire, T. M.; Finlayson-Pitts, B. J., Interaction of Gas-Phase Ozone at 296 K with

- Unsaturated Self-Assembled Monolayers: A New Look at an Old System. *Journal of Physical Chemistry A* 2004, 108, (47), 10473-10485.
81. Viececi, J.; Ma, O. L.; Tobias, D. J., Uptake and Collision Dynamics of Gas Phase Ozone at Unsaturated Organic Interfaces. *Journal of Physical Chemistry A* 2004, 108, (27), 5806-5814.
82. Sylvain, C.; Wagner, A.; Mioskowski, C., Ozone: a versatile reagent for solid phase synthesis. *Tetrahedron Letters* 1997, 38, (6), 1043-1044.
83. Vallant, T.; Kattner, J.; Brunner, H.; Mayer, U.; Hoffmann, H., Investigation of the Formation and Structure of Self-assembled Alkylsiloxane Monolayers on Silicon Using In Situ Attenuated Total Reflection Infrared Spectroscopy. *Langmuir* 1999, 15, (16), 5339-5346.
84. Cheng, S. S.; Scherson, D. A.; Sukenik, C. N., In Situ Attenuated Total Reflectance Fourier Transform Infrared Spectroscopy Study of Carboxylate-Bearing, Siloxane-Anchored, Self-Assembled Monolayers: A Study of Carboxylate Reactivity and Acid-Base Properties. *Langmuir* 1995, 11, (4), 1190-5.
85. Sagiv, J., Organized monolayers by adsorption. 1. Formation and structure of oleophobic mixed monolayers on solid surfaces. *Journal of the American Chemical Society* 1980, 102, (1), 92-8.
86. Mauersberger, K.; Hanson, D.; Barnes, J.; Morton, J., Ozone vapor pressure and absorption cross-section measurements: introduction of an ozone standard. *J. Geophys. Res.* 1987, 92, 8480.
87. Busch, K. W.; Busch, M. A., Introduction to cavity-ringdown spectroscopy. *ACS Symp. Ser.* 1999, 720, (Cavity-Ringdown Spectroscopy), 7-19.

88. Gauss, J.; Cremer, D., The IR spectra of carbonyl oxide and dioxirane: a theoretical investigation at a correlated level. *Chemical Physics Letters* 1987, 133, (5), 420-4.
89. Cremer, D.; Gauss, J.; Kraka, E.; Stanton, J. F.; Bartlett, R. J., A CCSD(T) investigation of carbonyl oxide and dioxirane. Equilibrium geometries, dipole moments, infrared spectra, heats of formation and isomerization energies. *Chemical Physics Letters* 1993, 209, (5-6), 547-56.
90. Stanton, J. F.; Lopreore, C. L.; Gauss, J., The equilibrium structure and fundamental vibrational frequencies of dioxirane. *Journal of Chemical Physics* 1998, 108, (17), 7190-7196.
91. Crehuet, R.; Anglada, J. M.; Cremer, D.; Bofill, J. M., Reaction Modes of Carbonyl Oxide, Dioxirane, and Methylenebis(oxy) with Ethylene: A New Reaction Mechanism. *Journal of Physical Chemistry A* 2002, 106, (15), 3917-3929.
92. Sharpe, S. Vapor phase infrared spectral library
(<https://secure.pnl.gov/nsd/nsd.nsf/Welcome>).
<https://secure.pnl.gov/nsd/nsd.nsf/Welcome>
93. Docherty, K. S.; Wu, W.; Lim, Y. B.; Ziemann, P. J., Contributions of Organic Peroxides to Secondary Aerosol Formed from Reactions of Monoterpenes with O₃. *Environmental Science and Technology* 2005, 39, (11), 4049-4059.
94. Neeb, P.; Sauer, F.; Horie, O.; Moortgat, G. K., Formation of hydroxymethyl hydroperoxide and formic acid in alkene ozonolysis in the presence of water vapor. *Atmospheric Environment* 1997, 31, (15), 1417-1423.

95. Kalberer, M.; Paulsen, D.; Sax, M.; Steinbacher, M.; Dommen, J.; Prevot, A. S. H.; Fisseha, R.; Weingartner, E.; Frankevich, V.; Zenobi, R.; Baltensperger, U., Identification of polymers as major components of atmospheric organic aerosols. *Science* 2004, 303, (5664), 1659-62.
96. Jang, M.; Czoschke Nadine, M.; Lee, S.; Kamens Richard, M., Heterogeneous atmospheric aerosol production by acid-catalyzed particle-phase reactions. *Science* 2002, 298, (5594), 814-7.
97. Gao, S.; Keywood, M.; Ng, N. L.; Surratt, J.; Varutbangkul, V.; Bahreini, R.; Flagan, R. C.; Seinfeld, J. H., Low-Molecular-Weight and Oligomeric Components in Secondary Organic Aerosol from the Ozonolysis of Cycloalkenes and α -Pinene. *Journal of Physical Chemistry A* 2004, 108, (46), 10147-10164.
98. Gao, S.; Ng, N. L.; Keywood, M.; Varutbangkul, V.; Bahreini, R.; Nenes, A.; He, J.; Yoo, K. Y.; Beauchamp, J. L.; Hodyss, R. P.; Flagan, R. C.; Seinfeld, J. H., Particle phase acidity and oligomer formation in secondary organic aerosol. *Environmental Science and Technology* 2004, 38, (24), 6582-6589.
99. Tolocka, M. P.; Jang, M.; Ginter, J. M.; Cox, F. J.; Kamens, R. M.; Johnston, M. V., Formation of Oligomers in Secondary Organic Aerosol. *Environmental Science and Technology* 2004, 38, (5), 1428-1434.
100. Neeb, P.; Moortgat, G. K., Formation of OH Radicals in the Gas-Phase Reaction of Propene, Isobutene, and Isoprene with O₃: Yields and Mechanistic Implications. *Journal of Physical Chemistry A* 1999, 103, (45), 9003-9012.

101. Fenske, J. D.; Hasson, A. S.; Paulson, S. E.; Kuwata, K. T.; Ho, A.; Houk, K. N., The Pressure Dependence of the OH Radical Yield from Ozone-Alkene Reactions. *Journal of Physical Chemistry A* 2000, 104, (33), 7821-7833.
102. Hawkins, M.; Kohlmeier, C. K.; Andrews, L., Matrix infrared spectra and photolysis and pyrolysis of isotopic secondary ozonides of ethylene. *Journal of Physical Chemistry* 1982, 86, (16), 3154-66.
103. Andrews, L.; Kohlmeier, C. K., Infrared spectra and photochemistry of the primary and secondary ozonides of propene, trans-2-butene, and methylpropene in solid argon. *Journal of Physical Chemistry* 1982, 86, (23), 4548-57.
104. Griesbaum, K.; Volpp, W.; Greinert, R.; Greunig, H. J.; Schmid, J.; Henke, H., Ozonolysis of tetrasubstituted ethylenes, cycloolefins, and conjugated dienes on polyethylene. *Journal of Organic Chemistry* 1989, 54, (2), 383-9.
105. Khachatryan, L.; Haas, Y.; Pola, J., Laser-induced decompositions of 3,5-dimethyl-1,2,4-trioxolane (secondary butene-2-ozonide) in the gas phase. *Perkin Transactions* 1997, 2, (6), 1147-1151.
106. Schauer, J. J.; Kleeman, M. J.; Cass, G. R.; Simonei, B. R. T., Measurement of emissions from air pollution sources. 4. C1-C27 organic compounds from cooking with seed oils. *Environmental science & technology* 2002, 36, (4), 567-75.
107. Presto, A. A.; Huff Hartz, K. E.; Donahue, N. M., Secondary Organic Aerosol Production from Terpene Ozonolysis. 1. Effect of UV Radiation. *Environmental Science and Technology* 2005, 39, (18), 7036-7045.
108. Seinfeld, J. H., Private communications. *Private communications* 2005, (D7).

109. Sander, S. P.; Friedl, R. R.; Golden, D. M.; Kurylo, M. J.; Huie, R. E.; L., O. V.; Moortgat, G. K.; Ravishankara, A. R.; Kolb, C. E.; Molina, M. J.; Finlayson-Pitts, B. J., *Chemical Kinetics and Photochemical Data for Use in Stratospheric Modeling: Evaluation Number 14*. JPL Publication 02-25 ed.; Jet Propulsion Laboratory: Pasadena, 2003.
110. Gomez, A.; Walser, M.; Park, J.; Lin, A.; Britigan, N.; Nizkorodov, S. A., Photolysis of oxidized undecylenic acid studied with infrared cavity-ring down spectroscopy. *J. Phys. Chem. A* 2005, accepted.
111. McIntire, T. M.; Lea, A. S.; Gaspar, D. J.; Jaitly, N.; Dubowski, Y.; Li, Q.; Finlayson-Pitts, B. J., Unusual aggregates from the oxidation of alkene self-assembled monolayers: a previously unrecognized mechanism for SAM ozonolysis? *Physical Chemistry Chemical Physics* 2005, 7, (20), 3605-3609.
112. Disselkamp, R. S.; Dupuis, M., A temperature-dependent study of the ozonolysis of propene. *Journal of Atmospheric Chemistry* 2001, 40, (3), 231-245.
113. Kuczkowski, R. L., The structure and mechanism of formation of ozonides. *Chemical Society Reviews* 1992, 21, (1), 79-83.
114. Fajgar, R.; Vitek, J.; Haas, Y.; Pola, J., Observation of secondary 2-butene ozonide in the ozonation of trans-2-butene in the gas phase. *Tetrahedron Letters* 1996, 37, (19), 3391-3394.
115. Griesbaum, K.; Miclaus, V.; Jung, I. C., Isolation of Ozonides from Gas-Phase Ozonolysis of Terpenes. *Environmental Science and Technology* 1998, 32, (5), 647-649.
116. Fajgar, R.; Vitek, J.; Haas, Y.; Pola, J., Formation of secondary ozonides in the gas phase low-temperature ozonation of primary and secondary alkenes. *Journal of the*

Chemical Society, Perkin Transactions 2: Physical Organic Chemistry 1999, (2), 239-248.

117. Dreyfus, M. A.; Tolocka, M. P.; Dodds, S. M.; Dykins, J.; Johnston, M. V., Cholesterol Ozonolysis: Kinetics, Mechanism, and Oligomer Products. *Journal of Physical Chemistry A* 2005, 109, (28), 6242-6248.

118. Hung, H.-M.; Katrib, Y.; Martin, S. T., Products and Mechanisms of the Reaction of Oleic Acid with Ozone and Nitrate Radical. *Journal of Physical Chemistry A* 2005, 109, (20), 4517-4530.

119. Griesbaum, K.; Hilss, M.; Bosch, J., Ozonides of mono-, bi- and tricyclic terpenes. *Tetrahedron* 1996, 52, (47), 14813-14826.

120. Schauer, J. J.; Kleeman, M. J.; Cass, G. R.; Simoneit, B. R. T., Measurement of Emissions from Air Pollution Sources. 1. C1 through C29 Organic Compounds from Meat Charbroiling. *Environmental Science and Technology* 1999, 33, (10), 1566-1577.

121. Hoffmann, T.; Odum, J. R.; Bowman, F.; Collins, D.; Klockow, D.; Flagan, R. C.; Seinfeld, J. H., Formation of organic aerosols from the oxidation of biogenic hydrocarbons. *Journal of Atmospheric Chemistry* 1997, 26, (2), 189-222.

122. Jang, M.; Kamens, R. M., Thermodynamic Approach Using Group Contribution Methods to Model the Partitioning of Semivolatile Organic Compounds on Atmospheric Particulate Matter. *Environmental Science and Technology* 1997, 31, (10), 2805-2811.

123. Griffin, R. J.; Cocker, D. R., III; Flagan, R. C.; Seinfeld, J. H., Organic aerosol formation from the oxidation of biogenic hydrocarbons. *Journal of Geophysical Research, [Atmospheres]* 1999, 104, (D3), 3555-3567.

124. Iinuma, Y.; Boge, O.; Gnauk, T.; Herrmann, H., Aerosol-chamber study of the α -pinene/O₃ reaction: influence of particle acidity on aerosol yields and products. *Atmospheric Environment* 2004, 38, (5), 761-773.
125. Calvert, J. G.; Atkinson, R.; Becker, K. H.; Kamens, R. M.; Seinfeld, J. H.; Wallington, T. H.; Yarwood, G., *The Mechanisms of Atmospheric Oxidation of the Aromatic Hydrocarbons*. 2001; p 464 pp.
126. Schank, K.; Marson, C.; Heisel, T.; Martens, K.; Wagner, C., Surprising results during the re-investigation of the formation and decomposition of triptene ozonide. *Helvetica Chimica Acta* 2000, 83, (12), 3312-3332.

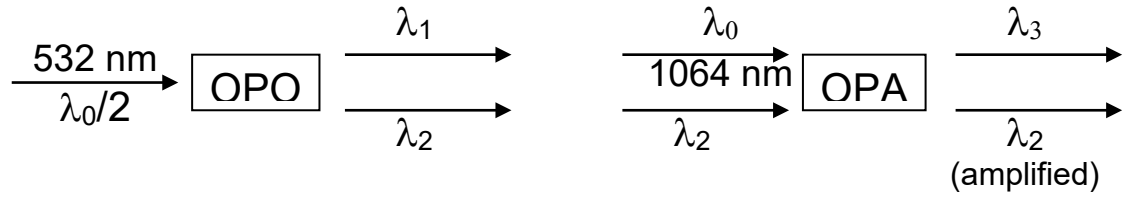
Appendix A

CRDS System in Detail

A.1 Lasers and Optics

At the root of the CRDS system (Fig A.1) is a seeded, 1064 nm pulsed Continuum Power Light 8000 Precision II 20 Hz Nd:YAG laser. The laser is capable of generating 20 watts of power in seeded mode. This power is tuned down to the OPO/OPA input power specifications of 10 to 11 watts by delaying the amplifier flash lamps with respect to the Q-Switch. The Q-Switch timing is set by the controller at 145 μs which is optimized for maximum overlap with the oscillator flash lamps. The flash lamp voltages are set to 1.31 kV with the oscillator and amplifier flash lamps delayed to 130 and 110 μs respectively on the main power supply dials.

The 1064 nm radiation pumps a Laser Vision OPO/OPA which provides tunable near IR. The OPO/OPA laser is tunable from 712 to 880 nm (λ_1) and 1350 to 5000 nm (λ_3), and outputs a 8 ns, ~ 10 mJ pulse with 0.1 cm^{-1} resolution (λ_3). From the OPA, λ_3 (NIR) is filtered from λ_2 and residual λ_0 with a polarizer, and is steered through irises to the CRDS cavity by gold-coated mirrors. A small fraction of the light is reflected to an optoacoustic cell with a CaF_2 window.



The OPO wavelengths are related as followed:

$$\frac{2}{\lambda_0} = \frac{1}{\lambda_1} + \frac{1}{\lambda_2}$$

The OPA wavelengths are related as followed:

$$\frac{1}{\lambda_0} = \frac{1}{\lambda_2} + \frac{1}{\lambda_3}$$

From these equations, we get

$$\nu_3 (cm^{-1}) = 10^7 (nm/cm) \times \left(\frac{1}{\lambda_1 (nm)} - \frac{1}{\lambda_0 (nm)} \right) \quad \lambda_0(\text{measured})=1064.09 \text{ nm}$$

The OPO/OPA motor positions are calibrated by observing the back reflection of λ_1 with an Ångstrom wave meter. λ_0 was also measured by an Ångstrom wave meter from scattered light from the Nd-YAG laser beam.

A.2 Optoacoustic Cell

An optoacoustic cell is operated in parallel with the CRDS to help calibrate and identify products in the absorption spectrum taken by the CRDS (see Fig 2.5 and 3.2). The cell is made up of a 1" × 3" cylindrical cavity with CaF₂ windows. It is outfitted with a hearing-aid microphone mounted in the middle of the cell, and an amplification circuit. The cell is normally filled with approximately 1 torr of formic acid vapor and 9 torr of buffer gas (e.g., He). Formic acid is chosen because it will be one of the gas-phase products of photolysis of organic aerosol particles; however other gases can also be used such as formaldehyde, methane, or water vapor.

A.3 IR CRDS Cavity

The CRDS setup has gone through two revisions where the central body was completely changed (Fig A.2). In the first incarnation, the body was all stainless steel and had a total volume of about 4 L. It was equipped with a rotating platter to minimize bleaching for photolysis experiments. Photolysis experiments were performed using an Oriol UV Lamp and either a cutoff filter ($\lambda > 295\text{nm}$) or a monochromator, and directing the output through a CaF₂ window on the top of the chamber. Gas reactants were admitted through ports on the top flange and the chamber was pumped through a sidearm. Its large volume and surface area caused problems with residence times and surface adsorption.

The second generation chamber improved upon many of the design features of the original chamber. The central body was replaced with an interchangeable 16" × 3/4" OD quartz tube. This new body minimized the total volume and surface area. Particles collected on filter paper, thin liquid films, SAMs and SAMs on SiO₂ particles could all be placed on or within the quartz tube. Since the whole central chamber is made of quartz, UV-photolysis could be directly performed through the tube. Oxidation reactions were performed by flowing a reactant gas through one of the inlet ports (#12) and the cell was pumped out through a port on the other end (#17) of the chamber allowing unidirectional product flow. Gas phase products from chemical and photochemical reactions are now constrained to the optical path of the CRDS increasing the effective sensitivity and allowing possible measurements of intermediates of reactions.

Consistent with both designs are the optics and sidearm adjusters. The CRDS optics consists of a pair Los Gatos Research 99.98% reflective mirrors optimized for 3300 nm, having a 0.8" OD, a 6 m radius of curvature and 60 cm spacing between them. These mirrors are ideal for looking at C-H stretching vibrations. To keep the mirrors clean of particles, a constant flow of N₂ was passed over both mirrors through ports #8. Each sidearm (stainless steel bellows) is fitted with an MDC model FGC-275 X-Y gimbal mount. The micrometer adjusters allow for fine tuning of the optical cavity. Components for the CRDS chamber include:

CRDS Version 1

1. 1" diameter Quartz window (UV Port)

2. NPT→1/4" Swagelock (Reactant Inlet)
3. SS ISO-100 blank flange: machined for 1 & 2
4. SS 5 arm cross. Top and bottom are ISO-100. Side arms are 6" CF. 5th arm (not shown) is a DN 40 KF connection for pumping.
5. SS 6" CF→2.75" CF reducer
6. MDC Standard Gimbal FGC-275-M
7. SS 3" Bellow with 2.75" CF
8. SS Double sides 2.75" CF with 1/8" NPT purge port
9. 0.8" CRDS mirror
10. SS 2.75" CF blank flange machined for CRDS mounting (see drawing below)
11. Machined mount
12. Belt drive gear for platter rotation via motor (not shown)
13. Rotary Feedthrough
14. 3" OD sample platter

CRDS Version 2

15. 16" × 3/4" Quartz tube
16. 3/4" Ultra-torr union
17. 3/4" OD SS tube welded through 2.75" CF machined flange. Total length 3.5"
18. 1/4" ports for pumping/Pressure gauge (100 torr Baratron)
19. Machined top cap for mount
20. Machined mount base
21. 1/4" ports for reactant gases

Note: CF flanges use fluoropolymer gaskets instead of copper.

A.4 Alignment

The CRDS requires two different types of alignment for the cavity depending on whether there are minor alignment issues (such as changing the cell pressure) or major alignment issues such as those that arise when replacing the CRDS mirrors after cleaning. These two processes will be outlined independently.

Major alignment—CRDS signal on the oscilloscope appears as a sharp spike < 1 μ s wide or is not visible at all. These issues require the installation of optional mirrors M3 and M4. Using only M3, the HeNe laser is aligned to the center of I1. Next using only M4, align the HeNe through the center of I2. Repeat this iterative process till the HeNe passes through the center of both I1 and I2. With only the right CRDS mirror (closest to the detector) installed, adjust the right CRDS mirror using the X-Y micrometers till the back reflection overlaps the primary HeNe reflection on M2. Install the left CRDS mirror and adjust its back reflection to center the primary reflection on M4 using only the X-Y micrometers on the left sidearm. Remove the temporary mirror and proceed to minor alignment corrections.

Minor alignment—CRDS signal of the empty cavity appears as either a multi order exponential or the early time window appears as saturated signal. These issues require M1 and M2 adjustments and/or left and right X-Y micrometer adjustments and/or reduction of input IR power for detector saturation. First close I1 and I2 to approximately 3mm diameter. Using M1 and M2, maximize the signal intensity on the

oscilloscope. Next use the micrometers to carefully align the cavity till you observe a ring-down signal. If you cannot achieve an exponential decay even with careful adjustments on via the micrometers, use small adjustments on M1 and M2 till you get an exponential decay. Follow up by further adjusting the micrometers. The lens in front of the detector may also need adjusting if the trace is fuzzy. This increases the S/N but does not change the average ring-down time.

A.5 Photolysis

Photolysis experiments were performed using an Oriel UV Lamp system using a Xe lamp and either a cutoff filter ($\lambda > 295$ nm) or an Oriel monochromator, and directing the output through either a CaF₂ window on the top of the chamber (CRDS v1) or directly through the quartz chamber (CRDS v2). Calibration of monochromatic light intensity was performed using a PowerMax PM30V1 thermopile.

A.6 Ozone Generation

Ozone is produced with a corona discharge ozone generator which is supplied with UHP oxygen via a flow controller. Transmission is via Teflon tubing with a glass/Teflon valve on the CRDS inlet. Ozone concentrations are measured using an Hg-lamp photometer (assuming $\sigma_{253.65\text{nm}}=1.136\times 10^{-17}$ cm²). Without dilutions, ozone can be supplied at concentrations from approximately 300 ppm up to 1% at 1atm. Because the

CRDS is operated at low pressure and reactant gas is diluted by purge gas, actual oxidation occurs on at 10^{13} to 10^{15} O₃ molec/cm³.

A.7 Detector

IR laser pulses that leak out of the CRDS cavity are focused onto a liquid nitrogen cooled, Judson Technology InSb detector (> 5 MHz bandwidth) by a CaF₂ lens. Detector sensitivity for the 60° FOV version used, is given in figure A.3 The detector signal is then amplified with a fast, low-noise circuit and sent to the oscilloscope for waveform capture which is analyzed in real time by a Labview program. For weak detection signals, an optional amplifier can be used. It is based on a Burr-Brown OPA637 IC with a bandwidth of 80 Mhz and a gain of 10.

A.8 Triggering

Triggering for the CRDS system is diagramed in figure A.4. The data acquisition is initially triggered by the Q-switch fixed synch output of the Nd:YAG. This pulse is sent to the DG535 delay generator, which converts it into several TTL-compatible trigger pulses with individually controllable delays. They trigger the SRS 250 boxcar averager, SRS 245 computer interface and the LeCroy oscilloscope. The optoacoustic signal is sent to the SRS 250 with a gate set up to average the pulse signal, and then sent to the SRS 245 and outputted to a computer via GPIB for data processing. The CRDS detector signal is sent to the oscilloscope where waveforms are captured and also sent via

GPIB to the computer. A custom Labview program was written to control the laser, data acquisition, and processing

Normal DG535 Digital Delay/Pulse Generator settings:

Ext Trigger: Thr = + 0.25 V; R = 50 ohm; (falling edge)

To: high Z; TTL; normal

A: A = T_o + 0; high Z; TTL, normal; output to

B: B=T_o + 0.00055 s; high Z; TTL; normal

SR250 settings:

Trigger: Ext.

Delay: 130 ns

Width: 150 μs*

Sensitivity: 0.1 V, filter = AC

Averaging: Last

*The SR250 was modified for wide gate operation by adding a 0.33 μF capacitor in parallel with C127 increasing the base gate-width value from 3 to 30 μs.

Connections:

Optoacoustic Out → SRS 250 Signal

CRDS Detector → Oscilloscope Ch1

SRS 250 Last Sample → SRS 245 Analog Chan1

SRS 250 Signal Out → Oscilloscope Ch. 2

SRS 535 To → Oscilloscope Ch. 4 (trigger)

SRS 535 Channel A → SRS 250 Trigger

SRS 535 Channel B → SRS 245 Digital Sync Ch. 1

SRS 245 → GPIB out to computer

Oscilloscope → GPIB to computer

A.9 GUI

System controls and data processing are performed via an in-house designed LabView program (Fig A.5). The program controls both the rate and scanning speed of the OPO as well as saving individual wave forms and calculating ringdown time based on user defined parameters.. Primary GUI controls are as follows:

- Speed—Sets the OPO scanning speed of λ_1 in nm/s
- Red/Blue—Sets the direction of scanning for λ_1
- Scanning mode—Select either scanning or free run (fixed wavelength). In free run, the data acquisition works but no actual laser scanning is done.
- Triggers per point—number of laser pulses used to average a waveform (normally set to 20)
- Starting point offset—Determines the starting point for exponential fitting

- Length to fit—total number of points after the starting point, to use for calculating exponential fit (normally 500 for weak signals, but can be as low as 200 when absorption is expected to be strong*)

*Because the laser line width is in some cases larger than the rotational line widths of the absorbing species, the CRDS will behave non-linearly. This manifests itself as a multi-order exponential decay. Fitting the exponential decay to an early time window and over a shorter time period is empirically found to result in a more linear response to the absorber's concentration. Typically, the starting point offset will be approximately 50 points after the laser pulse ($t = 0$) and the fit length is limited to 0.5 to 1 of the empty-cavity decay time. The trade-off for the increased linearity is a slightly higher noise level in fitting.

A.10 Figures

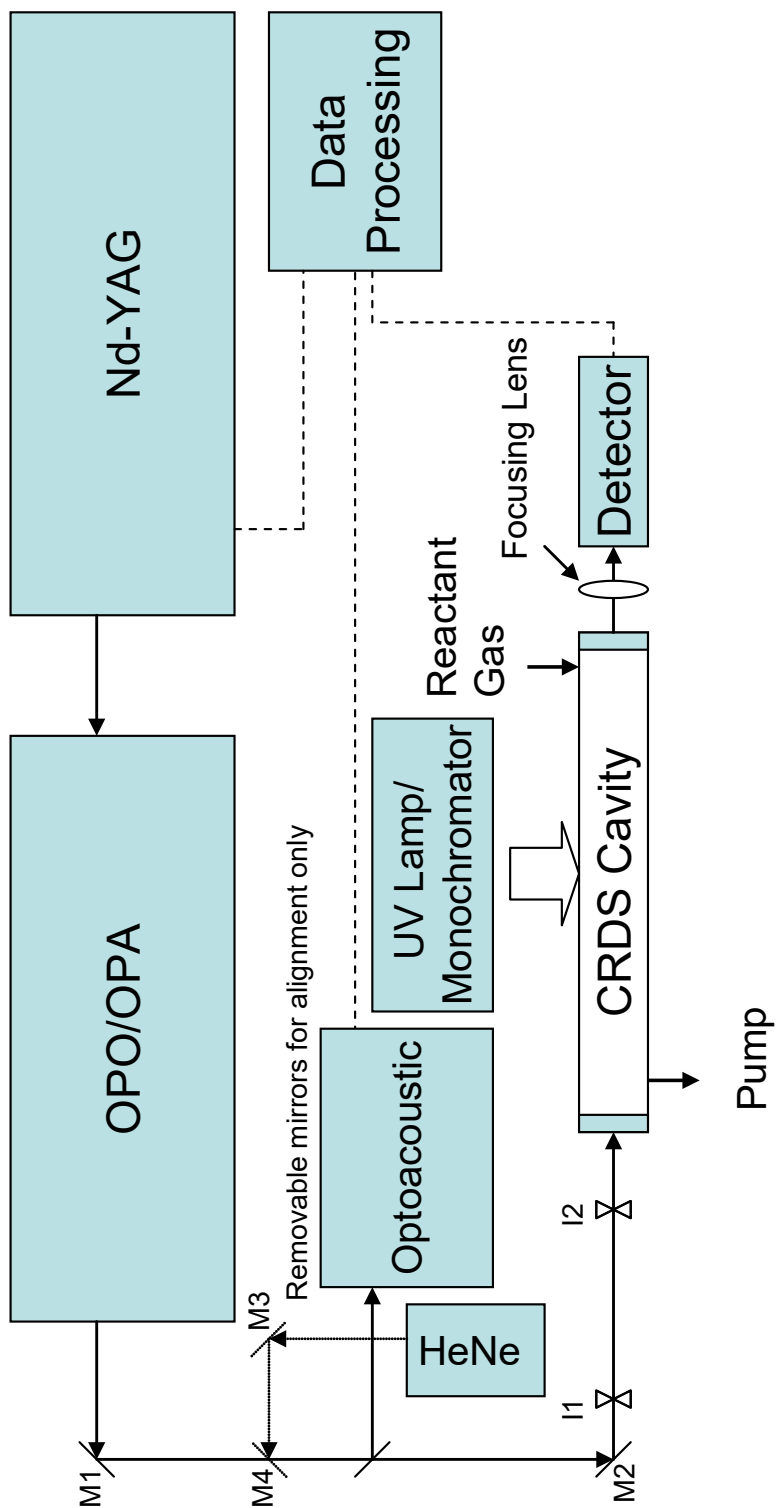


Figure A.1: Diagram of the IR CRDS system.

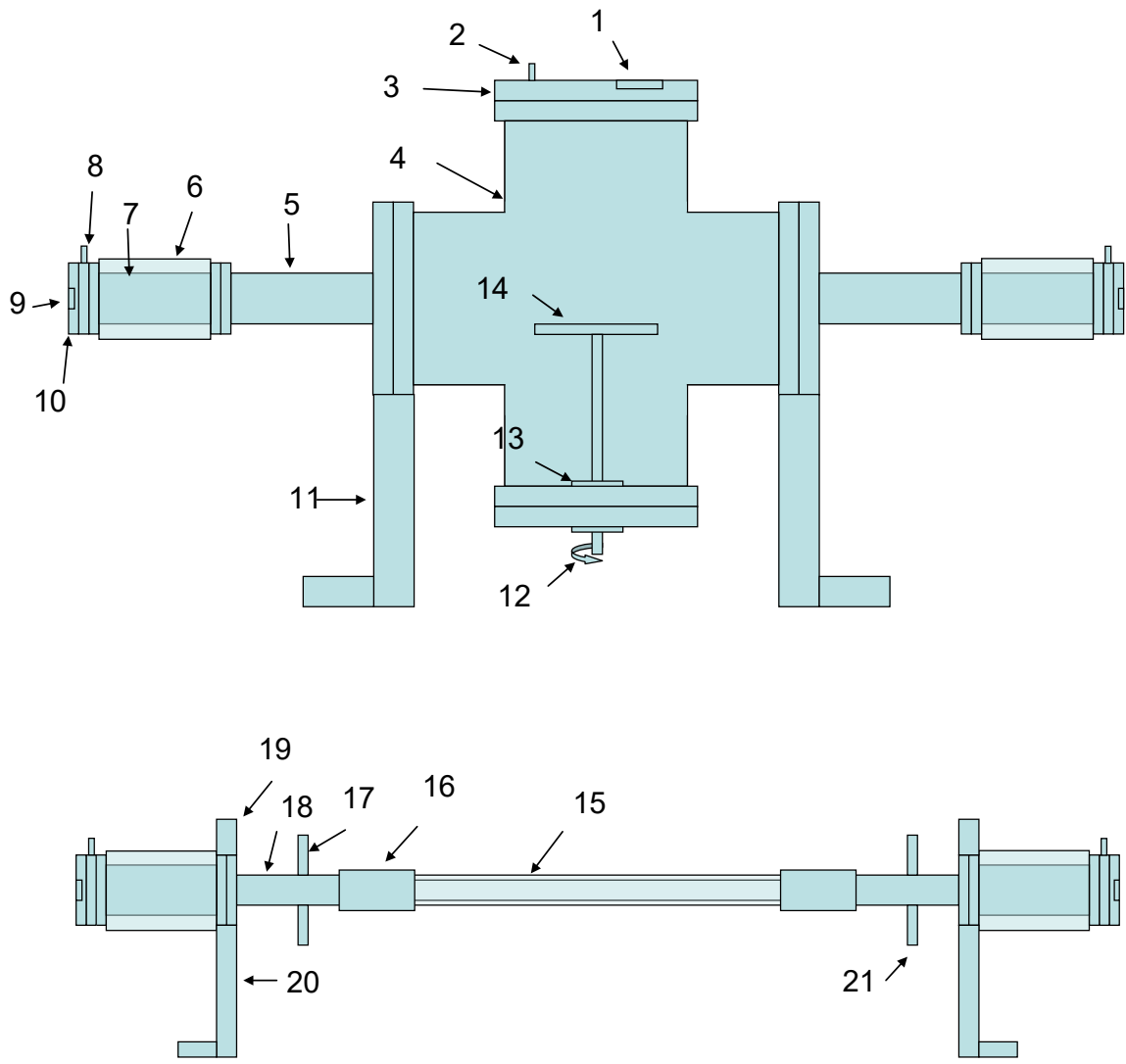


Figure A.2: Version 1 CRDS (top) and version 2 CRDS (bottom).

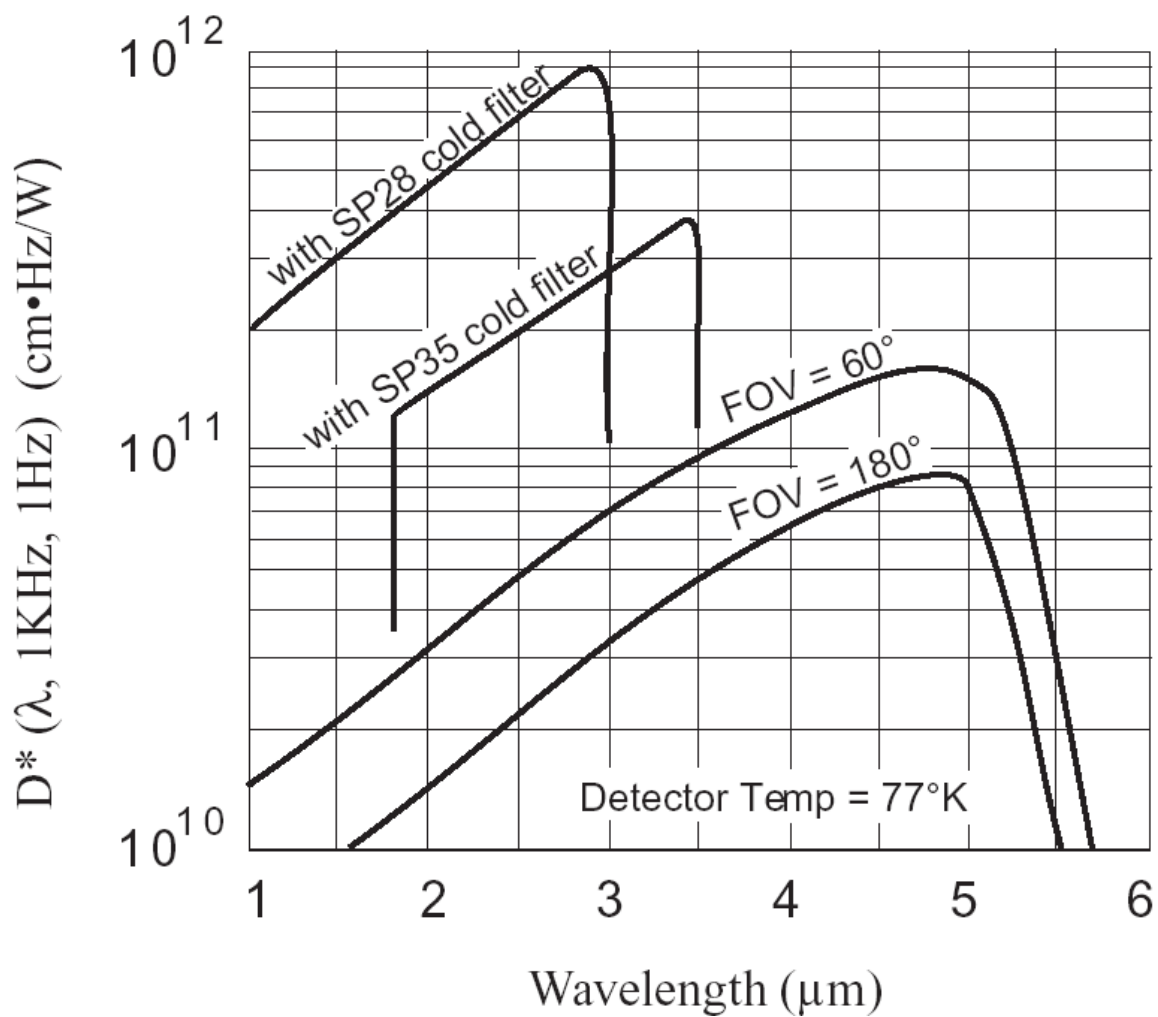


Figure A.4: Detection sensitivity for the CRDS detector. Detector is operated without a cold filter and has a 60° FOV.

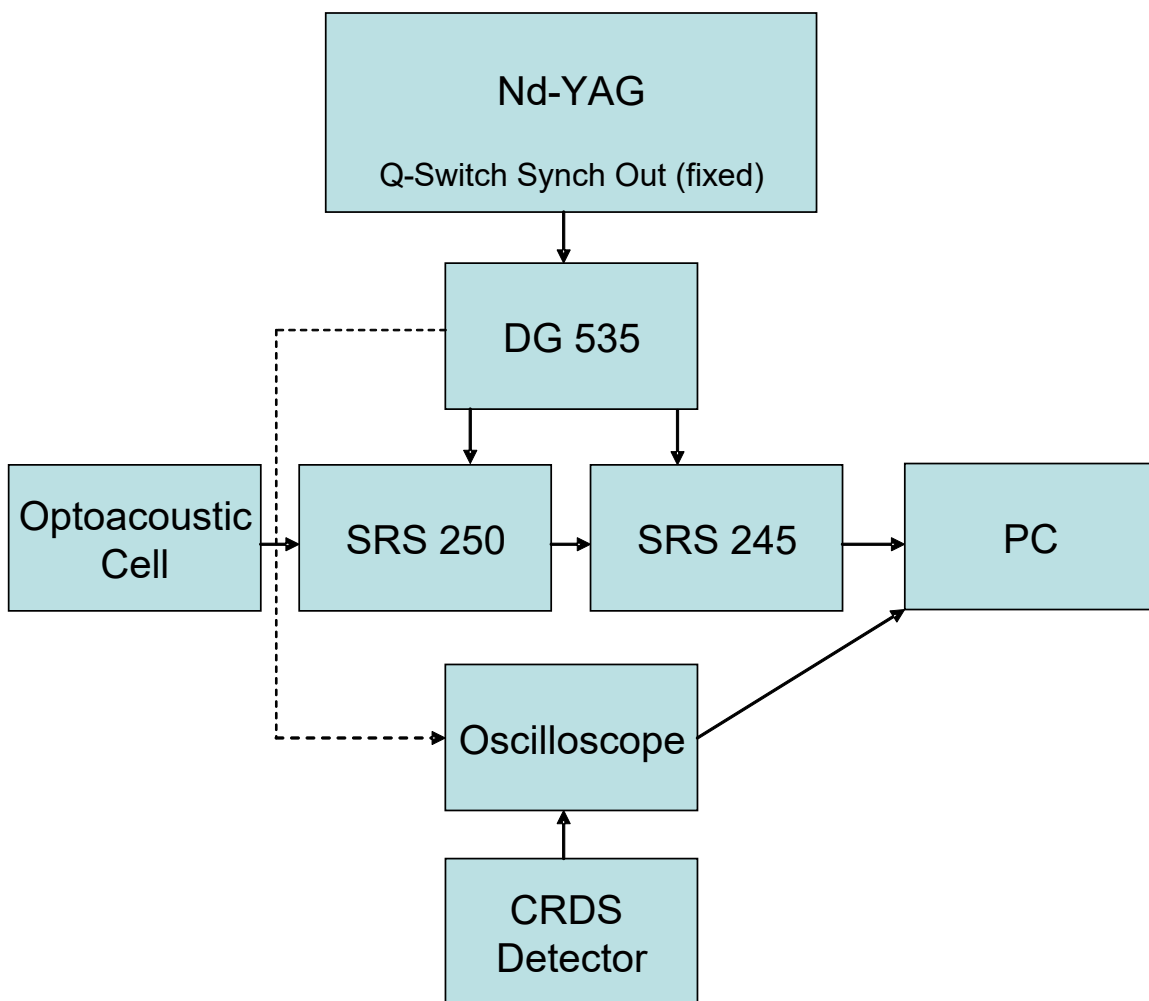


Figure A.4: Diagram of the CRDS data acquisition system.

